Applications of lattice field theory to large N and technicolor

Anne-Mari Mykkänen

Division of Elementary Particle Physics and
Helsinki Institute of Physics
Department of Physics
Faculty of Science
University of Helsinki
Helsinki, Finland

ACADEMIC DISSERTATION

To be presented, with the permission of the Faculty of Science of the University of Helsinki, for public criticism in the auditorium D101 at Physicum, Gustav Hällströmin katu 2 A, Helsinki, on December 5th 2012 at 12 o'clock.

Helsinki 2012

ISBN 978-952-10-8082-1 (printed version)
ISSN 0356-0961
ISBN 978-952-10-8083-8 (pdf version)
http://ethesis.helsinki.fi
Helsinki University Print
Helsinki 2012

A. Mykkänen: Applications of lattice field theory to large N and technicolor,
University of Helsinki, 2012, 61 pages,
University of Helsinki Report Series in Physics, HU-P-D199
ISSN 0356-0961
ISBN 978-952-10-8082-1 (printed version)
ISBN 978-952-10-8083-8 (pdf version)

Abstract

In this thesis we use lattice field theory to study different frontier problems in strongly coupled non-Abelian gauge theories, focusing on large-N models and walking technicolor theories.

Implementing lattice studies of technicolor theories, we consider the SU(2) gauge theory with two fermions transforming under the adjoint representation, which constitutes one of the candidate theories for technicolor. The early lattice Monte Carlo studies of this model have used an unimproved Wilson fermion formulation. However, large lattice cutoff effects can be expected with the unimproved formulation, and so we present the calculation of the $O(a)$ improved lattice Wilson-clover action. In addition to the adjoint representation fermions, we also determine the improvement coefficients for SU(2) gauge theory with two fundamental representation fermions.

In another work, we study the deconfined phase of strongly interacting matter, investigating Casimir scaling and renormalization properties of Polyakov loops in different irreducible representations, in SU(N) gauge theories at finite temperature. We study the approach to the large-N limit by performing lattice simulations of Yang-Mills theories with gauge groups from SU(2) to SU(6), taking the twelve lowest irreducible representations for each gauge group into consideration. We find clear evidence of Casimir scaling and identify the temperature dependence of the renormalized Polyakov loops.

The third study I present is related to the long-standing idea of non-Abelian gauge theories having a close relation to some kind of string theory. In the confining regime of SU(N) gauge theories, the flux lines between well separated color sources are expected to be squeezed in a thin, stringlike tube, and the interaction between the sources can be described by an effective string theory. One of the consequences of the effective string description at zero temperature is the presence of the Lüscher term - a Casimir effect due to the finiteness of the interquark distance - in the long distance interquark potential. To study the validity of this effective model, we compute the static quark potential in SU(3) and SU(4) Yang-Mills theories through lattice simulations, generalizing an efficient 'multilevel' algorithm proposed by Lüscher and Weisz to an improved lattice action.

Acknowledgements

The research for this thesis was done at the Division of Elementary Particle Physics in the University of Helsinki. The numerical calculations were performed at the Center for Scientific Computing (CSC) in Espoo, Finland and at EPCC, University of Edinburgh. I gratefully acknowledge the grants from the Magnus Ehrnrooth Foundation and the Academy of Finland.

I would like to thank my advisor, Kari Rummukainen, for initially presenting me the opportunity to do this Ph.D, and for all the invaluable guidance during these years. I would also like to thank Marco Panero for all the help and support during my studies, as well as Kimmo Tuominen, Jarno Rantaharju and Tuomas Karavirta for discussions and collaboration.

I am grateful to the pre-examiners, Tuomas Lappi and Biagio Lucini, for their comments and suggestions on the manuscript of this thesis.

Helsinki, November 2012
Anne-Mari Mykkänen

List of included publications

[1] T. Karavirta, A. Mykkänen, J. Rantaharju K. Rummukainen and K. Tuominen, *Nonperturbative improvement of SU(2) lattice gauge theory with adjoint or fundamental flavors*, JHEP **1106** (2011) 061, arXiv:1101.0154 [hep-lat]

[2] A. Mykkänen, M. Panero and K. Rummukainen, *Casimir scaling and renormalization of Polyakov loops in large-N gauge theories*, JHEP **1205** (2012) 069, arXiv:1202.2762 [hep-lat]

[3] A. Mykkänen, *The static quark potential from a multilevel algorithm for the improved gauge action*, arXiv:1209.2372 [hep-lat]

Author's contribution

In article [1] the author performed part of the numerical calculations. In article [2] the author performed analytical calculations related to the different representations used, contributed to writing the code, performed part of the numerical calculations, and wrote an early draft for the introductory part of the paper. The article [3] is a work done solely by the author.

Contents

Chapter 1

Non-Abelian gauge field theories

In gauge theories, transformations can depend on several variables, that do not necessarily commute, i.e. the order in which consecutive transformations are performed affects the result. Groups that contain these non-commuting transformations are called non-Abelian. The Standard Model is non-Abelian; it is based on the $\mathrm{SU(3)_{color}} \times (\mathrm{U(1)} \times \mathrm{SU(2)})$ gauge symmetries.

The efforts to extend the original concept of gauge theory from an Abelian group, e.g. quantum electrodynamics, to a non-Abelian group were motivated by the idea that weak and strong interactions could be derived from non-Abelian gauge theories. In 1954 Yang and Mills developed a modern formulation based on the $\mathrm{SU}(N)$ group [4], which however suffered from the inconvenience that the quanta of the fields had to be massless in order to maintain gauge invariance, thus imposing massless gauge bosons. The problem was settled in the 60's with the concept of particles aquiring mass through symmetry breaking, a work initially put forward by Goldstone, Nambu, and Jona-Lasinio [5, 6]. When applied to gauge theories, this mechanism is known as the Higgs mechanism [7, 8, 9], which explains how the W and Z bosons are massive.

In the context of gauge theories, Lie groups and their algebra hold an essential importance. The generators of a Lie group t^a form a basis for the vector space of infinitesimal transformations, i.e. Lie algebra. For non-Abelian groups, the following commutation relation holds:

$$[t^a, t^b] = C^{abc} t^c, \tag{1.1}$$

where the structure constants C^{abc} are antisymmetric with respect to the first two indices and independent of the representation; they define the multiplication properties of the Lie group. For the fundamental representation we can choose the generators to satisfy

$$\mathrm{Tr}(t^a t^b) = \frac{1}{2}\delta^{ab}. \tag{1.2}$$

In gauge theories the Lagrangian of a system is invariant under local symmetries, i.e. gauge invariant. This is because in gauge theories, the conventional derivatives ∂_μ are replaced with covariant derivatives

$$D_\mu = \partial_\mu + igA_\mu, \tag{1.3}$$

where A_μ is the gauge field, and the Lagrangian is given a kinetic energy term $-\frac{1}{4}F^a_{\mu\nu}F^{a\mu\nu}$:

$$L(\partial_\mu\psi(x),\psi(x)) \to L(D_\mu\psi(x),\psi(x)) - \frac{1}{4}F_{\mu\nu}F^{\mu\nu}. \tag{1.4}$$

The field strength tensor $F_{\mu\nu} = F^a_{\mu\nu}t^a$ is defined as

$$F_{\mu\nu} = \partial_\mu A_\nu - \partial_\nu A_\mu + g[A_\mu, A_\nu], \tag{1.5}$$

where g is the coupling constant. There are a number of constraints for the kinetic term; it should be Lorentz- and gauge-invariant, independent of the matter field, and also quadratic in the first derivatives of the gauge field.

The transformation rule for the gauge field A_μ reads:

$$A_\mu \to A'_\mu = \omega A_\mu \omega^{-1} + \frac{1}{g}\omega\partial_\mu\omega^{-1}, \tag{1.6}$$

and for the strength tensor:

$$F_{\mu\nu} \to F'_{\mu\nu} = \omega F_{\mu\nu}\omega^{-1}, \tag{1.7}$$

where $\omega = \exp(i\theta^a t^a)$ is an element of the group, with θ^a as the parameters of the transformation. Now we can construct a kinetic term for A_μ, that satisfies all the constraints listed above. Such a quantity is the trace of the product of the strength tensor with itself $\mathrm{Tr}(F_{\mu\nu}F^{\mu\nu})$, and it is gauge invariant due to the cyclicity of trace

$$\mathrm{Tr}(F_{\mu\nu}F^{\mu\nu}) \to \mathrm{Tr}(\omega F_{\mu\nu}F^{\mu\nu}\omega^{-1}) = \mathrm{Tr}(F_{\mu\nu}F^{\mu\nu}). \tag{1.8}$$

Using this property, we are able to construct a gauge invariant action.

In Euclidean space-time, the partition function can be written

$$Z = \int DA_\mu D\psi D\bar{\psi} e^{-S}, \tag{1.9}$$

where S is defined as an action containing both gauge fields and the fermionic fields:

$$S = \int d^4x (\frac{1}{4}F_{\mu\nu}F^{\mu\nu} - \bar{\psi}M\psi). \tag{1.10}$$

Here M is the Dirac operator, $\gamma^\mu\partial_\mu$ [10]. The fermionic fields are expressed with Grassmann variables $\bar{\psi}$ and ψ, and can be integrated out exactly, resulting in

$$Z = \int DA_\mu \mathrm{det}M e^{\int d^4x(-\frac{1}{4}F_{\mu\nu}F^{\mu\nu})}. \tag{1.11}$$

So, in the end, the fermionic contribution is contained in the term $\mathrm{det}M$, and we can write the action as a sum

$$\begin{aligned} S &= S_{\text{gauge}} + S_{\text{fermionic}} && (1.12)\\ &= \int d^4x(\frac{1}{4}F_{\mu\nu}F^{\mu\nu}) - \sum_i \log(\mathrm{det}M_i), && (1.13) \end{aligned}$$

where i are the flavors. In lattice simulations, in some cases one can employ the quenched approximation to simplify calculations, that is, one takes $\mathrm{det}M$ to be constant.

To obtain results for physical observables, we calculate expectation values:

$$\langle O \rangle = \frac{1}{Z} \int DA_\mu O e^{-S}, \tag{1.14}$$

In pratice, all dependence on fermions as dynamical fields is removed here, by expressing the fermionic fields in O in terms of fermion propagators, using Wick's theorem. Fermionic quantities are built with the Feynmann propagator

$$S_F(y, j, b; x, i, a) = (M^{-1})^{y,j,b}_{x,i,a} \tag{1.15}$$

A given element of the matrix $(M^{-1})^{y,j,b}_{x,i,a}$ is the amplitude for the propagation of a quark from site x with spin-color i, a to site-spin-color y, j, b [10].

1.1 Asymptotic freedom

A significant feature of gauge theories, is the asymptotic freedom. It was discovered by Gross, Wilczek [11], Politzer [12], and independently by 't Hooft [13]. Roughly speaking, asymptotic freedom means that as we go to shorter and shorter distances, the running coupling constant g decreases in such an extent, that the theory eventually appears to be a free theory. This can be characterized with the β-function, which in a perturbative expression reads

$$\mu \frac{\partial g}{\partial \mu} = \beta(g) = -(\beta_0 g^3 - \beta_1 g^5 + \ldots) \tag{1.16}$$

The function $\beta(g)$ is negative for non-abelian gauge groups. Here the leading terms β_0 and β_1 can be written

$$\beta_0 = \left(\frac{11N - 2n_f}{3} / 16\pi^2 \right), \tag{1.17}$$

$$\beta_1 = \left(\frac{34N^2}{3} - \frac{10Nn_f}{3} - \frac{n_f(N^2-1)}{N} \right) / (16\pi^2)^2, \tag{1.18}$$

and they are gauge and regularization scheme invariant. In the formulae N is the number of colors and n_f the number of flavors. For $n_f < \frac{11N}{2}$, we see that $\beta(x)$ is positive; a result that was essential when establishing QCD as the theory of strong interactions. This detail explained existing experimental data that implied that the strength of strong interactions decreases when the momentum exchanged in a process is increased [10].

A simple calculation with the equation (1.16) implies, that the coupling constant of non-abelian gauge theories depends logarithmically on the momentum scale of the process. For QCD, further analysis leads us to introduce Λ_{QCD}, the scale of the theory with dimensions of mass. In other words, for QCD, a theory with a dimensionless coupling constant and no intrinsic mass scale in the absence of quark masses, a mass scale is thus dynamically generated [10]. This is called the dimensional transmutation.

1.2 Confinement

Inversely to asymptotic freedom, when we go towards the other end of the scale, at larger and larger distances, the coupling constant increases, so that at one point perturbative calculations are no longer valid. When the coupling

constant is large, it means that gluons and fermions are bound more tightly together. This gives rise to another key feature of gauge theories, confinement [14].

Confinement has not been rigorously proven, but there is very compelling evidence that it exists. There are two possible ways to test if a theory is confining. For instance, one can demonstrate that the free energy of an isolated charge is infinite, or alternatively, one can show that the potential energy between two charges grows linearly with distance [10]. According to results obtained from lattice QCD computations, in general the potential between two quarks is proportional to the distance between them

$$V(r) \sim \sigma r. \tag{1.19}$$

where σ is the string tension. If we try to pull two quarks apart, at some point enough work has been done to create a new quark-antiquark pair, in which case the original "string" has been broken, but two new ones have appeared. This way, a single quark can never exist alone.

1.3 Chiral symmetry breaking

Chiral symmetry breaking is a key feature of quantum field theory with fermions. In QCD with N_f light flavors the standard expectation is that the $\mathrm{SU}(N_f)_L \times \mathrm{SU}(N_f)_R$ chiral symmetry group breaks spontaneously to $\mathrm{SU}(N_f)_{L+R}$.

For a massless fermion the action reads

$$S_F[\psi, \bar{\psi}, A] = \int d^4x L(\psi, \bar{\psi}, A), \tag{1.20}$$

$$L(\psi, \bar{\psi}, A) = \bar{\psi}\gamma_\mu(\partial_\mu + iA_\mu)\psi = \bar{\psi}D\psi, \tag{1.21}$$

where D is the massless Dirac operator. A chiral rotation of the fermion fields

$$\psi \to \psi' = e^{i\alpha\gamma_5}\psi, \qquad \bar{\psi} \to \bar{\psi}' = \bar{\psi}e^{i\alpha\gamma_5}, \tag{1.22}$$

where γ_5 is the chirality matrix acting in Dirac space and α is a constant, real parameter, leaves the Lagrangian density invariant

$$L(\psi', \bar{\psi}', A) = L(\psi, \bar{\psi}, A). \tag{1.23}$$

A mass term, however, breaks this invariance

$$m\bar{\psi}'\psi' = m\bar{\psi}e^{i2\alpha\gamma_5}\psi. \tag{1.24}$$

Furthermore, we introduce the right- and left-handed projectors

$$P_R = \frac{1+\gamma_5}{2}, \qquad P_L = \frac{1-\gamma_5}{2}, \tag{1.25}$$

with which we can define right- and left-handed fermion fields

$$\psi_R = P_R\psi, \qquad \psi_L = P_L\psi, \qquad \bar{\psi}_R = \bar{\psi}P_L, \qquad \bar{\psi}_L = \bar{\psi}P_R. \tag{1.26}$$

Further algebra shows the decoupling of left- and right-handed components

$$L(\psi, \bar{\psi}, A) = \bar{\psi}_L D\psi_L + \bar{\psi}_R D\psi_R \tag{1.27}$$

i.e., the left- and right-handed components "do not talk to each other". However, a mass term mixes the terms

$$m\bar{\psi}\psi = m(\bar{\psi}_R\psi_L + \bar{\psi}_L\psi_R). \tag{1.28}$$

The chiral symmetry of the action holds only for massless quarks, thus the limit of vanishing quark mass is often referred to as the chiral limit [15].

To summarize the essence of chiral symmetry, we can write the simple equation

$$D\gamma_5 + \gamma_5 D = 0, \tag{1.29}$$

i.e. the massless Dirac operator $D = \gamma_\mu(\partial_\mu + iA_\mu)$ anticommutes with γ_5.

Chapter 2

The Lattice

In the 70's Wilson formulated gauge fields on a discrete space-time grid [14]. The elegant lattice formulation was heavily motivated by the concept of a gauge field as a path-dependent phase factor, and remarkable in the way that the gauge freedom remained as an exact local symmetry. The lattice is a gauge invariant, non-perturbative regularization, that harnesses the Feynman path integral approach [16], converting the functional integral to a discrete collection of ordinary group integrals.

As summarized in [10], Wilson's approach to implement the path integral scheme consists of transcripting the gauge and fermion degrees of freedom into discretized space-time, constructing the action, defining the measure of integration in the path integral, and finally transcripting the operators that are to be used to probe the physics.

The lattice is a four dimensional $L_s^3 \times L_t$ grid, consisting of sites (fermionic fields) and the connecting links (gauge fields). It is defined in Euclidean space, where time is set imaginary $t \to \tau = it$, hence the metric is $g^{\mu\nu} = (++++)$. Since we are in Euclidean space, we can define the volume as

$$V = (aL_s)^3, \tag{2.1}$$

and with small temporal extent, it turns out that we can express the temperature as

$$T = \frac{1}{aL_t}. \tag{2.2}$$

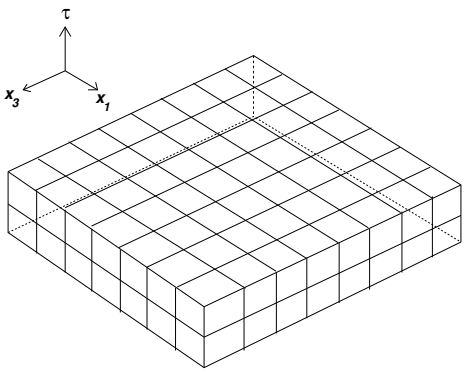

Figure 2.1: A lattice

Here a is the lattice spacing. The fermionic fields, which belong to the fundamental representation of SU(N), are transcripted to the lattice by anticommuting Grassmann variables. In pratice however, it turns out that one does not need to pass the Grassmann variables on the lattice, and implement the Pauli exclusion principle; since the fermion action is linear in both $\bar{\psi}$ and ψ, the rules for Grassmann variables can be used to integrate over them [10].

The gauge fields $A_\mu(x)$ mediate the interactions between neighboring sites. The link variables belong to the gauge group SU(N), and thus satisfy

$$U_\mu^\dagger = U_\mu^{-1}, \qquad \det U = 1. \tag{2.3}$$

With each link we can associate a discrete version of the path ordered product [10]

$$U(x, x+\hat{\mu}) = U_\mu(x) = e^{iagA_\mu(x+\frac{\hat{\mu}}{2}a)} \tag{2.4}$$

where the average field A_μ is defined at the midpoint of the link.

Naturally, on the lattice the continuous rotation group is replaced by the discrete hypercubic group. The allowed momenta are discrete and periodic

$$k = \frac{2\pi n}{aL}, \qquad n = 0, 1, ..., N, \tag{2.5}$$

conserved modulo $2\pi/a$.

Let us denote a local gauge transformation by $V(x)$. The effect on the variables $\psi(x)$ and U can be written

$$\psi(x) \rightarrow V(x)\psi(x) \tag{2.6}$$
$$\bar{\psi}(x) \rightarrow \bar{\psi}(x)V^\dagger(x) \tag{2.7}$$
$$U_\mu(x) \rightarrow V(x)U_\mu(x)V^\dagger(x+\hat{\mu}) \tag{2.8}$$

where $V(x)$ is, like $U_\mu(x)$, an SU(N) matrix. These definitions come in handy when we want to build gauge invariant quantities. There are two types, in fact. First, a string formed by a path ordered product of links, with a fermion and an antifermion at the ends of the string. Futhermore, if the lattice has periodic boundaries, and the string is closed by the periodicity, the fermion-antifermion pair is not needed. Such a quantity is called the Polyakov loop, or alternatively, the Wilson line

$$L = \mathrm{Tr}\prod_{t=1}^{L_t} U(t). \tag{2.9}$$

Another gauge invariant object is the closed Wilson loop, the simplest one being the plaquette

$$W_{\mu\nu}^{1\times1} = \mathrm{ReTr}(U_\mu(x)U_\nu(x+\hat{\mu})U_\mu^\dagger(x+\hat{\nu})U_\nu^\dagger(x)). \tag{2.10}$$

Using gauge invariant strings and loops, one is able to construct a gauge invariant action. The objects can be of arbitrary shape and size, and can also lie in any representation of SU(N), providing that, in the end, we get the familiar continuum theory in the $a \rightarrow 0$ limit [10]. A simple action can be built using plaquettes

$$S_W = \frac{2N}{g_0^2}\sum_x\sum_{\mu<\nu}(1 - \frac{1}{N}\mathrm{ReTr}W_{\mu\nu}^{1\times1}(x)). \tag{2.11}$$

This is known as the Wilson action, which in the naive continuum limit tends to $\frac{1}{4}\int d^4x(F^a_{\mu\nu})^2$ [10]. The prefactor in (2.11) is often denoted with β

$$\beta = \frac{2N}{g_0^2}. \tag{2.12}$$

The partition function can now be written as

$$Z = \int \sum_{x,\mu} dU_\mu(x) e^{-S_W}, \tag{2.13}$$

and the expectation values of physical observables as

$$\langle O \rangle = \frac{1}{Z} \int \prod_{x,\mu} dU_\mu(x) O e^{-S_W}. \tag{2.14}$$

The finite-dimensional integration measure dU_μ for the link variables is specified as an invariant group measure, the Haar measure. It is defined such that for any elements V and W of the group

$$\int dU f(U) = \int dU f(UV) = \int dU f(WU), \tag{2.15}$$

where $f(U)$ is an arbitrary function over the group. Furthermore, we can normalize the measure by defining

$$\int dU = 1. \tag{2.16}$$

2.1 Continuum limit

Naturally, we would eventually like to extract the continuum results from the lattice, i.e. get rid of the lattice spacing a. However, just taking a to be zero would bring all the dimensionful physical quantities to either zero or infinity. In lattice theories, in general, we need to adjust the other free parameter, the coupling g. In renormalizable theories fixing g enables the physical quantities to have their real, finite physical values.

The Callan-Symanzik β-function [17, 18, 19] expresses the unique functional dependence between g and a

$$\beta(g) = -a\frac{\partial g(a)}{\partial a}. \tag{2.17}$$

$\beta(g)$ can be determined with perturbation theory. For example, for sufficiently small bare coupling we can write

$$\beta(g) = -\frac{11}{16\pi^2}\left(\frac{11N_C}{3} - \frac{2N_f}{3}\right) g^3 + O(g^5) = \beta_0 g^3 \tag{2.18}$$

In the small coupling region $\beta(g)$ is negative, and we can see from the Callan-Symanzik equation that when the lattice spacing is decreased, g will approach the fixed point $g = 0$, corresponding to a zero of the β-function. In the case when g is small enough to validate (2.18), this approximation will improve along decreasing a, and the continuum limit will be realized at vanishing bare coupling. This is actually the property of asymptotic freedom, explained on the level of

the bare coupling constant; As the lattice spacing a diminishes, the coupling diminishes accordingly, to keep the physics the same. In other words, as the lattice moves on to describe higher momentum physics, the interaction weakens, approaching free theory.

A more practical way to describe how we approach the continuum limit is to talk about the observables. On the lattice we run simulations at different values of the lattice parameters and measure different observables. Suppose we measure the correlation length between two Polyakov loops, for example, at a certain value of β, and then repeat the simulation at larger values of β. We get that the correlation length in terms of the lattice spacing will grow. Since we want the correlation length to be physical, the lattice spacing a therefore has to get shorter and shorter in the subsequent simulations with larger β.

This way, by running simulations where the correlation length in lattice units becomes divergent, we get the continuum limit $a \to 0$. Note that the divergence happens only when the lattice theory has a continuous phase transition. In non-Abelian gauge theories, at zero temperature, such a transition occurs only for

$$\beta = \frac{2N}{g_0^2} \to +\infty, \tag{2.19}$$

namely for $g_0 \to 0$, giving rise yet again to the idea of asymptotic freedom.

How fast the continuum limit is actually reached, depends on the action. The discretization procedure is not unique. Nonetheless, different lattice actions have to give the same continuum limit. For an illustration, the expectation value of an arbitrary operator ϕ on the lattice can be written as a sum of the expectation value in the continuum theory and the deviation or "lattice artefact" caused by the discretization

$$\langle \phi \rangle_{\text{lat}} = \langle \phi \rangle + O(a^p), \tag{2.20}$$

where the exponent p expresses how fast the discretized action converges to the continuum action. For the Wilson action $p = 2$, but with improved actions with larger p, it is possible to approach the continuum limit faster [20]. It is still quite a delicate balance, since an action too complicated can slow down the simulation significantly, and in the end, the optimal choice may depend on the observable in question [20].

2.2 Phase structure and the Polyakov loop

At high temperatures, Yang-Mills theories are known to have a deconfined phase, where confined hadronic matter has transformed into a plasma of non-color-singlet constituents. One way to characterize the temperature region of deconfinement in Yang-Mills theories, is through the gauge-invariant trace of a temporal Wilson line, or Polyakov loop. The Polyakov loop is an order parameter [21, 22], that describes the dynamics of the system and signals the onset of phase transition.

The Polyakov loop L is the trace of path ordered product of the link matrices pointing in the time direction in a specific point in space, and winding around the euclidean time direction. Beyond periodic gauge transformations, the lattice action of the pure SU(N) gauge theory has also another symmetry, the center Z(N) symmetry [21]. By studying the behavior of the Polyakov loop under the center Z(N) symmetry, we can access some essential features of the physics behind the deconfinement phase transition.

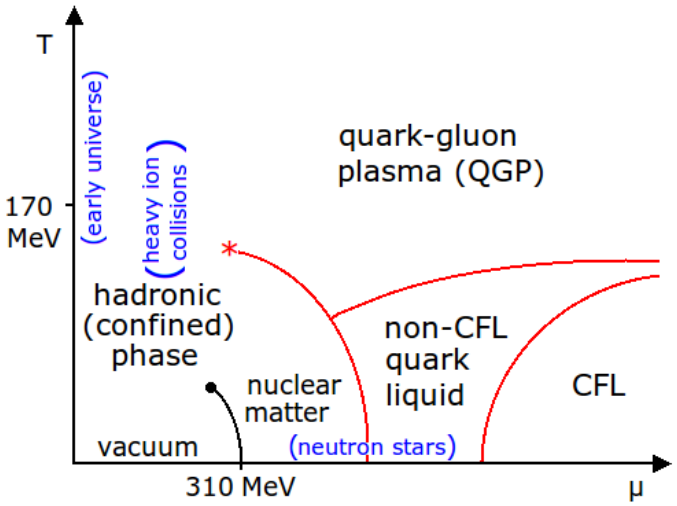

Figure 2.2: The QCD phase diagram.

The center Z(N) of the group SU(N) consists of all elements z for which

$$zgz^{-1} = g, \qquad g \in \mathrm{SU}(N). \tag{2.21}$$

The elements of $SU(N)$ that belong to the center of the group are given by $\exp(i2\pi n/N)$, $n = 1 \ldots N$.

Multiplying all link matrices oriented in the lattice time direction, at time $x_0 = 0$, by an element z of the center

$$U(\bar{n}, 0) \rightarrow U'(\bar{n}, 0) = zU(\bar{n}, 0), \tag{2.22}$$
$$U(\bar{n}, x_0 \neq 0) \rightarrow U'(\bar{n}, x_0 \neq 0) = U(\bar{n}, x_0 \neq 0), \tag{2.23}$$
$$\tag{2.24}$$

a time-space plaquette in $x_0 = 0$ changes as

$$U_{i0}(\bar{n}) = U_i(\bar{n}, 0)U_0(\bar{n} + \hat{e}_i, 0)U_i^\dagger(\bar{n}, 1)U_0^\dagger(\bar{n}, 0) \tag{2.25}$$
$$\rightarrow U_i(\bar{n}, 0)zU_0(\bar{n} + \hat{e}_i, 0)U_i^\dagger(\bar{n}, 1)U_0^\dagger(\bar{n}, 0)z^\dagger. \tag{2.26}$$

Demanding that z commutes with all link matrices, the plaquette - and therefore the action - remain invariant. Thus the center Z(N) symmetry is indeed a symmetry of the action.

The Polyakov loop, however, changes as

$$L(\bar{n}) \rightarrow \Big(zU(\bar{n}, 0)\Big) \prod_{j=1}^{L_t-1} U(\bar{n}, j) = zL(\bar{n}), \tag{2.27}$$

so, it is invariant only in the case, when it is zero.

The physical meaning of the Polyakov loop is in the free energy of a system with a single heavy quark. To elaborate how this comes about, we can write the partition function of a system of an infinitely heavy quark coupled to a fluctuating gauge potential in the form

$$Z = \sum_s \langle s | e^{\frac{1}{T}H} | s \rangle. \tag{2.28}$$

Here $\frac{1}{T} = a \times L_t$. Furthermore, (2.28) can be written in the form

$$Z = \mathrm{Tr}(e^{-\frac{1}{T}H}), \tag{2.29}$$

and expressed in path integral formalism,

$$Z = \int DA e^{-S^{(1/T)}_{\mathrm{Gauge}}[A]}. \tag{2.30}$$

Thus, considering the translational invariance of the vacuum, we conclude that

$$e^{-\frac{1}{T}F_q} = \langle L \rangle = \frac{1}{V}\sum_{\vec{x}} \langle L(\vec{x}) \rangle. \tag{2.31}$$

Here V is the spatial volume of the lattice. (The left hand side of (2.31) is replaced by $e^{-\frac{1}{T}\hat{F}_q}$ on the lattice, $\hat{F}_q$ being the free energy measured in lattice units) [15].

The Polyakov loop can be interpreted as the world line of a static quark, implying that the free energy of a static quark (located at, say, $\vec{x} = \vec{n}a$) and an antiquark (at $\vec{y} = \vec{m}a$) can be obtained from the correlation function of two loops

$$\Gamma(\vec{n}, \vec{m}) = \langle L(\vec{n}) L^\dagger(\vec{m}) \rangle. \tag{2.32}$$

This equation is related to the free energy $\hat{F}_{q\bar{q}}(\vec{n}, \vec{m})$ of a static quark-antiquark pair, measured relative to that in the absence of the $q\bar{q}$ pair [15]:

$$\Gamma(\vec{n}, \vec{m}) = e^{-\frac{1}{T}\hat{F}_{q\bar{q}}(\vec{n}, \vec{m})}. \tag{2.33}$$

Now, when $|\vec{n} - \vec{m}| \to \infty$,

$$\langle L(\vec{n}) L^\dagger(\vec{m}) \rangle \to |\langle L \rangle|^2. \tag{2.34}$$

Thus, we state

$$\langle L \rangle = 0 \qquad \text{(confinement)}, \tag{2.35}$$

and

$$\langle L \rangle \neq 0 \qquad \text{(deconfinement)}. \tag{2.36}$$

Looking back at equation (2.27), we note that the center Z(N) symmetry is realized in the low temperature confining phase, and correspondingly, in the deconfined phase it is necessarily broken. The center Z(N) symmetry is thus a symmetry of the Polyakov loop only in the confined phase, and a deconfinement phase transition is accompanied by a breakdown of the center symmetry [21]. In this respect, the pure Yang-Mills theory provides a cleaner theoretical setup than QCD, where the finite-temperature deconfinement at physical values of the quark masses is actually a *crossover*. In QCD, because of fermionic contribution, the Polyakov loop is actually an *approximate* order parameter with physical values of the quark masses: It has a small, yet non-vanishing, value in the confined phase, and a large value in the deconfined phase.

Of course the expectation value of the Polyakov loop extracted from lattice simulations is a bare quantity, affected by ultraviolet divergences. An appropriate renormalization, in a given scheme is thus required [23]. There is an additive shift in the logarithm of the bare Polyakov loop expectation value, which can be interpreted as the free energy of a static, infinitely heavy color source probing the system. The Polyakov loop renormalization is studied in the second included publication of this thesis, [2].

2.3 Fermions on the lattice and the doubling problem

In general, N_f light flavors can be presented in 'left' and 'right' components, following a symmetry pattern

$$\mathrm{U}(N_f)_L \otimes \mathrm{U}(N_f)_R = \mathrm{SU}(N_f)_V \otimes \mathrm{SU}(N_f)_A \otimes \mathrm{U}(1)_V \otimes \mathrm{U}(1)_A. \tag{2.37}$$

$\mathrm{SU}(N_f)_V$ is conserved, whereas $\mathrm{SU}(N_f)_A$ is spontaneously broken, thus introducing pions, the Goldstone bosons of this symmetry breaking. $\mathrm{U}(1)_V$ is conserved, corresponding to baryon number conservation, and $\mathrm{U}(1)_A$ is explicitly broken by anomalies due to quantum fluctuations. In the classical continuum theory (and for massless fermions), the chiral symmetry

$$\{\not{D}, \gamma_5\} = \not{D}\gamma_5 + \gamma_5\not{D} = 0, \tag{2.38}$$

would imply the conservation of an axial-vector current, that is if there wasn't the explicit breaking of $\mathrm{U}(1)_A$.

On the lattice, the attempt to discretize the Dirac action in the simplest way, leads to the naive fermion action [10]:

$$\begin{aligned} S_F^{\mathrm{Naive}} &= m_q \sum_x \bar{\psi}(x)\psi(x) \qquad (2.39)\\ &\quad + \frac{1}{2a}\sum_x \bar{\psi}(x)\gamma_\mu[U_\mu(x)\psi(x+\hat{\mu}) - U_\mu^\dagger(x-\hat{\mu})\psi(x-\hat{\mu})] \\ &= \sum_x \hat{\psi}(x) M_{xy}^N[U]\psi(y), \qquad (2.40) \end{aligned}$$

with the interaction matrix M^N

$$M_{i,j}^N[U] = m_g\delta_{i,j} + \frac{1}{2a}\sum_\mu [\gamma_\mu U_{i,\mu}\delta_{i,j-\mu} - \gamma_\mu U_{i-\mu,\mu}^\dagger \delta_{i,j+\mu}]. \tag{2.41}$$

Translations by a, as well as C, P and T leave the fermion action invariant. The naive action has a global symmetry $\mathrm{U}(1)_V$, i.e

$$\begin{aligned} \psi(x) &= e^{i\phi}\psi(x) \qquad (2.42)\\ \bar{\psi}(x) &= \bar{\psi}(x)e^{-i\phi} \qquad (2.43) \end{aligned}$$

with a continuous parameter ϕ. On a lattice with finite lattice spacing, the axial-vector current is conserved. The drawback is the existence of corresponding extra excitations, 'doublers'.

When naively trying to put fermionic fields on the lattice, the spurious states, doublers, appear, such that one ends up having 2^d fermionic particles for each original fermion. Thus, the naive action does not converge to the continuum action as a $a \to 0$. Nielsen and Ninomiya examined the problem further, which resulted in the formulation of the so called no-go -theorem [24, 25]. The theorem states, that it is not possible to remove the doublers from the action without breaking chiral symmetry. More precisely, fermion doubling is inevitable with a local, real, free fermion lattice action, that has chiral and translational invariance.

Let us look at the problem of the naive fermion action closer. Using the formulae above, we can define a propagator as the inverse of the interaction

matrix M:

$$\langle\bar{\psi}_x\psi_y\rangle = \frac{1}{Z}\int[d\psi d\bar{\psi}e^{-S_F^{\text{Naive}}}]\bar{\psi}_x\psi_y \quad (2.44)$$

$$= M^{-1}_{x,y}. \quad (2.45)$$

In momentum space, the field variables are transformed as

$$\psi(x) = \frac{1}{\sqrt{N}}\sum_p e^{-ip_\mu x_\mu}\psi(p), \quad (2.46)$$

where

$$p_i = \frac{2\pi n_i}{aN_s}, \quad n_i = 0, ..., N_s - 1 \quad (2.47)$$

$$p_0 = \frac{2\pi n_0}{aN_t}, \quad n_0 = \frac{1}{2}, \frac{3}{2}, ..., N_t - \frac{1}{2}. \quad (2.48)$$

In this space,

$$S_F^{\text{Naive}} = \sum_p \bar{\psi}_p[a^4(m + ia^{-1}\sum_\mu \gamma_\mu \sin(p_\mu a))]\psi_p \quad (2.49)$$

$$= \bar{\psi}_p M_p \psi_p \quad (2.50)$$

and the inverse propagator is thus

$$\Delta^{-1} = M_p = m + ia^{-1}\sum_\mu \gamma_\mu \sin(p_\mu a). \quad (2.51)$$

At small values of p we get

$$M_p \approx m + i\gamma_\mu p_\mu \quad (2.52)$$

and up to this point all is well. However, now near the edge of the Brillouin zone, $p_\mu \sim \frac{\pi}{a}$

$$\frac{1}{a}\sin(p_\mu a) \sim (p_\mu - \frac{\pi}{a}) \quad (2.53)$$

and again, we have a zero point. Since $p_\mu = (p_0, p_1, p_2, p_3)$ and $p \approx 0, \frac{\pi}{a}$ we end up with $2^4 = 16$ light modes. Thus it turns out, that instead of just one, our action is a model for sixteen light fermions. This is the so called doubling problem. There are various suggestions on how to circumvent the problem, accepting the limitation stated by the no-go theorem. The most well established, for example, the Kogut-Susskind staggered fermions [26] [27], Wilson fermions [14, 28], the perfect action [29, 30], domain wall fermions [31, 32] and overlap fermions. Wilson's fix to the doubling problem was to assign a heavy mass to the doublers, which would then decouple.

2.4 Wilson fermions

To get rid of the doublers in the fermionic part of the naive action, Wilson proposed [28] adding a term to it, that contains a second derivative

$$-\frac{r}{2}\sum_n \bar{\psi}(n)\partial_\mu\partial_\mu\psi(n) \quad (2.54)$$

with r as an arbitrary constant. This extra term is proportional to a, therefore it raises the masses of the unwanted doublers proportional to $1/a$, and on the other hand, vanishes in the continuum limit $a \to 0$. The action with "Wilson fermions" takes the form

$$\begin{aligned} S_F^{\text{Wilson}} &= \sum_n (ma + 4r)\bar{\psi}(n)\psi(n) \\ &\quad -\frac{1}{2}\sum_{n,\mu} \bar{\psi}(n)(r - \gamma_\mu)U_\mu(n)\psi(n + a\hat{\mu}) \\ &\quad +\bar{\psi}(n + a\hat{\mu})(r + \gamma_\mu)U_\mu^\dagger(n)\psi(n). \end{aligned} \tag{2.55}$$

As already noted, Wilson's fix accepts the limitations set by the no-go theorem, i.e. the chiral symmetry is broken explicitly [10]. This happens for $r \neq 0$, even for zero quark masses on a lattice. In the continuum limit however, one expects the chiral symmetry to be restored. Reaching the chiral limit requires some fine tuning, since the Wilson term also leads to an additive renormalization of the quark mass.

Chapter 3

Technicolor

The Higgs field was postulated to resolve inconsistencies in the Standard Model, primarily to provide a mechanism for the spontaneous electroweak symmetry breaking. Although phenomenologically successful at the electroweak energy scale, the Standard Model with the Higgs field has several well-known theoretical problems at much higher energies, such as the hierarchy problem, the stability of the electroweak vacuum, triviality bounds etc [33]. These difficulties arise from the fact that the Higgs field is in fact the only scalar field of the theory.

The motivation for Technicolor [34, 35] comes from analogy with QCD. By itself QCD already contributes to the electroweak symmetry breaking: even without the Higgs field in the Standard model, the electroweak charge of the chiral $\bar{q}q$ condensate would alone break the electroweak gauge symmetry and give rise to W and Z boson masses [33]. However, these masses would be very much smaller than the physical values of m_W and m_Z. As it is, Technicolor theories address the electroweak symmetry breaking by substituting the fundamental Higgs scalar with a QCD-like chiral condensate. One introduces a new non-Abelian gauge field, technigauge, and massless fermions, techniquarks Q. Like quarks in the Standard model, the techniquarks are taken to have both technicolor and electroweak charge. The chiral $\bar{Q}Q$ condensate breaks the electroweak symmetry, and the magnitude of the chiral condensate takes the role of the Higgs condensate. As in QCD, there are several bound states also in technicolor models, which would be observable in experiments [33].

3.1 Extended Technicolor and Walking

Despite of all, the classic technicolor scenario described above fails to provide for the Standard Model fermion mass terms. To fix this, extended technicolor (ETC) theories [36, 37], where a Yukawa-like coupling is produced to the technifermion condensate, have been considered. As discussed in [33], ETC can be modeled with a gauge boson, with mass M_{ETC}, coupled to the SM fermions q and techniquarks Q (figure 3.1, taken from [33]). Now, at energies smaller than M_{ETC}, the coupling

$$\frac{g_{\mathrm{ETC}}^2}{M_{\mathrm{ETC}}^2}\bar{Q}Q\bar{q}q, \tag{3.1}$$

gives fermion masses

$$m_q \propto \frac{\langle\bar{Q}Q\rangle}{M_{\mathrm{ETC}}^2}, \tag{3.2}$$

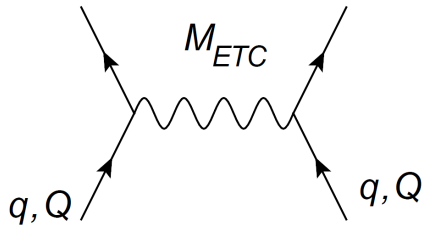

Figure 3.1:

and the term

$$\frac{g^2_{\rm ETC}}{M^2_{\rm ETC}}\bar{q}q\bar{q}q, \tag{3.3}$$

contributes to unwanted flavour changing neutral currents.

Related to the latter, in ETC we have the generic constraint $M_{\rm ETC} > 1000\Lambda_{\rm EW}$. Together with the requirement of the electroweak symmetry breaking pattern, $\langle\bar{Q}Q\rangle_{TC} \propto \Lambda^3_{\rm TC} \approx \Lambda^3_{\rm EW}$, we are lead to having too small SM fermion masses. The problem can be avoided by enhancing the condensate at the extended technicolor scale, so that $\langle\bar{Q}Q\rangle_{\rm ETC} \propto m_q\Lambda^2_{ETC}$ [33].

Looking at the renormalization group evolution of the technifermion condensate

$$\langle\bar{Q}Q\rangle_{\rm ETC} = \langle\bar{Q}Q\rangle_{\rm TC}\exp\Big[\int_{\Lambda_{\rm TC}}^{M_{\rm ETC}}\frac{\gamma(g^2)}{\mu}d\mu\Big], \tag{3.4}$$

we can note that in a weakly coupled theory the anomalous exponent $\gamma \sim 0$, and the condensate $\langle\bar{Q}Q\rangle$ remain approximately constant. This would imply that satisfying the above constraints is not possible in a QCD-like theory, with a large coupling only in a narrow energy range above the chiral symmetry breaking. Thus, we introduce the walking coupling [38, 39, 40, 41]. Walking means, that g^2 remains almost constant $\sim g^2_\star$ over the whole energy range from TC to ETC. Now we can write the condensate enhancement as

$$\langle\bar{Q}Q\rangle_{\rm ETC} \approx \Big(\frac{\Lambda_{\rm ETC}}{\Lambda_{\rm TC}}\Big)^{\gamma(g^2_\star)}\langle\bar{Q}Q\rangle_{\rm TC} \tag{3.5}$$

The β-function of the walking theory

$$\beta = \mu\frac{dg}{d\mu} \tag{3.6}$$

comes very close to zero at some value of the coupling. At $g^2 = g^2_\star$, it means that the theory has an infrared fixed point (IRFP), with conformal and scale invariant long distance behaviour. Both walking theory, and a theory with an IRFP are suitable starting points for a technicolor model, since the latter can be deformed to the walking case with the introduction of a scale [33].

The 2-loop scheme-invariant β-function of SU(N) gauge theory, with N_f fermions of representation R, reads

$$\beta = \mu\frac{dg}{d\mu} = -\beta_0\frac{g^3}{16\pi^2} - \beta_1\frac{g^5}{(16\pi^2)^2} + O(g^7) \tag{3.7}$$

where

$$\beta_0 = \frac{11}{3}N - \frac{4}{3}T(R)N_f, \tag{3.8}$$

$$\beta_1 = \frac{34}{3}N^2 - \frac{20}{3}NT(R)N_f - 4C_2(R)T(R)N_f \tag{3.9}$$

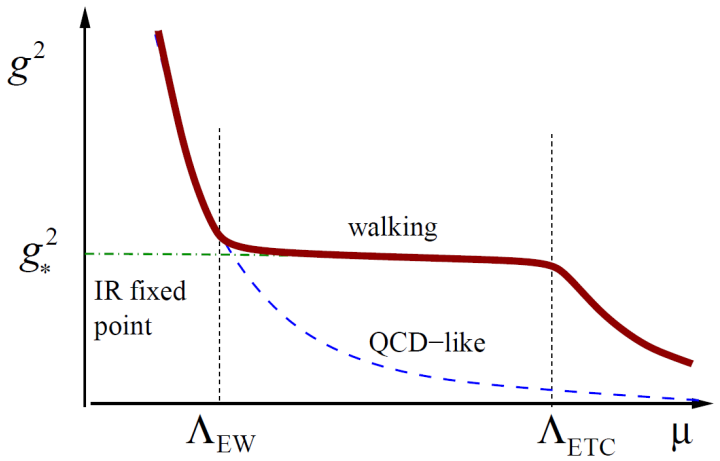

Figure 3.2: The evolution of the walking coupling, versus the QCD-like coupling and the coupling with an infrared fixed point [33].

Here $C_2(R)$ is the second Casimir invariant of the fermion representation R, and $T(R)$ is defined by the relation $T(R)\delta^{ab} = TrT^aT^b$. To ensure asymptotic freedom, β_0 must be positive. If $\beta_1 < 0$, the theory is QCD-like, otherwise, if $\beta_1 < 0$, the theory has an IRFP at some coupling [33].

3.2 The Conformal Window

Asymptotically free (at high energies) theories, that have an IRFP in the renormalization group flow of their couplings, are said to be inside the *conformal window* [42]. The conformal window in SU(N) gauge field theory with N_f fermion flavours in different fermion representations is presented in figure 3.3, taken from [33]. In the figure, the upper edges are where β_0 changes sign, and below the lower lines the system is expected to have chiral symmetry breaking. The lines below the shaded regions is where β_1 changes sign. A potentially walking technicolor theory is required to be close to the lower edge of the conformal window; it is just below the window where walking coupling behaviour is exhibited. Just within the window the theory can be easily deformed into a walking theory by adding a mass or momentum scale to it. At energy scales less than the mass term, the physics is dominated by the gauge fields and the theory is confining [33].

It has been noted that the conformal window can be reached with a smaller number of fermions, if one uses higher than fundamental representations [43, 44, 45]. Of these, the adjoint representation and 2-index symmetric representation have proven to be the most interesting; the two most compelling theories are SU(2) gauge theory with two adjoint fermions, and SU(3) with two 2-index symmetric representation fermions [33].

3.3 Minimal Walking Technicolor; lattice study

The above-mentioned SU(2) gauge field theory with two adjoint fermions is know as “minimal walking technicolor (MWTC). The MWTC model has been

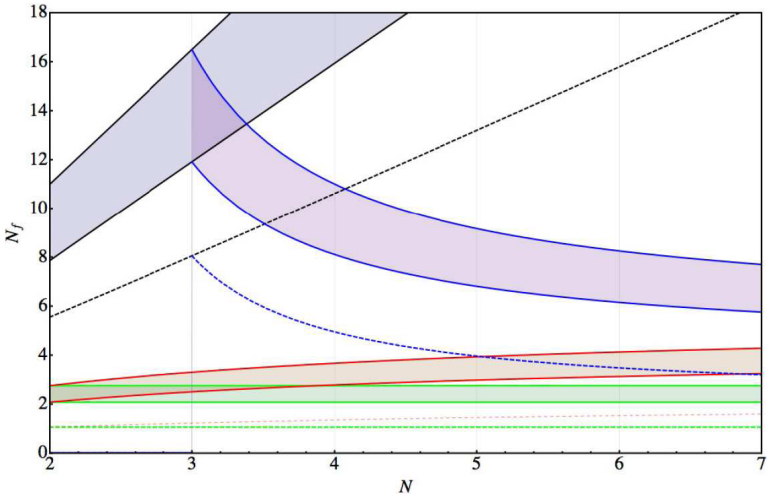

Figure 3.3: The conformal window in SU(N) gauge field theory with N_f fermion flavours in different fermion representations. From top to bottom: the fundamental, two-index antisymmetric, two-index symmetric and the adjoint represenation. The upper edge of the bands correspond to the loss of the asymptotic freedom, and the lower edge of the band has been calculated using the ladder approximation [33, 43, 44, 45]

studied in a number of works, including, in particular, [46, 47, 48, 49, 50].

One of the ways to determine non-perturbatively the β-function of this theory is the Schrödinger functional method [51], in which we have a constant background field with special boundary conditions and we measure the response of the system when this background field is changed. In this method, the eigenvalues of the fermion Dirac matrix are governed by the fixed boundary conditions. As a result, simulations with exactly massless fermions become possible [33].

Following an analysis in [33], let's consider a lattice with volume $V = L^4 = (Na)^4$, where a is the lattice spacing. We fix the spatial gauge links on the $x_0 = 0$ and $x_0 = L$ so that we obtain color diagonal boundary gauge fields

$$A_i(x_0 = 0) = \mu\sigma_3/(g_0 L) \tag{3.10}$$
$$A_i(x_0 = L) = (\pi - \mu)\sigma_3/(g_0 L), \tag{3.11}$$

where σ is the third Pauli matrix and g_0 the bare gauge coupling. These boundary conditions generate a constant Abelian chromoelectric background field at the classical level. Differentiating the action with respect to μ,

$$\frac{\partial S^{\text{class}}}{\partial \mu} = \frac{k(N,\mu)}{g_0^2}, \tag{3.12}$$

where $k(N, h)$ is a known function. Generalizing to the quantum level,

$$\left\langle \frac{\partial S^{\text{class}}}{\partial \mu} \right\rangle = \frac{k(N,\mu)}{g^2} \tag{3.13}$$

After taking the derivative, $\mu = \pi/4$ is fixed. The obtained coupling is defined at length scale L (i.e., lattice size). Thus, at fixed lattice spacing a, the evolution of the coupling can be measured by varying the size of the lattice [33].

When we look at the behavior of the β-function, MWTC differs greatly from QCD, i.e. the coupling constant does not simply increase with the lattice size. In MWTC, with small coupling, $g^2(L)$ increases very slowly with increasing lattice size L/a. The rate of growth slows as the coupling increases, until finally, at $g^2 > 3$, g^2 decreases with increasing L, provided that L is large enough [33]. A decreasing coupling constant indicates a positive β-function.

The value of the lattice spacing is a priori unknown, but we do know it is a function of the bare lattice gauge coupling $b_L \equiv 4/g_0^2$. Thus, we can use the measurements of $g^2(L)$ to match lattices of different sizes. However, artifacts due to finite lattice spacing, such as the small L behaviour, make this more complicated. To obtain reliable results, a proper continuum limit extrapolation is required. One option would be to use step scaling, but since in MWTC the evolution of $g^2(L)$ is very slow, compared to for example QCD, the method becomes questionable due to finite lattice artifacts. To go around this problem, improved actions could be the key.

To check the consistency of results obtained from a large volume data, one can fit to the β-function ansatz [33]

$$\beta = -L\frac{dg}{dL} = -b_1 g^3 - b_2 g^5 - b_3 g^\delta \tag{3.14}$$

where b_1, b_2 are perturbative constants, and b_3 and δ are fit parameters.

Nevertheless, there remains the question of validity of the different lattice results that are obtained with the unimproved Wilson fermion action. Regarding this, studies of SU(3) gauge with 2-index symmetric representation fermions have shown a large dependence on the action used [52]. The unimproved action has large $O(a)$ errors, causing small lattice sizes ($L/a < 10$) to be ineligible. It is thus an object of interest to define a non-perturbatively $O(a)$ improved action for MWTC, and repeat the analysis.

In the first included publication of this thesis, [1], an $O(a)$ improvement is carried out non-perturbatively for SU(2) gauge theory with adjoint and fundamental flavors. Details related to this will be discussed in the next chapter.

Chapter 4

Improving the action

The case of SU(2) gauge fields with two fermions in the two-index symmetric representation, also known as minimal walking technicolor (MWTC), has been studied for its applications in Beyond Standard Model building. The lattice studies of this theory with unimproved Wilson fermion action and are however subject to large $\mathcal{O}(a)$ lattice artifacts that increase errors and hinder the convergence to the continuum limit. With $\mathcal{O}(a)$ improvement, one pursues constructing an action canceling lattice effects of order a in the effective continuum theory. The idea is quite simply to add a suitable counterterm to the Wilson fermion action. We write

$$S_{\text{impr}}(U, \bar{\psi}, \psi) = S(U, \bar{\psi}, \psi) + \delta S(U, \bar{\psi}, \psi) \tag{4.1}$$

where

$$\delta S(U, \bar{\psi}, \psi) = a^5 \sum_x c_{\text{sw}} \bar{\psi}(x) \frac{i}{4} \sigma_{\mu\nu} \hat{F}_{\mu\nu}(x) \psi(x) \tag{4.2}$$

is an improvement that first appeared in a paper by Sheikholeslami and Wohlert in 1985 [53]. c_{sw} is called the Sheikholeslami-Wohlert coefficient, and $F_{\mu\nu}(x)$ is the "clover term". We can write the definition

$$\hat{F}_{\mu\nu}(x)\psi(x) = \frac{1}{8a^2}(Q_{\mu\nu}(x) - Q_{\nu\mu}(x)) \tag{4.3}$$

where $Q_{\mu\nu}(x)$ is the sum of four plaquettes, depicted in figure (4.1). Due to the shape of the graphical representation, the improved action goes also by the name clover action.

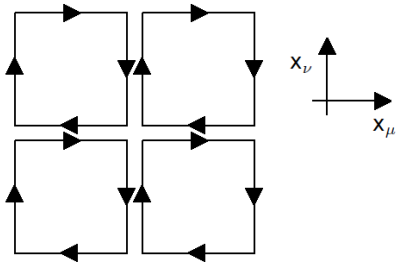

Figure 4.1: Graphical representation of the clover term

4.1 Schrödinger functional method and boundary conditions

In the attempt to obtain a fully $\mathcal{O}(a)$ improved action, we can make use of the Schrödinger functional method [54, 55, 56, 57]. The basic idea is to generate chromoelectric background field, and define the running coupling constant as the response of the system to this field. On the lattice, the values of the quantum fields are prescribed by the boundaries of the Euclidean path integral, at $x_0 = 0$ and $x_0 = L$. The classical path corresponds to a minimal action field configuration which interpolates between the boundary values [58].

Consider the space-time as a cylinder with spatial size L and time-like extent T. For the spatial directions, we take periodic boundaries, and for the temporal direction, fixed Dirichlet boundaries, chosen in such a way that a constant background chromoelectric field is generated. The fixed boundaries bring a $\mathcal{O}(a)$ contribution to the gauge part of the action. To account for it, we consider

$$S_{\mathrm{G,impr}} = \frac{\beta_L}{4} \sum_p w(p) Tr(1 - U(p)) \tag{4.4}$$

where

$$w(p) = \begin{cases} 1 & \text{plaquettes in the bulk} \\ c_s/2 & \text{spatial plaquettes at } x_0 = 0 \text{ and } T \\ c_t & \text{time-like plaquettes attached to a boundary plane} \end{cases}$$

The parameters c_s and c_t, which to leading order in perturbation theory are 1, can be tuned to reduce the $\mathcal{O}(a)$ boundary contributions. Terms proportional to c_s do not contribute for the electric background field considered here [1].

At the boundaries only half of the Dirac components are defined and fixed to some prescribed values $\rho, ..., \bar{\rho}'$ [59], which are the source fields for correlation functions. These are set to zero when generating configurations in simulations. Introducing the projectors $P_\pm = \frac{1}{2}(1 \pm \gamma_0)$, the boundary conditions of the quark and antiquark fields read

$$P_+ \psi(x)|_{x_0=0} = \rho(x) \qquad P_- \psi(x)|_{x_0=T} = \rho'(x) \tag{4.5}$$

$$\bar{\psi}(x) P_-|_{x_0=0} = \bar{\rho}(x) \qquad \bar{\psi}(x) P_+|_{x_0=T} = \bar{\rho}'(x) \tag{4.6}$$

The complementary components are expected to vanish [59]. In the spatial directions we introduce a "twist" for the phase of the fermion fields [55]

$$\psi(x + L\hat{k}) = e^{i\phi_k} \psi(x), \qquad \hat{\psi}(x + L\hat{k}) = \hat{\psi}(x) e^{-i\phi_k}. \tag{4.7}$$

which, together with the Dirichlet boundary conditions, regulates the fermion matrix in such a way, that it becomes possible to do simulations at zero fermion masses [1].

The improved lattice action can now be written

$$S_{\mathrm{impr}} = S_{\mathrm{G,impr}} + S_F + \delta S_{\mathrm{sw}} + \delta S_{F,b}. \tag{4.8}$$

where

$$\delta S_{F,b} = a^4 \sum_x (\tilde{c}_t - 1) \frac{1}{a} \bar{\psi}(x) \psi(x) (\delta(x_0 - a) - \delta(x_0 - (a - L))) \tag{4.9}$$

is a counterterm that captures the boundary effects. We only have to take into account the contribution controlled by $\tilde{c}_t$, since the one proportional by $\tilde{c}_s$ vanishes if we set the fermionic fields to zero on the boundaries [1]. $\tilde{c}_t$ is known to be 1 up to leading order.

In conclusion, obtaining full $\mathcal{O}(a)$ improvement boils down to determining the parameters c_t, $\tilde{c}_t$ and c_{sw}. Of these, c_t and $\tilde{c}_t$ can be determined perturbatively, whereas the Sheikholeslami-Wohlert coefficient c_{sw} demands a non-perturbative determination [1].

4.2 Non-perturbative tuning of c_{SW}

For fundamental representation fermions we fix the gauge field Dirichlet boundary conditions as follows [55, 1]

$$U(x_0 = 0) = \exp(iC), \qquad C = -\frac{\pi}{4}\frac{a\sigma^3}{L} \tag{4.10}$$

$$U(x_0 = T) = \exp(iC'), \qquad C' = -\frac{3\pi}{4}\frac{a\sigma^3}{L}. \tag{4.11}$$

The Fourier components of the boundary quark fields can be interpreted as operators that create quarks and anti-quarks [59]. We denote

$$\zeta(x) = \frac{\delta}{\delta\bar{\rho}(x)}, \qquad \bar{\zeta} = \frac{\delta}{\delta\rho(x)} \tag{4.12}$$

as the boundary quark field and anti-quark field, respectively. The product

$$\mathcal{O} = a^6 \sum_{y,z} \bar{\zeta}(y)\gamma_5 \frac{1}{2}\tau^a \zeta(z) \tag{4.13}$$

creates a quark and an anti-quark with zero momenta at time $x_0 = 0$. Similarly at $x_0 = T$

$$\mathcal{O}' = a^6 \sum_{y,z} \bar{\zeta}'(y)\gamma_5 \frac{1}{2}\tau^a \zeta'(z) \tag{4.14}$$

Using this notation, we write the correlation functions

$$f_A(x_0) = -\frac{1}{3}\langle A_0^a(x)\mathcal{O}\rangle \tag{4.15}$$

$$f_P(x_0) = -\frac{1}{3}\langle P^a(x)\mathcal{O}\rangle \tag{4.16}$$

corresponding to axial current and the related axial density.

In the continuum limit, the partially conserved axial current relation, PCAC relation, is expected to be satisfied

$$\partial_\mu A_\mu^a = 2MP^a. \tag{4.17}$$

Here P^a denotes the associated axial density and M the physical quark mass. The equation can be written as

$$\frac{1}{2}(\partial_\mu + \partial_\mu^*)\langle (A_I)_\mu^a(x)\mathcal{O}\rangle = 2M\langle P^a(x)\mathcal{O}\rangle \tag{4.18}$$

The correlation functions, the position x and chosen boundary conditions all affect the result of the obtained M. Differences in the results are of order a in general and are reduced to $\mathcal{O}(a^2)$ by improvement.

So, defining the quark mass via the PCAC relation

$$M = \frac{1}{2}\frac{\frac{1}{2}(\partial_0^* + \partial_0)f_A(x_0) + c_A a\partial_0^*\partial_0 f_P(x_0)}{f_P(x_0)}. \tag{4.19}$$

More compactly, this can be written as:

$$M(x_0) = r(x_0) + c_A s(x_0) \tag{4.20}$$

where

$$r(x_0) = \frac{1}{4}(\partial_0^* + \partial_0)f_A(x_0)/f_P(x_0) \tag{4.21}$$

$$s(x_0) = \frac{1}{2}a\partial_0^*\partial_0 f_P(x_0)/f_P(x_0). \tag{4.22}$$

The bare mass is tuned by making $M(T/2)$ vanish. We define M' correspondingly and note that the quantity

$$\Delta M(x_0) = M(x_0) - M'(x_0) \tag{4.23}$$

can be used as the condition to fix $c_{\rm sw}$ and c_A, since it vanishes up to corrections of $\mathcal{O}(a^2)$, if both $c_{\rm sw}$ and c_A have their proper values [1].

To ensure correct tree level behaviour we fix M and ΔM to their tree level values, and obtain a small correction to the relations [1]

$$\Delta M(x_0) = M(x_0) - M'(x_0) - \delta = 0, \qquad M(x_0) = \delta M. \tag{4.24}$$

The above method is effective for fermions in the fundamental representation, however, if we want to study fermions in the adjoint representation, changes have to be made to the boundary conditions. Due to a component in the color vector, that does not see the background field, at long distances the adjoint fermion correlation functions behave as if there was no background field [1]. Therefore, we need to use boundary conditions which maximize the difference between the two boundaries. Choosing

$$U(x_0 = T, k) = I \tag{4.25}$$

$$U(x_0 = 0, k) = \exp(aC_k), \qquad C_k = \frac{\pi}{2}\frac{\tau^k}{iL} \tag{4.26}$$

the boundaries create a strong enough chromomagnetic field at the $x_0 = 0$ boundary, so that the PCAC relation can be used to tune $c_{\rm sw}$ [1].

Chapter 5

Large-N

Studying Yang-Mills theories with a large number of colors N, i.e. in the large-N limit, provides important fundamental insights on QCD [60, 61], as first pointed out in the works by 't Hooft [62]. The large-N limit also offers viewpoints on Yang-Mills thermodynamics in general, and is crucial in the exploration of gauge/string correspondances. The technical and conceptual simplifications that come with taking the large-N limit in SU(N) gauge theories, make many quantities easier to study, and in QCD, certain features get a more intuitive explanation in terms of combinatorics. Migdal and Makeenko observed [63, 64] that in SU(N) gauge theories, expectation values factorize at large-N, so that disconnected diagrams, with the most traces, dominate. Works in which various properties of large-N gauge theories were studied include [65, 66, 67, 68, 69, 70, 71, 72, 73, 74, 49, 75, 76, 77, 78]. The second included publication of this thesis, [2], discusses Casimir scaling and renormalization of Polyakov loops in large-N gauge theories

5.1 't Hooft coupling and the double line notation

Generally, the physical coupling in QFT runs with the energy scale, and thus it is not a "natural" small expansion parameter. For instance, in $D = 3+1$ space-time dimensions, Yang-Mills theories have a dimensionless coupling g^2 and are classically invariant under scale transformations; however, quantum fluctuations make this scale invariance anomalous, so setting g^2 to some particular value is useful only close to the scale where the physical running coupling takes that value. In the 70's, from the considerations of QCD 't Hooft came up with the novel approach [62] to use $1/N$ as an expansion parameter - which is less obvious but more general. Namely, one replaces the gauge group SU(3) by SU(N), take the limit $N \to \infty$, and performs an expansion in $1/N$. All this is done taking the coupling $g \to 0$, such that the so called 't Hooft coupling

$$\lambda = g^2 N \tag{5.1}$$

is kept fixed. This way we obtain a generalized theory, with degrees of freedom that are the gluon fields $A^i_{\mu j}$ and the quark fields q^i_a. Here $i, j = 1, \ldots, N$ and $a = 1, \ldots, N_f$, with N_f the number of quark flavours. As we know, the number of independent degrees of freedom in SU(N) Yang-Mills theories is proportional to $N^2 - 1$, however, working in the limit $N \to \infty$, it is justified to consider it

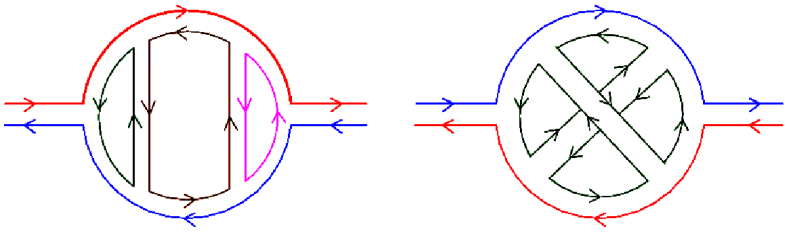

Figure 5.1: Two Feynman diagrams drawn in the double line notation. The one on the left is a planar diagram with three internal gluon loops, and the one on the right is a non-planar diagram, with only one internal loop. The number of vertices, however, is the same.

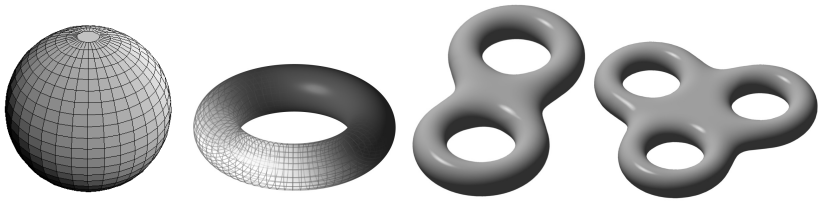

Figure 5.2: As the complexity of diagrams increase, so does the complexity of the surface on which they can be drawn on. The simplest, planar diagram can be drawn on the surface of a sphere, the non-planar diagram on a torus, etc. (pictures:[79]).

as N^2 alone. The number of gauge degrees of freedom is much larger than that of the quarks, $N_f N$, hinting at gluon dominance in the large-N limit.

To portray what happens in the level of Feynman diagrams of physical processes, we introduce the double line notation. This consists of simply replacing the line associated to a gluon in the Feynman diagram with a pair of lines, the fundamental line which is associated with a quark, and its conjugate which is associated with an anti-quark. The simplest type of these diagrams can be drawn on a surface of the sphere, but more complicated diagrams require more complicated topologies. In this notation, each vertex gives a factor g, and each closed loop carrying a fundamental or antifundamental index gives a factor N. Now, if we contemplate the diagrams with different topologies, while keeping $\lambda = g^2 N$ fixed, we see that the non-planar diagrams are suppressed by factors of $1/N^2$. For example, in the picture (5.1) the first diagram has g^6 and N^3, thus giving

$$g^6 N^3 = (g^2 N)^3 = \lambda^3, \tag{5.2}$$

whereas the second one has g^6, and N, giving

$$g^6 N = \frac{1}{N^2} g^6 N^3 = \frac{1}{N^2} \lambda^3. \tag{5.3}$$

In addition, using this notation one can also see that quark loops are suppressed with a factor $1/N$, and are thus negligible, making large-N effectively a quenched theory. Internal quark loops are represented by just one line, since fermions in the fundamental representation are described by fields with only one colour index.

The diagrams with internal quark loops, instead of gluon loops, have therefore fewer free color lines, and hence fewer powers of N. Also, since the flavour

of the quark running in the loop must be summed over, we also get an additional power of N_f, making internal quark loops suppressed by powers of N_f/N with respect to gluon loops. So, like earlier speculated, in the 't Hooft limit the dynamics of gluons indeed dominates and it is therefore legitimate to consider only the gluodynamic sector of the theory on the lattice in this limit, thus avoiding the complications arising from lattice fermions.

5.2 SU(∞), SU(3) and the lattice

Though the theory with SU(∞) gauge group is not simple enough to be solved analytically, some things become very simple in a large-N confining theory. As the number of colors increases, the probability of any quarks or gluons forming a color singlet in a dynamical process decreases, since the singlet itself becomes a large construction of increasing amount of components. Other simplifications that follow from the coupling $g^2 \propto 1/N$ going to zero, include mesons becoming stable, supression of mixing, perfect OZI rule, and the absence of color singlet scattering [80].

The important question is of course, if the difference between SU(3) and $SU(\infty)$ is 'small' for typical physical quantities. This question has been addressed, for example, in the review [81] an references therein; one can calculate the masses of the lightest glueballs, express them in units of the simultaneously calculated string tension and extrapolate the ratios to the continuum limit to obtain values of m/σ. Repeating this for various N, and plotting the resulting ratios against $1/N^2$ (since the leading large-N correction should be $O(1/N^2)$), it can be observed that the $O(1/N^2)$ corrections are indeed small, thus SU(3) appears to be close to SU(∞). Also, in the large-N limit, mathematical arguments show that certain irreducible representations should become equivalent. Observed in [82], this seems to be approximately the case also for SU(3), which is thus "close" to SU(∞) in this respect.

It is important to study if the properties of the gauge theory at finite temperature depend strongly on Nor not.A question we should ask, is whether the SU($N \to \infty$) gauge theory is confining at low temperatures. To address this question, we can refer to an example from [80, 83], where SU(6) was considered in $3+1$ dimensions. Suppose we calculate the mass of the lightest state, in which one unit of fundamental flux closes upon itself by winding once around a spatial torus of length l. If we have linear confinement, the flux will organise itself into a flux tube and the mass will grow linearly with l for large l, $m(l) = \sigma l$ [80]. Indeed, this is observed to happen, and furthermore, the largest values of l are large compared to the flux tube width, reassuring us that what is seen is the onset of an asymptotic linear behaviour.

5.3 QCD_∞ and QCD_3

Even though in the pure gauge theory we see SU(3) $\sim$ SU(∞), considering glueballs alone does not fully establish a phenomenological relevance of the large-N limit. We need to study, whether the mesonic spectrum of QCD_3 is close to QCD_∞. Fields in the fundamental representation, like quarks, introduce $O(1/N)$ corrections in the lattice calculations, whereas in the pure gauge theory the leading correction is $O(1/N^2)$. This implies, that it is not guaranteed that the mesonic spectrum will be as well-behaved as the gluonic one [80].

At the moment, questions of how close SU(∞) is to SU(3), and in which respects, can only be addressed numerically, and the results are somewhat varied. One way to proceed would be to perform the meson spectrum calculation [84, 74] with the quenched approximation at various finite N, and extrapolate the results to $N = \infty$. Without quark loops, the leading correction should now be $O(1/N^2)$, and the extrapolated values are the correct values for (the dynamically quenched) QCD_∞ theory [80]. The obtained spectrum can be compared with experimental data or full lattice QCD calculations. Of course, quenched QCD at finite N is not unitary, however problems due to this appear mainly at small quark masses and can be avoided in the extrapolations in most part. Also, current calculations are probably not precise enough to be sensitive to such pathologies [80].

5.4 Large-N physics at high temperature

High temperature translates to a small coupling, so that hadronic states cannot be formed. To study this region, perturbation theory has been, and still is the method of choice, see for example [85] and references therein. However, close to the critical temperature T_c, the coupling is usually not so small anymore and therefore perturbation theory does not continue to produce such accurate results. In this temperature region, lattice computations can be used.

As lattice studies have indicated, and experiments like RHIC and ALICE confirmed, above the deconfining temperature T_c there is a large range of T where the plasma is strongly interacting. The phase transition happens at a value of T where the free energies of the confined and deconfined phases are equal, $F_c = F_d$. The number of gluons being $O(N^2)$, we can expect $F_d \propto N^2$, but one could naively also expect $F_c \propto N^0$, since there are only colour singlet states in the confined phase. From this it follows, that as $N \to \infty$, $T_c \to 0$. Numerical results however show that this is not the case [80]. Indeed, the vacuum energy density brings an $O(N^2)$ contribution to F_c in the confined phase, thus the large-N limit T_c is precisely determined by the balance between this and the $O(N^2)$ part of F_d.

One can also ask how the gluon plasma behaves at large-N; will it continue to be strongly coupled close to T_c? This can be assessed with calculations of the pressure and its deviation from the Stefan-Boltzmann value. The pressure can be obtained by integrating the average plaquette over β, with the value of the pressure at $T = 0$ subtracted to remove ultraviolet divergences

$$a^4[p(T) - p(0)] = 6 \int_{\beta_0}^{\beta} d\beta' (\langle u_p \rangle_T - \langle u_p \rangle_0). \tag{5.4}$$

Denoting $p(T) - p(0) \to p(T)$, $T = (aL_t)^{-1}$ we rewrite

$$\frac{p(T)}{T^4} = 6L_t^4 \int_{\beta_0}^{\beta} d\beta' (\langle u_p \rangle_T - \langle u_p \rangle_0). \tag{5.5}$$

For SU(3) the ratio of the pressure and the Stefan-Boltzmann value is far below unity, even to quite high T, indicating strong coupling nature for the gluon plasma.

Similar calculations have been made at larger N to test if the ratio continues to reside far from unity. In [86] it was seen that there is essentially no change in the normalised value of p/T^4 when going from $N = 3$ to $N = 8$. This was

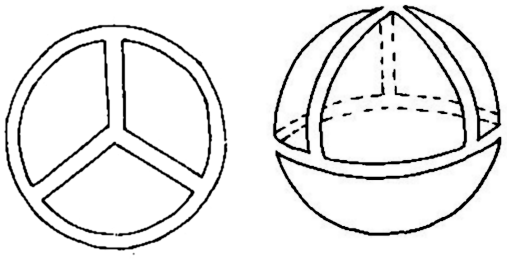

Figure 5.3: A Rieman surface associated to a planar diagram

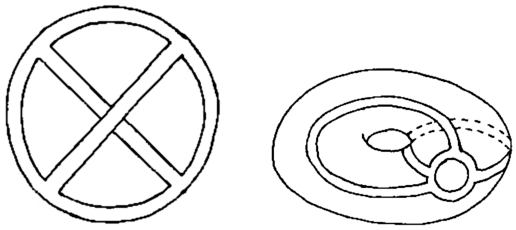

Figure 5.4: A Rieman surface associated to a non-planar diagram

shown to hold in the range $1 \leq T/T_c \leq 2$, but studies extending over a larger range of T/T_c [87] have also indicated the same. Therefore, one can say that the $N = \infty$ plasma is as strongly coupled as $N = 3$ one [80].

The finite-T physics is also an interesting subject for gauge-gravity duality calculations. These are typically applicable to $\mathcal{N} = 4$ supersymmetric (SUSY) theories, and only valid at large N and g^2, thus they don't really correspond to QCD or SU(3) gauge theory in the low-T confining phase. However, at finite-T $\mathcal{N} = 4$ SUSY is broken as the adjoint fermions acquire $O(T)$ Matsubara masses from the anti-periodic fermionic boundary conditions in the Euclidean time direction. Because SUSY is broken, the adjoint scalars also become massive, leaving only the gauge field as light fields. This way, we arrive at something that looks like a gauge theory at $T > T_c$. Moreover, since $N = \infty$ plasma and $N = 3$ seem to be strongly coupled at temperatures close to T_c, this raises the interest of applying gauge-gravity duality in this area.

5.5 Connections to String theory

Beyond QCD, the large-N limit has also broader implications, entailing deep connections with string theory. As previously presented, the Feynman diagrams can be drawn using the double line notation, leading to a topological classification of the diagrams. Now, we can associate a Riemann surface to each Feynman diagram in the following way. First of all, each line in a diagram is a closed loop, that is thought of as the boundary of a two dimensional surface. The loops are then glued together along their boundaries, as depicted in (5.3) and (5.3), and with the addition of 'the point at infinity to the loop associated to the external line in the diagram, we obtain a compact Riemann surface. Further analysis shows, that the power of N associated to a given Feynman diagram is exactly N^χ, where χ is the Euler number of the corresponding Riemann surface [88].

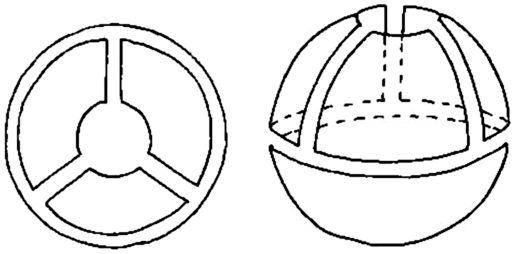

Figure 5.5: A Rieman surface associated to a planar diagram with an internal quark loop

This leads to the realization, that the expansion of any gauge theory amplitude in Feynman diagrams can be written as

$$A = \sum_{g=0}^{\infty} N^{\chi} \sum_{n=0}^{\infty} c_{g,n} \lambda^n, \tag{5.6}$$

where g is the genus of the compact orientable surface on which the diagram in double line notation can be drawn, $\chi = 2 - 2g$, and $c_{g,n}$ are constants. Furthermore, the first sum, a topological series, is recognized as the loop expansion in Riemann surfaces for a closed string theory with coupling constant $g_s \sim 1/N$, and the second sum, a perturbative series in the t'Hooft coupling, proves out to be the so called α' expansion in the string theory [88]. In turn, quark loops in a given Feynman diagram, as illustrated in (5.5), corresponds in terms of the Riemann surfaces to introducing a boundary. The power of N associated with the Feynman diagram remains N^{χ}, but the Euler number is $\chi = 2 - 2g - b$, where b is the number of boundaries. In the large-N expansion we therefore have to also sum over the boundaries, which implies that the expansion is for a theory with both closed and open strings. The coupling constant of the open strings is $g_{open} \sim N_f g_s^{1/2} = N_f/N$ [88].

Because of the conjunctions above, it was hoped that string theory would be a "reformulation" of all the topological classes of diagrams in the large-N limit.

5.6 Flux tubes as strings

It has been long speculated, that the SU(N) gauge theory could be closely related to some kind of string theory [89, 90, 91]. Indeed, one type of connection derives from the following observation: When separating two static quarks far apart from each other, a connecting gauge field, that appears to be squeezed into a flux tube, is generated. This "flux tube" exhibits string-like behavior with fixed ends, and thus the interaction between the static quark-antiquark pair can be described by an effective string theory. It has been suggested that the expectation values of large Wilson loops have a correspondance with amplitudes of an effective bosonic string theory [92, 89]. The string-like features of the flux tube have been studied with calculations using various gauge groups: $\mathbb{Z}_2$ [93, 94, 95, 96], $\mathbb{Z}_4$ [97], U(1) [98, 99, 100], SU(2) [101, 102, 96, 103], SU(3) [92, 104, 105], as well as with SU($N > 3$) [106, 107, 108, 109], and even in a random percolation model [110, 111]. The third included publication of this thesis, [3], concentrates on studying the string effects with SU(3) and SU(4).

5.6.1 Static quark potential and the Lüscher term

In the confining regime of SU(N) gauge theories, the asymptotic behavior of $V(r)$ at large distances is a linear rise, and the flux lines between the well separated color sources are expected to be squeezed in a thin, string-like tube [112, 113, 114]. This "confining string" can be considered as a basic object, in particular when it is stable, i.e. when there is no matter in representations of non-zero N-ality. By studying the low-energy effective action on the string we want to understand the low-energy fluctuations and the light excitations of long strings. In large-N gauge theories the confining string can be thought of as a weakly coupled fundamental string subject to some effective action which, if known, can be used to study the low-energy dynamics of the model. Unfortunately, in general the effective string action is not known. However, lattice simulations may offer a way to study the low energy effective action of a confining string and give insights on its properties. Furthermore, the general properties of the effective string can be derived based on the symmetries it should have [115, 116, 117, 118, 119].

In a confining theory, the static quark potential has the large distance asymptotic expansion [92]

$$V(r) = \sigma r + \mu + \gamma/r + O(1/r^2), \tag{5.7}$$

where σ is the string tension, μ a constant (a regularization-dependent mass), and γ is the Lüscher term, a Casimir effect, which is due to the finiteness of the interquark distance r

$$\gamma = -\frac{\pi}{24}(D-2). \tag{5.8}$$

Here D as the dimension of the space-time [112, 113]. The presence of the Lüscher term in the long distance inter-quark potential is one of the consequences of the effective string description at zero temperature; it can be seen as an indication of the effective string behavior of the flux tube. The term includes a coefficient that depends only on the dimension of the space-time and is not influenced by higher order corrections of the effective string action.

5.6.2 Nambu-Goto string

The simplest effective action for a bosonic string is simply the string tension σ times the area of the string worldsheet, i.e. the Nambu-Goto action [120, 121, 122]

$$S_{\text{eff}} = \sigma \int d^2\xi \sqrt{\det g_{\alpha\beta}}. \tag{5.9}$$

In the so called "physical gauge" the integrand reads

$$\sqrt{1 + (\partial_0 h)^2 + (\partial_1 h)^2 + (\partial_0 h \times \partial_1 h)^2} \tag{5.10}$$

where h is the displacement of the world sheet surface in the transverse directions. Expanding this in a perturbative series in $1/(\sigma r^2)$, at leading order we get the following expression for the Polyakov loop correlation function (see, e.g. [98] for a discussion)

$$\langle P^\star(r) P(0)\rangle = \frac{e^{-\sigma r L - \mu L}}{\left(\eta\left(i\frac{L}{2r}\right)\right)^{D-2}}, \tag{5.11}$$

where we have used Dedekind's η function

$$\eta(\tau) = q^{\frac{1}{24}} \prod_{n=1}^{\infty}(1-q^n), \qquad q = e^{2\pi i \tau}. \tag{5.12}$$

When $\frac{L}{2r} \gg 1$, eq. (5.11) gives the Lüscher term in the quark-antiquark potential.

The spectrum of the Nambu-Goto string can be obtained by canonical quantization [123, 124]: the energy levels for a string with fixed ends are

$$\begin{aligned} E_n(r) &= \sigma r \sqrt{1 + \frac{2\pi}{\sigma r^2}\Big(n - \frac{D-2}{24}\Big)}, \qquad n \in \mathbb{N}, & (5.13)\\ &= \sigma r - \frac{(D-2-24n)\pi}{24r} + O(1/r^3). & (5.14) \end{aligned}$$

As a consequence, the partition function describing the string with fixed ends reads

$$Z = \sum_{n=0}^{\infty} \omega_n e^{-E_n(r)L} \tag{5.15}$$

where ω_n are the number of states.

Finally, the effective string model also gives a prediction for the form of the inter-quark potential in finite temperature gauge theories [103, 101, 125].

5.6.3 QCD string

In a pure gauge theory the ground state inter-quark potential $V(r)$ of a heavy $Q\bar{Q}$ pair can be expressed in terms of the two-point correlation function $G(r)$ of Polyakov lines

$$V(r) = -\frac{1}{L}\log G(r) = -\frac{1}{L}\log\langle P^\star(r)P(0)\rangle, \tag{5.16}$$

where r is the interquark distance and L the system size in the time-like direction [98]. Assuming that the low energy dynamics of the pure gauge model is described by the effective string, and neglecting excited state decays, we can write the Polyakov loop two-point correlation function as a string partition function

$$\langle P^\star(r)P(0)\rangle = \int \mathcal{D}h e^{-S_{\text{eff}}}, \tag{5.17}$$

where S_{eff} is the effective action for the world sheet spanned by the string.

The dynamics of the confining string is not known, but it should respect the expected rotational symmetries. This implies that only the terms that are rotationally symmetric can be part of the effective string action. In fact these constraints are more general and they restrict the form of the effective action (at least at the lowest orders in $1/\sigma r^2$) to be the Nambu-Goto one. Lattice simulations for pure Yang-Mills theories in $D = 3$ and $D = 4$ show the effective action being very well approximated by this form. However, deviations from Nambu-Goto can be derived at higher orders [126].

There are two main approaches that have been studied in the past to constrain the effective action of a confining string. In the Polchinski-Strominger approach [127, 128, 129] the degrees of freedom in the effective action are the D embedding coordinates of the string in a conformal gauge worldsheet. Requiring

the effective action to have the correct critical central charge, one is left with constraints that have been shown to imply the four-derivative effective action to agree with the Nambu-Goto form. This approach seems to be difficult to extend to higher orders, however.

Another approach [112, 113, 130] is to write the effective action in static gauge, such that the degrees of freedom are only the $(D-2)$ transverse fluctuations of the string worldsheet. The string action is constrained by the fact that the Lorentz symmetry is non-linearly realized on the Nambu-Goldstone bosons. This is to say, that the action should non-linearly realize the Lorentz symmetry rotating the direction in which the string propagates, and the transverse directions. Following the suggestion of Lüscher and Weisz in [130], the effective action is constrained by computing the partition function of long winding strings, and expressing it as a sum over string states. From [130], an active line of research followed, in particular the method was further generalized in [131] to any D and to the closed strings. In [117] it was apprehended, that the the Lorentz symmetry of the underlying Yang-Mills theory had a crucial role in the Lüscher-Weisz argument, and in fact, the whole Nambu-Goto action was necessary to respect the Lorentz symmetry.

Even though the interquark potential $V(r)$ and related quantities have been studied extensively on the lattice since the eighties (see, for example, [105, 132, 133] for references), the question whether the picture given by effective string models is satisfactory, is still under debate. Previous results [105, 132] have shown prominent support for the bosonic string prediction, in particular, the Lüscher term has been shown to be a universal feature of the IR regime of confined gauge theories. However, results from recent, high precision Monte Carlo simulations [100, 134, 92, 95, 135, 102, 136, 101, 137, 138] suggest that higher order corrections to $V(r)$ might not be universal, and do not trivially fit the Nambu-Goto string predictions. In fact, there are also theoretical arguments suggesting that the effective string action is different from the Nambu-Goto one at higher orders.

Another aspect of interest is the excitation spectrum description. According to the bosonic string picture, the excitations are expected to be described by a tower of harmonic oscillator modes with energies

$$E = E_0 + \frac{\pi}{r} n, \qquad n \in \mathbb{N}. \tag{5.18}$$

In the ground state potential the Lüscher term is supported by numerical evidence down to very short distances, but for the excited states the lattice results seem to be much more difficult to fit into this simple harmonic oscillator pattern [98]. The mismatch between effective string predictions [139] and numerical results have been shown in [140, 104, 141, 96].

5.7 AdS/CFT

The conjectured equivalence between gauge and string models, from yet another perspective, manifests in the AdS/CFT correspondance. It has been noted [142] that maximally supersymmetric Yang-Mills theory with $\mathcal{N} = 4$ supercharges in four dimensions is equivalent to supersymmetric type IIB string theory in a 10-dimensional space, $\mathrm{AdS}_5 \times \mathrm{S}^5$, where AdS stands for anti-de Sitter space and S^5 is a five-dimensional sphere. The dual string model reduces to its weakly-coupled gravity limit when the rank of the group of the gauge theory and the 't Hooft coupling are large. Thus large-N plays an important role in this correspondence,

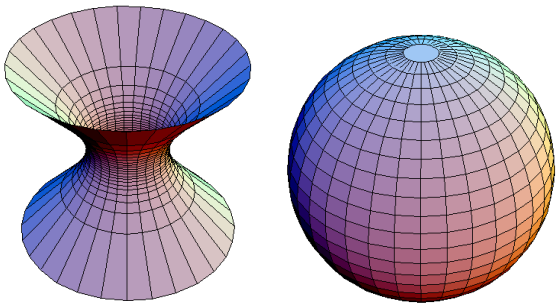

Figure 5.6: The AdS_5 space with a five dimensional sphere makes up $AdS_5 \times S^5$ space. (picture: [79])

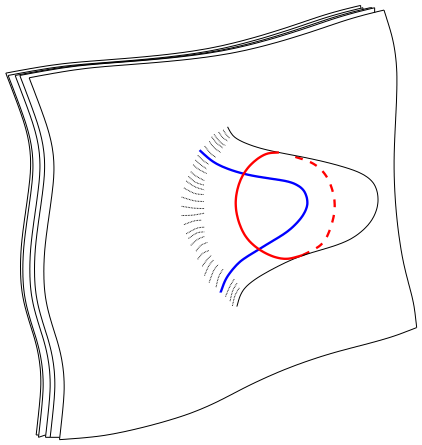

Figure 5.7: A stack of D3 branes, with closed string (red) and an open string (blue)

which can provide powerful analytical tools to study strongly coupled theories, possibly including QCD with three colors, if the dependence on N is not strong (In fact, there is already convincing evidence from lattice calculations of many different observables that this is indeed the case [81]; [74, 84]).

The concept of gauge-string duality goes with understanding D3-branes. D-branes in general are are a class of extended objects in ten-dimensional spacetime where open strings can end, and a D3-brane is a D-brane that extends in three spatial dimensions and in the time direction. If we look at a single D3-brane, the low energy excitations are described by a $\mathcal{N} = 4$ supersymmetric U(1) gauge theory, whereas, if we stack N D3-branes on top of each other, the excitations are described by a $\mathcal{N} = 4$ supersymmetric U(N) Yang-Mills gauge theory [143]. The latter splits into a free $U(1)$ part, relating to the center of mass motions of the stack of D3-branes, and to an interacting SU(N) part, relating to the relative motions of the branes [144]. A string running from one brane to another in the stack represents a gluon of these gauge theories. For example (from [144]), considering the case with three colors, $N = 3$, we can label the branes as R, G, and B. Now, a string running from R to B has the color quantum numbers $\bar{R}B$, as expected for a gluon of SU(3) gauge theory.

D3 branes are sources for a tensor field with four indices, C_4. The exterior

derivative of C_4 is a field strength with five indices, F_5, for which

$$\int_{S^5} F_5 = N, \tag{5.19}$$

where N is the number of branes. This field strength is self-dual in 10 dimensions. The D3-branes are able to deform the spacetime into a solution of the ten-dimensional Einstein equations coupled to the 5-form, because they have a definite mass per unit volume and a charge under a 5-form field strength. It turns out that this solution takes the form $AdS_5 \times S^5$ close to the D3-branes, and that the low-energy excitations of this system can be described in terms of $\mathcal{N} = 4$ supersymmetric Yang-Mills theory. This exposes a connection between gauge theories with SU(N) and string theory. The so called AdS/CFT correspondence was first formulated by Maldacena [142], and formally, it states that the maximally supersymmetric $\mathcal{N} = 4$ Yang-Mills theory in four dimensions is dual to type IIB string theory in an $\mathrm{AdS}_5 \times \mathrm{S}^5$ space.

When it comes to performing calculations affiliated to gauge-string duality, the large-N limit has proven a crucial aid. As the number of colors in the gauge theory is increased, the corresponding parameters in the string theory are driven towards the limit of the theory of classical gravitation in AdS space. In other words, the large-N limit allows one to study non-perturbatively the strongly-coupled regime of a field theory, by mapping it to the weak-coupling limit of a gravity model.

Let us take a closer look at D3-branes that are at zero temperature, where they can be described by a vacuum state of $\mathcal{N} = 4$ super-Yang-Mills theory. The metric of these objects is [144]

$$ds_{10}^2 = H^{-1/2}(dt^2 + d\bar{x}^2) + H^{1/2}(dr^2 + r^2 d\Omega_5^2), \tag{5.20}$$

with

$$H = 1 + \frac{L^4}{r^4}. \tag{5.21}$$

L is related to the number of the 'stacked' D3-branes as

$$L^4 = \frac{\kappa}{2\pi^{2/5}} N = g_{\mathrm{YM}}^2 N \alpha'^2, \tag{5.22}$$

introducing

$$\kappa = \sqrt{8\pi G_{10}} \tag{5.23}$$

$$g_{YM} = \sqrt{4\pi g_{\mathrm{string}}}, \tag{5.24}$$

i.e. the gravitational coupling in ten-dimensional supergravity, and the gauge coupling of $\mathcal{N} = 4$ super-Yang-Mills, respectively. N is the number of D3-branes, and α' is the Regge slope parameter of fundamental strings, inversely proportional to their tension.

Now, we shall focus on the region $r \ll L$, i.e. we are close to the D3-branes. Zooming in to the D3-brane means dropping the 1 from equation (5.21). By doing this, we lose track of the asymptotically flat region, and the resulting geometry is a direct product of AdS_5 and S^5 [144]

$$ds_{10}^2 = \frac{r^2}{L^2}(-dt^2 + d\bar{x}^2) + \frac{L^2}{r^2} dr^2 + L^2 d\Omega_5^2 \tag{5.25}$$

This way, the branes are replaced by a curved geometry. Concluding, the gauge theory dynamics built from strings on the branes is indeed equivalently captured by the geometry.

It is common to denote the radial variables

$$z = \frac{L^2}{r}, \qquad u = \frac{r}{L^2}, \tag{5.26}$$

where z has dimensions of length, while u has dimensions of energy. Using z we write

$$ds_5^2 = \frac{L^2}{z^2}(-dt^2 + d\bar{x}^2 + dz^2), \tag{5.27}$$

i.e., the AdS_5 space is conformal to flat space. Loosely speaking the gauge theory is said to be defined at the boundary $z = 0$. The string theory, in turn, lives in the bulk of AdS_5. The region of AdS_5 where u is large corresponds to ultraviolet (UV) physics, whereas the region where u is small corresponds to infrared (IR) physics. Moreover, u can be regarded as a typical energy scale concerning processes that take place in AdS_5 at a depth u [144].

Chapter 6

Simulation methods

6.1 Updating gauge fields

The standard approach in simulating gauge field theories is to apply Monte Carlo (MC) simulation methods. A MC program begins with some initial configuration of the fields, and proceeds in sequences of (pseudo)random changes on these variables. The changes should be such, that the ultimate probability density of a configuration is proportional to the Boltzmann factor. The goal is to provide a set of configurations, that are typical of the thermal equilibrium in the statistical analogue [21, 145, 146].

The initial configuration of a lattice simulation can be either cold or hot. In a cold start the link variables are set to unit matrices, whereas in the hot start we kick off the simulation with random group elements. The link matrices are then updated to create new configurations in a Markovian chain [147]. Due to autocorrelations in a Markov chain, a configuration is strongly correlated with the previous one generated. Thus, if we begin with a configuration far from the equilibrium Boltzmann distribution, the consequent configurations will also be such. It is only after several iterations that the configurations produced by the algorithm reach the equilibrium, i.e. thermalize, and can be accepted as the calculation data.

There are some criteria a good update algorithm should fulfill. First, it should preserve the equilibrium Boltzmann distribution, which is the so called detailed balance condition [147, 146]. Furthermore, it should be ergodic, meaning that if we start from any configuration, repeating the algorithm would bring us arbitrarily close to any other configuration [146].

It is common to use algorithms, that make a small local change in the field configuration at each step. This way it is not needed to calculate the action of the whole lattice at each step. Instead we use a local action on the lattice

$$S_\mu^{\mathrm{loc}}(U_\mu(x), P_\mu(x)) = \beta\Big[1 - \frac{1}{N_C}\mathrm{ReTr}P_\mu^\dagger U_\mu(x)\Big]. \tag{6.1}$$

In the case of the Wilson action, the sum of staples $P_\mu^\dagger$ can be written

$$P_\mu^\dagger = \sum_{\nu\neq\mu}^{d}[U_\nu(x+a\hat{e}_\mu)U_\mu^\dagger(x+a\hat{e}_\nu)U_\nu^\dagger(x)$$
$$+U_\nu(x-a\hat{e}_\nu)U_\mu^\dagger(x+a\hat{e}_\mu)U_\nu^\dagger(x+a\hat{e}_\mu-a\hat{e}_\nu)], \tag{6.2}$$

where a is the lattice spacing. The original action can be written using the local action

$$S = \frac{1}{4}\sum_{x,\mu} S_\mu^{\rm loc}(U_\mu(x), P_\mu(x)). \tag{6.3}$$

The factor 1/4 is due to every link contributing to four plaquettes.

Heat bath is a commonly used algorithm for updating the link variables. Usually applied to SU(2) gauge theory, this algorithm is a very effective way of thermalizing the lattice, using only local updates. For SU(2) the heat bath method is quite simple, but for other groups with higher N, different methods have to be pursued, such as the Cabibbo-Marinari method [148], which can be used for any N. This method works by decomposing the members of the SU(N) group into subgroups of SU(2), which can be then treated with the SU(2) heat bath algorithm. The overrelaxation algorithm [149] provides faster decorrelation compared to many other methods. The basic idea of overrelaxation is to use a transformation, under which the action is invariant, and apply it to a link matrix. Combined with heat bath, overrelaxation satisfies the ergodicity and detailed balance conditions, and again for SU(2) it is simple. Like with heat bath, larger groups should be divided into SU(2) subgroups.

6.2 Hybrid Monte Carlo

To simulate the computationally complex, full QCD with dynamical Wilson fermions, Hybrid Monte Carlo (HMC) [150] algorithms are used. In the standard HMC, one introduces pseudo-fermion fields that take into account the contribution of the fermion determinant. The evolution of the gluon fields through phase space is carried out for all degrees of freedom simultaneously, using for example the leap-frog algorithm. The HMC algorithm is a general global Monte Carlo procedure, and it is ergodic, fully parallelizable, and shows surprisingly short autocorrelation times [151]. Nevertheless, simulations of full QCD are computationally very demanding, especially when approaching the chiral limit of small quark mass. HMC is discussed in detail in reference [151], and in the subsections 6.2.1 and 6.2.2 we will follow the notation of this reference.

6.2.1 Quenched case

Let us start by looking at the quenched case, where $\det M$ is considered as constant. HMC consists two steps; First the gauge field is evolved through phase space, and an artificial guidance Hamiltonian $\mathcal{H}$ is introduced. Second, the equations of motion are chosen, in such a way that $\mathcal{H}$ is conserved.

We write

$$\mathcal{H} = S_g(U) + \frac{1}{2}\sum_{x,\mu,\rm color} {\rm Tr} H_\mu^2(x), \tag{6.4}$$

$$Z = \int (dH)(dU) e^{-\mathcal{H}}, \tag{6.5}$$

and we wish to find a suitable H. Since $U \in$ SU(3) under the evolution, and Taylor expanding $U(\tau+\delta\tau)$ leads to $U(\tau)\dot{U}^\dagger(\tau) + \dot{U}(\tau)U^\dagger(\tau) = 0$, we find the first equation of motion

$$\dot{U} = iHU. \tag{6.6}$$

H is represented by the generators of SU(3), thus it is hermitian and traceless. $H_\mu(x) = \sum_{a=1}^{8} \lambda^a h_\mu^a(x)$, where each h_μ^a is a Gaussian distributed random number. The second equation of motion comes from requiring $\dot{\mathcal{H}} = 0$ and $\dot{H}$ to stay explicitly traceless under the evolution. This boils down to

$$i\dot{H}(x) = -\frac{\beta}{6}(U_\mu(x)P_\mu(x) - h.c.), \tag{6.7}$$

[151], where $P_\mu(x)$ are the staples, corresponding to a gluonic force term. Numerical integration can not ensure for the Hamiltonian $\mathcal{H}$ to be exactly conserved, therefore we add an accept/reject step

$$P_{\text{acc}} = \min(1, e^{-\Delta\mathcal{H}}) \tag{6.8}$$

to obtain a canonical distribution for U. Furthermore, the integration scheme must lead to a time reversible trajectory and preserve the phase-space volume to ensure detailed balance. Symplectic integration is thus employed [151].

6.2.2 Including dynamical fermions

Consider the fermionic determinant in

$$Z = \int \sum_{x,\mu} dU_\mu(x) \det(M(U)) e^{-\beta S_g}. \tag{6.9}$$

In HMC, dynamical fermions are included in form of a stochastic Gaussian representation for the determinant [151]. We need the interaction matrix to be hermitean, so that the Gauss integral converges. The Wilson fermion matrix, being a complex matrix, can not be represented directly, so we consider the two light quarks u and d as mass degenerate. With the identity $\det^2 M = \det M^\dagger M$, the representation can be written

$$\det(M^\dagger M) = \int \Big(\sum_x (d\bar{\phi}_x)(d\phi_x) \Big) e^{-\phi_x^* (M^\dagger M)^{-1}_{x,y} \phi_y}, \tag{6.10}$$

with the bosonic field ϕ, which can be related to a vector R of Gaussian random numbers. With $\phi = M^\dagger R$, we get the starting distribution $R^\dagger R$, equivalent to $\phi^*(M^\dagger M)^{-1}\phi = \phi^* X$ [151]. As discussed in [151], we add the fermionic action to $\mathcal{H}$, and the time derivate reads

$$\frac{dS_f}{d\tau} = \kappa \sum_{x,\mu} \text{Tr}[\dot{U}_\mu(x) F_\mu(x) + h.c], \tag{6.11}$$

$$F_\mu(x) = [MX]_{x+e_\mu} X_x^\dagger (1+\gamma_\mu) + X_{x+e_\mu} [MX]_x^\dagger (1-\gamma_\mu). \tag{6.12}$$

Due to the fermionic force F the second equation of motion becomes

$$i\dot{H}(x) = -\frac{\beta}{6}(U_\mu(x)V_\mu(x) + \kappa \text{Tr} F_\mu(x) - h.c.). \tag{6.13}$$

To perform the finite time-step integration of the equation of motion, we can use the leap-frog scheme. This method provides an integration process that is reversible, conserves the phase-space volume, and shows only small deviation from the surface $\mathcal{H} = \text{const}$ [151]. Leap-frog consists of a sequence of triades:

$$H_\mu(x, \tau + \frac{\Delta\tau}{2}) = H_\mu(x,\tau) + \frac{\Delta\tau}{2}\dot{H}_\mu(x,\tau) \tag{6.14}$$

$$U_\mu(x, \tau + \Delta\tau) = e^{i\Delta\tau H_\mu(x, \tau + \frac{\Delta\tau}{2})} U_\mu(x,\tau) \tag{6.15}$$

$$H_\mu(x, \tau + \Delta\tau) = H_\mu(x, \tau + \frac{\Delta\tau}{2}) + \frac{\Delta\tau}{2}\dot{H}_\mu(x, \tau + \Delta\tau). \tag{6.16}$$

It can be shown that for each triade $\mathcal{H}$ is approximated correctly up to $O(\Delta t^2)$ [151].

6.3 Multilevel algorithm

The multilevel algorithm was introduced by Lüscher and Weisz in [152], and it has been shown to be usefull in many contexts where one has to cope with an exponentially decaying signal-to-noise ratio. In lattice calculations of the Polyakov loop correlation function, the algorithm has been shown to provide an exponential reduction of the statistical errors. In this algorithm the lattice is split into sublattices that do not communicate with one another, and the final observables are built combining the independent measurements of each sublattice. Of course, from time to time the boundaries between the sublattices are updated, so that the final results are the same as in the usual theory.

Following the discussion in [101], suppose we measure an observable $\mathcal{O}$ by combining the results of averages $\mathcal{O}_{sub}$ computed in $\mathcal{N}$ different sublattices. With N sublattice measurements, the combination of the sublattice averages $\mathcal{O}_{sub}$ corresponds to $(N)^{\mathcal{N}}$ measurements of $\mathcal{O}$, i.e. we get an estimate of $\mathcal{O}$ as if $(N)^{\mathcal{N}}$ measurements would have been performed. However, due to the links that have been kept frozen at the boundaries of the sublattices, this estimate is biased by a background field, but this bias is removed by averaging over the boundary configurations.

Using the notation of [101], consider the correlation function of two Polyakov loops

$$\begin{aligned}\langle P(\vec{0})P(\vec{x})^*\rangle &= \frac{1}{Z}\int\prod_{y,\mu}dU_{y,\mu}\mathrm{Tr}\Big[U_{(\vec{0},0),t}\dots U_{(\vec{0},L-1),t}\Big] \\ &\times \mathrm{Tr}\Big[U^*_{(\vec{x},0),t}\dots U^*_{(\vec{x},L-1),t}\Big]e^{-S[U]}. \qquad (6.17)\end{aligned}$$

Next, we slice the lattice along the temporal direction into $\mathcal{N} = N_t/n_t$ sublattices, i.e. n_t is the temporal thickness of each sublattice in units of the lattice spacing a. Now, to obtain sublattices isolated from each other, we fix the set V^s_k of all spatial links with time coordinates kn_t, $k = 0,\dots,(\mathcal{N}-1)$. This way, the dynamics of every sublattice depends only on the background field of the two frozen time slices, and hence are totally independent from one another.

As in [101], we rewrite (6.17) as

$$\begin{aligned}\langle P(\vec{0})P(\vec{x})^*\rangle &= \int\prod_k dU^{(s)}_k T^{\alpha\gamma\beta\delta}_{\vec{0},(\vec{x})}[V^{(s)}_0, V^{(s)}_1] \qquad (6.18)\\ &\dots\quad T^{\epsilon\alpha\rho\beta}_{\vec{0},(\vec{x})}[V^{(s)}_{\mathcal{N}-1}, V^{(s)}_0]\mathcal{P}[V^{(s)}_k] \qquad (6.19)\end{aligned}$$

where

$$\begin{aligned}T^{\alpha\gamma\beta\delta}_{\vec{0},(x)}[V^{(s)}_i, V^{(s)}_j] &\equiv \int\prod_{y,\mu}dU_{y,\mu}\Big[U_{(\vec{0},0),t}\dots U_{(\vec{0},n_t-1),t}\Big]_{\alpha\gamma} \qquad (6.20)\\ &\times \Big[U^*_{(\vec{x},0),t}\dots U^*_{(\vec{x},n_t-1),t}\Big]_{\beta\delta}\frac{e^{-S[U;V^{(s)}_i,V^{(s)}_j]}}{Z[V^{(s)}_i,V^{(s)}_j]}. \qquad (6.21)\end{aligned}$$

The partition function of the sublattice with fixed temporal boundaries reads

$$Z[V^{(s)}_i, V^{(s)}_j] \equiv \int\prod_{y,\mu}dU_{y,\mu}e^{-S[U;V^{(s)}_i,V^{(s)}_j]} \qquad (6.22)$$

in which $S[U; V_i^{(s)}, V_j^{(s)}]$ is the action in the sublattice with fixed temporal boundaries $V_i^{(s)}$ and $V_j^{(s)}$. Here we denote the color indices as α, β, γ and δ, and $T^{\alpha\gamma\beta\delta}$ are gauge-invariant quantities under sublattice gauge transformations. $\mathcal{P}[V_k^{(s)}]$ is the probability for the spatial links with time coordinates kn_t, $k = 0, \ldots, (\mathcal{N}-1)$, to be $V_k^{(s)}$, and can be written

$$\mathcal{P}[V_k^{(s)}] = \frac{1}{Z} \int \prod_{y,\mu} dU_{y,\mu} \prod_k \delta(U_k^{(s)} - V_k^{(s)}) e^{-S[U]} \tag{6.23}$$

Iterating this procedure and averaging the background field according to the probability distribution of eq. (6.23) gives a numerical estimate for the integral (6.18) [101]. This technique is the so-called "single level algorithm". A more general "multilevel algorithm" by Lüscher and Weisz involves a feature, that the updating frequency of the background field $V_k^{(s)}$ is not the same for the various time slices k. However, for many purposes the single level algorithm seems to be more efficient [92, 101].

In numerical simulations with the single level algorithm, three parameters have to be fixed: the temporal sublattice thickness n_t, the number N of sublattice measurements and the number M of background field configurations to integrate over $V^{(s)}$. These parameters are dependent on each other as well as on the temporal extension N_t of the whole lattice and on the distance between the two Polyakov loops. Finding the optimal choice for them is thus not trivial. Some results on the optimization step can be found in [135, 153].

When measuring the Polyakov loop correlation function $\langle P(\vec{0})P(\vec{x})^* \rangle$ the final error bar is the combination of the uncertainties of the sublattice averages and their fluctuations, due to different background fields. With n_t fixed, a large distance between two loops requires both N and M to be large. N is typically order of several thousands and M of few hundreds [101]. It should be noted that N does not depend on N_t whereas M does. With the Lüscher and Weisz algorithm, exponential gain in the accuracy of the numerical estimation of $\langle P(\vec{0})P(\vec{x})^* \rangle$ is possible only in the temporal direction. Every sublattice estimate decreases exponentially with the distance, but it is still estimated with an error reduction proportional to $1/\sqrt{N}$ [101].

Bibliography

[1] T. Karavirta, A. Mykkänen, J. Rantaharju, K. Rummukainen, and K. Tuominen. Nonperturbative improvement of SU(2) lattice gauge theory with adjoint or fundamental flavors. *JHEP*, 1106:061, 2011.

[2] A. Mykkänen, M. Panero, and K. Rummukainen. Casimir scaling and renormalization of Polyakov loops in large-N gauge theories. *JHEP*, 1205:069, 2012. arXiv:1202.2762v2 [hep-lat].

[3] A. Mykkänen. The static quark potential from a multilevel algorithm for the improved gauge action, Sep 2012. arXiv:1209.2372 [hep-lat].

[4] N. Yang and R. L. Mills. Conservation of isotopic spin and isotopic gauge invariance. *Phys. Rev.*, 96:191, Jun 1954.

[5] Y. Nambu and G. Jona-Lasinio. Dynamical model of elementary particles based on an analogy with superconductivity. I. *Physical Review*, 122:345358, Apr 1961.

[6] Y. Nambu and G. Jona-Lasinio. Dynamical model of elementary particles based on an analogy with superconductivity. II. *Physical Review*, 124:246254, Oct 1961.

[7] P. W. Higgs. Broken Symmetries and the Masses of Gauge Bosons. *Phys. Rev. Lett.*, 13 (16):508509, 1964.

[8] F. Englert and R. Brout. Broken Symmetry and the Mass of Gauge Vector Mesons. *Phys. Rev. Lett.*, 13 (9):321323, 1964.

[9] G. S. Guralnik, C. R. Hagen, and T. W. B. Kibble. Global Conservation Laws and Massless Particles. *Phys. Rev. Lett.*, 13 (20):585587, 1964.

[10] R. Gupta. Introduction to lattice QCD. Jul 1998. arXiv:hep-lat/9807028v1.

[11] D.J. Gross and F. Wilczek. Ultraviolet behavior of non-abelian gauge theories. *Physical Review Letters*, 30 (26):13431346, 1973.

[12] H.D. Politzer. Reliable perturbative results for strong interactions. *Physical Review Letters*, 30 (26):13461349, 1973.

[13] G. 't Hooft, Jun 1972. Unpublished talk at the Marseille conference on renormalization of Yang-Mills fields and applications to particle physics.

[14] K. G. Wilson. Confinement of quarks. *Phys. Rev. D*, 10:24452459, 1974.

[15] C. Gattringer and C.B. Lang. *Quantum Chromodynamics on the Lattice, An Introductory Presentation.* Lect. Notes Phys. 788 (Springer, Berlin Heidelberg), 2010.

[16] R.P.Feynman. Space-time approach to non-relativistic quantum mechanics. *Reviews of Modern Physics*, 20(2):367, Apr 1948.

[17] C. G. Callan. Broken scale invariance in scalar field theory. *Phys. Rev. D*, 2:15411547, 1970.

[18] K. Symanzik. Small distance behaviour in field theory and power counting. *Commun. math. Phys.*, 18:227, 1970.

[19] K. Symanzik. Small-distance-behaviour analysis and Wilson expansions. *Commun. math. Phys.*, 23:49, 1971.

[20] G. Endrődi. QCD thermodynamics with dynamical fermions, Apr 2011. arXiv:1104.3730v1 [hep-lat].

[21] H.J.Rothe. *Lattice gauge theories, an introduction.* World Scientific Publishing Co.Pte.Ltd, second edition, 1997.

[22] N. Weiss. Effective potential for the order parameter of gauge theories at finite temperature. *Phys. Rev.D*, 24:475, Jul. 1981.

[23] V.S. Dotsenko and S.N. Vergeles. Renormalizability of phase factors in the nonabelian gauge theory. *Nucl. Phys. B*, 169:527, 1980.

[24] H. B. Nielsen and M. Ninomiya. Absence of neutrinos on a lattice. *Nucl. Phys. B*, 185:20, 1981.

[25] H. B. Nielsen and M. Ninomiya. No go theorem for regularizing chiral fermions. *Phys. Lett. B*, 105:219, 1981.

[26] J. Kogut and L. Susskind. *Phys. Rev. D*, 11:395, 1975.

[27] L. Susskind. *Phys. Rev. D*, 16:3031, 1977.

[28] K. G. Wilson. *Plenum Press*, 1977. in New Phenomena in Subnuclear Physics, ed. A. Zichichi.

[29] P. Hasenfratz and F. Niedermayer. *Nucl. Phys. B*, 414:785, 1994.

[30] P. Hasenfratz. *Nucl. Phys. (Proc. Suppl.) B*, 63:53, 1998.

[31] D. Kaplan. *Phys. Lett. B*, 288:342, 1992.

[32] Y. Shamir. *Nucl. Phys. B*, 406:90, 1993.

[33] K. Rummukainen. QCD-like technicolor on the lattice. *AIP Conf.Proc.*, 1343:51–56, Jan 2011. arXiv:1101.5875v1 [hep-lat].

[34] S. Weinberg. Implications of dynamical symmetry breaking: An addendum. *Phys. Rev. D*, 19:1277, 1979.

[35] L. Susskind. Dynamics of spontaneous symmetry breaking in the Weinberg-Salam theory. *Phys. Rev. D*, 20:2619, 1979.

[36] E. Eichten and K. D. Lane. *Phys. Lett. B*, 90:125, 1980.

[37] C. T. Hill and E. H. Simmons. *Phys. Rept.*, 381:235, 2003. [Erratum-ibid. 390, 553 (2004)].

[38] B. Holdom. *Phys. Rev. D*, 24:1441, 1981.

[39] K. Yamawaki, M. Bando, and K. i. Matumoto. *Phys. Rev. Lett.*, 56:1335, 1986.

[40] T.W. Appelquist, D. Karabali, and L. C. R.Wijewardhana. *Phys. Rev. Lett.*, 57:957, 1986.

[41] T. Appelquist, A. Ratnaweera, J. Terning, and L. C. R. Wijewardhana. *Phys. Rev. D*, 58:105017, 1998.

[42] L. Del Debbio. The conformal window on the lattice. Feb 2011. arXiv:1102.4066v1 [hep-lat].

[43] F. Sannino and K. Tuominen. *Phys. Rev. D*, 71:051901, 2005. arXiv:hep-ph/0405209.

[44] D. D. Dietrich, F. Sannino, and K. Tuominen. *Phys. Rev. D*, 72:055001, 2005. arXiv:hep-ph/0505059.

[45] D. D. Dietrich and F. Sannino. *Phys. Rev. D*, 75:085018, 2007. arXiv:hep-ph/0611341.

[46] L. Del Debbio, B. Lucini, A. Patella, C. Pica, and A. Rago. Conformal versus confining scenario in SU(2) with adjoint fermions. *Phys.Rev.*, D80:074507, 2009.

[47] L. Del Debbio, B. Lucini, A. Patella, C. Pica, and A. Rago. The infrared dynamics of Minimal Walking Technicolor. *Phys.Rev.*, D82:014510, 2010.

[48] L. Del Debbio, B. Lucini, A. Patella, C. Pica, and A. Rago. Mesonic spectroscopy of Minimal Walking Technicolor. *Phys.Rev.*, D82:014509, 2010.

[49] B. Lucini. Strongly Interacting Dynamics beyond the Standard Model on a Spacetime Lattice. *Phil.Trans.Roy.Soc.Lond.*, A368:3657–3670, 2010.

[50] F. Bursa, L. Del Debbio, D. Henty, E. Kerrane, B. Lucini, et al. Improved Lattice Spectroscopy of Minimal Walking Technicolor. *Phys.Rev.*, D84:034506, 2011.

[51] M. Lüscher, R. Narayanan, P. Weisz, and U. Wolff. *Nucl. Phys. B*, 384:168, 1992. arXiv:hep-lat/9207009.

[52] T. DeGrand, Y. Shamir, and B. Svetitsky. *Phys. Rev. D*, 82:054503, 2010. arXiv:1006.0707 [hep-lat].

[53] B. Sheikholeslami and R. Wohlert. *Nucl. Phys. B*, 259:572, 1985.

[54] M. Lüscher, P. Weisz, and U. Wolff. *Nucl. Phys. B*, 359:221, 1991.

[55] M. Lüscher, R. Sommer, U. Wolff, and P. Weisz. Computation Of The Running Coupling In The SU(2) Yang-Mills Theory. *Nucl. Phys. B*, 389:247, 1993. arXiv:hep-lat/9207010.

[56] M. Lüscher, S. Sint, R. Sommer, P. Weisz, and U. Wolff. *Nucl. Phys. B*, 491:323, 1997. arXiv:hep-lat/9609035.

[57] K. Jansen and R. Sommer [ALPHA collaboration]. *Nucl. Phys. B*, 530:185, 1998. [Erratum-ibid. B 643, 517 (2002)] arXiv:hep-lat/9803017.

[58] S. Sint and R. Sommer. The running coupling from the QCD Schrödinger functional – a one-loop analysis. *Nucl.Phys. B*, 465:71–98, 1996. arXiv:hep-lat/9508012v1.

[59] M. Lüscher, S. Sint, R. Sommer, and P. Weisz. Chiral symmetry and $O(a)$ improvement in lattice QCD. *Nucl.Phys. B*, 478:365–400, 1996. arXiv:hep-lat/9605038v1.

[60] E. Witten. Baryons in the $1/N$ expansion. *Nucl. Phys. B*, 160:57, 1979.

[61] A. V. Manohar. Large N QCD. arXiv:hep-ph/9802419.

[62] G. 't Hooft. A planar diagram theory for strong interactions. *Nucl. Phys. B*, 72:461, 1974.

[63] Yu. M. Makeenko and A. A. Migdal. *Phys. Lett. B*, 212:221, 1980.

[64] A. A. Migdal. *Phys. Rep.*, 102:199, 1983.

[65] B. Lucini and M. Teper. Confining strings in SU(N) gauge theories. *Phys.Rev.*, D64:105019, 2001.

[66] B. Lucini and M. Teper. SU(N) gauge theories in four-dimensions: Exploring the approach to $N =$ infinity. *JHEP*, 0106:050, 2001.

[67] B. Lucini, M. Teper, and U. Wenger. The High temperature phase transition in SU(N) gauge theories. *JHEP*, 0401:061, 2004.

[68] B. Lucini, M. Teper, and U. Wenger. Properties of the deconfining phase transition in SU(N) gauge theories. *JHEP*, 0502:033, 2005.

[69] B. Lucini, M. Teper, and U. Wenger. Glueballs and k-strings in SU(N) gauge theories: Calculations with improved operators. *JHEP*, 0406:012, 2004.

[70] B. Lucini, M. Teper, and U. Wenger. The Deconfinement transition in SU(N) gauge theories. *Phys.Lett.*, B545:197–206, 2002.

[71] B. Lucini and M. Teper. SU(N) gauge theories in $(2 + 1)$-dimensions: Further results. *Phys.Rev.*, D66:097502, 2002.

[72] B. Lucini and M. Teper. The $k = 2$ string tension in four dimensional SU(N) gauge theories. *Phys.Lett.*, B501:128–133, 2001.

[73] B. Lucini, M. Teper, and U. Wenger. Topology of SU(N) gauge theories at $T = 0$ and $T = T(c)$. *Nucl.Phys.*, B715:461–482, 2005.

[74] L. Del Debbio, B. Lucini, A. Patella, and C. Pica. Quenched mesonic spectrum at large N. *JHEP*, 0803:062, 2008. arXiv:0712.3036v2 [hep-th].

[75] B. Lucini, A. Rago, and E. Rinaldi. Glueball masses in the large N limit. *JHEP*, 1008:119, 2010.

[76] B. Lucini and G. Moraitis. The Running of the coupling in SU(N) pure gauge theories. *Phys.Lett.*, B668:226–232, 2008.

[77] B. Lucini. The Large N limit from the lattice. *Few Body Syst.*, 36:161–166, 2005.

[78] B. Lucini, A. Rago, and E. Rinaldi. SU(N_c) gauge theories at deconfinement. *Phys.Lett.*, B712:279–283, 2012.

[79] Wikipedia; a picture released into the public domain.

[80] M. Teper. Large N and confining flux tubes as strings - a view from the lattice, Dec 2009. arXiv:0912.3339v1[hep-lat].

[81] M. Teper. Large N. PoS LATTICE2008, 2008. arXiv:0812.0085v1 [hep-lat].

[82] A. Dumitru, Y. Hatta, J. Lenaghan, K. Orginos, and R. D. Pisarski. Deconfining phase transition as a matrix model of renormalized Polyakov loops. *Phys.Rev.D*, 70:034511, 2004. arXiv:hep-th/0311223v2.

[83] H. Meyer and M. Teper. Confinement and the effective string theory in SU($N \to \infty$) : a lattice study. *JHEP*, 0412:031, 2004. arXiv:hep-lat/0411039.

[84] G. Bali and F. Bursa. Mesons at large N_c from lattice QCD, 2008. arXiv:0806.2278v3 [hep-lat].

[85] K. Kajantie, M. Laine, K. Rummukainen, and Y. Schröder. The pressure of hot QCD up to $g^6\ln(1/g)$. *Phys. Rev. D*, 67:105008, 2003. arXiv:hep-ph/0211321v2.

[86] B. Bringoltz and M. Teper. *Phys. Lett. B*, 628:113, 2005. hep-lat/0506034.

[87] M. Panero. *Phys. Rev. Lett.*, 103:232001, 2009. arXiv:0907.3719.

[88] D. Mateos. String theory and quantum chromodynamics. *Class.Quant.Grav.*, 24:S713–S740, 2007. arXiv:0709.1523v1[hep-th].

[89] Y. Nambu. QCD and the string model. *Phys. Lett. B*, 80:372, 1979.

[90] A.M. Polyakov. String representations and hidden symmetries for gauge fields. *Physics Letters B*, 82:247–250, 1979.

[91] J.L. Gervais and A. Neveu. The quantum dual string wave functional in Yang-Mills theories. *Phys. Lett. B*, 80:255, 1979.

[92] M. Lüscher and P. Weisz. Quark confinement and the bosonic string. *JHEP*, 0207:049, Jul 2002. arXiv:hep-lat/0207003v1.

[93] M. Caselle, R. Fiore, F. Gliozzi, M. Hasenbusch, and P. Provero. String effects in the Wilson loop: a high precision numerical test. *Nucl. Phys. B*, 486:245, 1997. arXiv:hep-lat/9609041v1.

[94] A. Rajantie, K. Rummukainen, and D. J. Weir. Form factor and width of a quantum string. Oct 2012. arXiv:1210.1106v1 [hep-lat].

[95] M. Caselle, M. Hasenbusch, and M. Panero. String effects in the 3d gauge Ising model. *JHEP*, 0301:057, Jan 2003. arXiv:hep-lat/0211012.

[96] K. J. Juge, J. Kuti, and C. Morningstar. QCD string formation and the Casimir energy, Jan 2004. arXiv:hep-lat/0401032.

[97] P. Giudice, F. Gliozzi, and S. Lottini. The conformal anomaly of k-strings. *JHEP*, 0705:010, 2007. arXiv:hep-th/0703153v1 16 Mar 2007.

[98] M. Panero. A numerical study of confinement in compact QED. *JHEP*, 0505:066, May 2005. arXiv:hep-lat/0503024v3.

[99] M. Panero. A numerical study of a confined $Q\bar{Q}$ system in compact U(1) lattice gauge theory in $4D$. *Nucl.Phys.Proc.Suppl.*, 140:665–667, 2005. arXiv:hep-lat/0408002v3.

[100] Y. Koma, M. Koma, and P. Majumdar. Static potential, force, and flux-tube profile in $4D$ compact U(1) lattice gauge theory with the multi-level algorithm. *Nucl. Phys. B*, 692:209–231, Jun 2004. arXiv:hep-lat/0311016v2.

[101] M. Caselle, M. Pepe, and A. Rago. Static quark potential and effective string corrections in the $(2+1)-d$ SU(2) Yang-Mills theory. *J. High Energy Phys.*, 10:005, Jun 2004. arXiv:hep-lat/0406008v1.

[102] M. Caselle, M. Pepe, and A. Rago. String effects in SU(2) lattice gauge theory. *Nucl. Phys. Proc. Suppl.*, 129:721, 2004. arXiv:hep-lat/0310005.

[103] C. Bonati. Finite temperature effective string corrections in $(3+1)D$ SU(2) lattice gauge theory, Aug 2011. arXiv:hep-lat/1106.5920v3.

[104] K. J. Juge, J. Kuti, and C. Morningstar. Fine structure of the QCD string spectrum. *Phys. Rev. Lett.*, 90:161601, 2003. arXiv:hep-lat/0207004.

[105] G. S. Bali. QCD forces and heavy quark bound states. *Phys. Rept.*, 343:1–136, May 2001. arXiv:hep-ph/0001312.

[106] A. Athenodorou, B. Bringoltz, and M. Teper. Closed flux tubes and their string description in $D = 3+1$ SU(N) gauge theories. *JHEP*, 1102:030, 2011. arXiv:1007.4720v2 [hep-lat].

[107] A. Athenodorou, B. Bringoltz, and M. Teper. Closed flux tubes and their string description in $D = 2+1$ SU(N) gauge theories, Mar 2011. arXiv:1103.5854v1 [hep-lat].

[108] A. Athenodorou, B. Bringoltz, and M. Teper. The closed string spectrum of SU(N) gauge theories in $2+1$ dimensions. *Phys. Lett. B*, 656:132, 2007. arXiv:hep-lat/0709.0693.

[109] B. Bringoltz and M. Teper. Strings in SU(N) gauge theories in $2+1$ dimensions: beyond the fundamental representation, 2007. arXiv:0708.3447 [hep-lat].

[110] F. Gliozzi, S. Lottini, M. Panero, and A. Rago. Random percolation as a gauge theory. *Nucl.Phys.*, B719:255–274, 2005.

[111] P. Giudice, F. Gliozzi, and S. Lottini. The confining string beyond the free-string approximation in the gauge dual of percolation, Jan 2009. arXiv:0901.0748 [hep-lat].

[112] M. Lüscher, K. Symanzik, and P. Weisz. Anomalies of the free loop wave equation in the Wkb approximation. *Nucl. Phys. B*, 173:365, 1980.

[113] M. Lüscher. Symmetry breaking aspects of the roughening transition in gauge theories. *Nucl. Phys. B*, 180:317, 1981.

[114] M. Lüscher, G. Munster, and P. Weisz. *Nucl. Phys. B*, 180:1, 1981.

[115] F. Gliozzi and M. Meineri. Lorentz completion of effective string (and p-brane) action. arXiv:1207.2912v1 [hep-th].

[116] H. B. Meyer. Poincare invariance in effective string theories. *JHEP*, 05:066, 2006. arXiv:hep-th/0602281.

[117] O. Aharony and M. Field. On the effective theory of long open strings. *JHEP*, 1101:065, 2011. arXiv:1008.2636 [hep-th].

[118] O. Aharony and M. Dodelson. Effective string theory and nonlinear Lorentz invariance. *JHEP*, 12:008, 2012. arXiv:1111.5758 [hep-th].

[119] O. Aharony, M. Field, and N. Klinghoffer. The effective string spectrum in the orthogonal gauge. *JHEP*, 04:048, 2012. arXiv:1111.5757 [hep-th].

[120] Y. Nambu. Symmetries and quark models. ed. R. Chand, (Gordon and Breach, New York, 1970).

[121] T. Goto. *Prog. Theor. Phys*, 46:1560, 1971.

[122] Y. Nambu. *Phys. Rev. D*, 10:4262, 1974.

[123] J. F. Arvis. The exact $q\bar{q}$ potential in Nambu string theory. *Phys. Lett. B*, 127:106, 1983.

[124] O. Alvarez. Static potential in string models. *Phys. Rev. D*, 24:440, 1981.

[125] M. Caselle, A. Feo, M. Panero, and R. Pellegrini. Universal signatures of the effective string in finite temperature lattice gauge theories. *J. High Energy Phys.*, 1104:020, Apr 2011. arXiv:hep-lat/1102.0723.

[126] B. B. Brandt. Probing boundary-corrections to Nambu-Goto open string energy levels in $3d$ SU(2) gauge theory. *JHEP :,*, 1102:040, 2011. arXiv:1010.3625v2 [hep-lat].

[127] J. Polchinski and A. Strominger. Effective string theory. *Phys. Rev. Lett.*, 67:1681, 1991.

[128] J. M. Drummond. Universal subleading spectrum of effective string theory. arXiv:hep-th/0411017; J. M. Drummond, Reply to hep-th/0606265, arXiv:hep-th/0608109.

[129] N. D. Hari Dass and P. Matlock. Universality of correction to Lüescher term in Polchinski-Strominger effective string theories. arXiv:hep-th/0606265; N. D. H. Dass and P. Matlock, Our response to the response hep-th/0608109 by Drummond, arXiv:hep-th/0611215; N. D. Hari Dass and P. Matlock, Covariant Calculus for Effective String Theories, arXiv:0709.1765 [hep-th].

[130] M. Lüscher and P. Weisz. String excitation energies in SU(N) gauge theories beyond the free-string approximation. *JHEP*, 0407:014, Jul 2004. arXiv:hep-th/0406205.

[131] O. Aharony and E. Karzbrun. On the effective action of confining strings, Mar 2009. arXiv:hep-th/0903.1927v4.

[132] G. Bali and A.M. Green. Two quark potentials, Oct 2004. arXiv:nucl-th/0410080v2.

[133] J. Kuti. Lattice QCD and string theory, 2006. PoS JHW2005, 009 (2006), arXiv:hep-lat/0511023.

[134] M. Caselle, M. Panero, and P. Provero. String effects in Polyakov loop correlators. *JHEP*, 0206:061, June 2002. arXiv:hep-lat/0205008.

[135] P. Majumdar. The string spectrum from large wilson loops. *Nucl. Phys. B*, 664:213, 2003. arXiv:hep-lat/0211038v3.

[136] M. Caselle, M. Hasenbusch, and M. Panero. Short distance behaviour of the effective string. *JHEP*, 0405:032, May 2004. arXiv:hep-lat/0403004.

[137] P. Majumdar. Continuum limit of the spectrum of the hadronic string, Jun 2004. arXiv:hep-lat/0406037.

[138] M. Caselle, M. Hasenbusch, and M. Panero. Comparing the Nambu-Goto string with LGT results. *JHEP*, 0503:026, May 2005. arXiv:hep-lat/0501027.

[139] J. Ambjørn, P. Olesen, and C. Peterson. *Phys. Lett. B*, 142:410, 1984. Nucl. Phys. B244 (1984) 262.

[140] K. J. Juge, J. Kuti, and C. J. Morningstar. Quark confinement and surface critical phenomena. *Nucl. Phys. Proc. Suppl.*, 83:503, 2000. arXiv:hep-lat/9911007.

[141] K. J. Juge, J. Kuti, and C. Morningstar. The Casimir energy paradox of the QCD string. *Nucl. Phys. Proc. Suppl.*, 129:686, 2004. arXiv:hep-lat/0310039.

[142] J. M. Maldacena. The large N limit of superconformal field theories and supergravity. *Adv.Theor.Math.Phys.*, 2:231–252, 1998. arXiv:hep-th/9711200v3.

[143] E. Witten. Bound States Of Strings And p-Branes. *Nucl.Phys.B*, 460:335–350, 1996. arXiv:hep-th/9510135.

[144] S. S. Gubser and A. Karch. From gauge-string duality to strong interactions: a Pedestrian's Guide. *Ann.Rev.Nucl.Part.Sci.*, 59:145–168, 2009. arXiv:0901.0935v2 [hep-th].

[145] M.Creutz. *Quarks, gluons and lattices.* Cambridge University Press, 1983.

[146] K. Rummukainen. Monte Carlo simulation methods. Lecture notes, University of Oulu, 2007.

[147] J-S. Wang. Cluster Monte Carlo algorithms and their applications, Oct. 1995. arXiv:cond-mat/9510082v1.

[148] N. Cabibbo and E. Marinari. *Phys. Lett. B*, 119:387, 1982.

[149] S. L. Adler. Overrelaxation algorithms for lattice field theories. *Phys. Rev. D*, 37(2):458, Jan. 1988.

[150] S. Duane, A. D. Kennedy, B. J. Pendleton, and D. Roweth. *Phys. Lett. B*, 195:216. 1987.

[151] T. Lippert. The Hybrid Monte Carlo algorithm for quantum chromodynamics, Dec 1997. arXiv:hep-lat/9712019v1.

[152] M. Lüscher and P. Weisz. Locality and exponential error reduction in numerical lattice gauge theory. *High Energy Phys.*, 09:010, 2001.

[153] H. B. Meyer. The Yang-Mills spectrum from a two-level algorithm. *JHEP*, 0401:030, Jan 2004. arXiv:hep-lat/0312034v2.

Preprint typeset in JHEP style - HYPER VERSION

Nonperturbative improvement of SU(2) lattice gauge theory with adjoint or fundamental flavors

Tuomas Karavirta[*]
Department of Physics, P.O.Box 35 (YFL), FI-40014 University of Jyväskylä, Finland, and Helsinki Institute of Physics, P.O. Box 64, FI-00014 University of Helsinki, Finland.

Anne Mykkanen[†]
Department of Physics and Helsinki Institute of Physics, P.O.Box 64, FI-00014 University of Helsinki, Finland

Jarno Rantaharju[‡]
Department of Physics and Helsinki Institute of Physics, P.O.Box 64, FI-00014 University of Helsinki, Finland

Kari Rummukainen[§]
Department of Physics and Helsinki Institute of Physics, P.O.Box 64, FI-00014 University of Helsinki, Finland

Kimmo Tuominen[¶]
Department of Physics, P.O.Box 35 (YFL), FI-40014 University of Jyväskylä, Finland, and Helsinki Institute of Physics, P.O. Box 64, FI-00014 University of Helsinki, Finland.

Abstract: SU(2) gauge theory with two fermions transforming under the adjoint representation may appear conformal or almost conformal in the infrared, and is one of the candidate theories for building models for technicolor. Early lattice Monte Carlo studies of this model have used unimproved Wilson fermion formulation, which can be expected to have large lattice cutoff effects. In this paper we present the calculation of the $O(a)$ improved lattice Wilson-clover action of the theory. The Sheikholeslami-Wohlert coefficient has been determined non-perturbatively, and various boundary improvement terms, needed for the Schrödinger functional formalism, have been calculated in perturbation theory. For comparison, we have also determined the improvement coefficients for SU(2) gauge theory with two fundamental representation fermions. The calculation paves way for more accurate lattice Monte Carlo analyses of the theory in the future.

Keywords: Lattice field theory, Conformal field theory.

Contents

1. Introduction

Quantum field theories with nontrivial infrared fixed points of the β- function have recently been studied due to their applications in beyond Standard Model model building. In these theories the coupling runs when probed at very short distances, but becomes a constant over some energy range in the infrared and the theory appears conformal. One of the phenomenological connections is the unparticle [1, 2, 3], i.e. the possibility of a fully conformal sector coupled only weakly to the Standard Model through effective operators at low energies. Another phenomenological motivation to study theories which either feature an infrared fixed point or are, in theory space, close to one which does, originates from technicolor (TC) and the associated extended technicolor (ETC) models. These models were devised to explain the mass patterns of the Standard Model gauge bosons and fundamental fermions without the need to introduce a fundamental scalar particle [4, 5, 6, 7].

Early TC models, based on a technicolor sector straightforwardly extrapolated from a QCD-like strongly interacting theory, lead to too large flavor changing neutral currents due to the extended technicolor interactions.The problems of these simple TC models are solved in so called walking technicolor theories [8, 9, 10, 11]. These theories are quasi-conformal, i.e. the evolution of the coupling constant is, over a wide range of energy, governed by an attractive quasi-stable infrared fixed point at strong coupling.

*tuomas.karavirta@jyu.fi
†anne-mari.mykkanen@helsinki.fi
‡jarno.rantaharju@helsinki.fi
§kari.rummukainen@helsinki.fi
¶kimmo.tuominen@jyu.fi

To build walking TC models one needs to tune the gauge and matter degrees of freedom so that the desired quasi-conformality arises. To achieve this in SU(N) gauge theory with fermions in the fundamental representation several $\mathcal{O}(10)$ Dirac flavors are required. These contribute to the precision parameter S, which becomes too large to be compatible with the current observations. To obtain enough screening, as required for quasi-conformality, but with smaller number of flavors, one considers fermions in higher representations. It has been suggested [12] that an ideal candidate for minimal walking technicolor theory would be the one with just two (techni)quark flavors in the two-index symmetric representation of SU(2) or SU(3).

Reliable quantitative studies of the models, especially evaluating the β-functions, require lattice Monte Carlo simulations. There are several recent studies of both SU(2) [13, 14, 15, 16, 17, 18, 19, 20, 21, 22] and SU(3) [23, 24, 25, 26, 27] gauge theories with two-index symmetric representation fermions. For related studies in QCD-like theories with fundamental representation fermions see [28, 29, 30, 31, 32, 33, 34, 35, 36, 37, 38, 39, 40].

In this paper we consider the case of SU(2) gauge fields with two fermions in the two-index symmetric representation, which, for SU(2), is equivalent to the adjoint representation. So far the lattice studies of this theory have been performed using unimproved Wilson fermion action and are hence subject to large $\mathcal{O}(a)$ lattice artifacts. In this paper we present the computation of $\mathcal{O}(a)$-improvement. This is a generalisation of the program used earlier to compute the improved action for two fundamental representation fermions in SU(3) gauge theory [41, 42, 43, 44, 45, 46]. The early results of this calculation have been presented in refs. [47, 48].

The Wilson fermion action can be improved for on-shell quantities by adding the well-known clover term. We tune the coefficient of the clover term (Sheikholeslami-Wohlert coefficient [49]) non-perturbatively, using the Schrödinger functional method. For the measurement of the coupling constant we also need the improvement coefficients of certain boundary terms. This computation is done using perturbative analysis. For comparison, we also calculate the improvement for SU(2) gauge theory with two flavors of fundamental representation fermions.[1]

The paper is structured so that in section 2 we first recall the basics of the model as well as of the lattice formulation we use. In section 3 we present our perturbative results for the boundary terms and nonperturbative results for the improvement coefficients are presented in section 4. In section 5 we conclude and outline the directions of our future work.

2. Lattice formulation: the model and $\mathcal{O}(a)$ improvement

We study SU(2) gauge theory with two different matter contents: two mass-degenerate flavors of Dirac fermions either in the adjoint or in the fundamental representation. The

[1]Non-perturbative improvement of the clover term has been recently published for SU(3) gauge field theory with 2-index symmetric (sextet) fermions, using the HYP-smeared link clover action [50].

continuum theory in Euclidean spacetime is defined by

$$\mathcal{L} = \frac{1}{2}\mathrm{Tr}\, F_{\mu\nu}F_{\mu\nu} + \sum_{\alpha} \bar{\psi}_\alpha(i\not{D} + m)\psi_\alpha \tag{2.1}$$

where $F_{\mu\nu}$ is the usual SU(2) field strength, and the gauge covariant derivative is

$$D_\mu\psi = \left(\partial_\mu - igA^a_\mu T^a\right)\psi \tag{2.2}$$

where $a = 1, 2, 3$ and the generators T^a are taken either in the fundamental ($T^a = \sigma^a/2$) or in the adjoint representation ($[T^a]^{bc} = -i\epsilon^{abc}$). The summation in Eq. (2.1) is over $\alpha = \mathrm{u}, \mathrm{d}$.

Our main goal in this work is to establish nonperturbative $\mathcal{O}(a)$ improved lattice implementation of these theories. While the improvement has been discussed in detail in existing literature for SU(3) gauge field with fundamental fermions, the studies of adjoint flavors require some alterations. Hence we find it necessary and useful to repeat essential parts of the analysis in detail here.

First recall the usual $\mathcal{O}(a)$ improvement obtained by Sheikholeslami and Wohlert [49]. The lattice action, split to the gauge and fermionic parts S_G and S_F, is

$$S_0 = S_G + S_F. \tag{2.3}$$

Here we use the standard Wilson plaquette gauge action

$$S_G = \beta_L \sum_{x;\mu<\nu} \left(1 - \frac{1}{2}\mathrm{Tr}\, P_{x;\mu\nu}\right) \tag{2.4}$$

where $\beta_L = 4/g_0^2$ and the plaquette is written in terms of the SU(2) fundamental representation link matrices $U_\mu(x)$, which act as parallel transporters between sites x and $x + a\hat{\mu}$:

$$P_{x;\mu\nu} = U_\mu(x)U_\nu(x + a\hat{\mu})U^\dagger_\mu(x + a\hat{\nu})U^\dagger_\nu(x). \tag{2.5}$$

The Wilson fermion action, S_F, for N_f (degenerate) Dirac fermions in the fundamental or adjoint representation of the gauge group is

$$S_{\mathrm{F}} = a^4 \sum_{\alpha} \sum_{x} \bar{\psi}_\alpha(x)(iD + m_{q,0}\mathbb{1})\psi_\alpha(x), \tag{2.6}$$

where the usual Wilson-Dirac operator is

$$D = \frac{1}{2}(\gamma_\mu(\nabla^*_\mu + \nabla_\mu) - a\nabla^*_\mu\nabla_\mu), \tag{2.7}$$

involving the gauge covariant lattice derivatives ∇_μ and ∇^*_μ defined as

$$\nabla_\mu\psi(x) = \frac{1}{a}[\widetilde{U}_\mu(x)\psi(x + a\hat{\mu}) - \psi(x)], \tag{2.8}$$

$$\nabla^*_\mu\psi(x) = \frac{1}{a}[\psi(x) - \widetilde{U}^{-1}_\mu(x - a\hat{\mu})\psi(x - a\hat{\mu})]. \tag{2.9}$$

Here, the link variables are the usual ones, $\widetilde{U}_\mu(x) = U_\mu(x)$, for fermions in the fundamental representation while for the adjoint representation they are

$$\widetilde{U}^{ab}_\mu(x) = 2\mathrm{Tr}\,(T^a U_\mu(x) T^b U^\dagger_\mu(x)), \tag{2.10}$$

where T^a, $a = 1, 2, 3$, are the generators of the fundamental representation, normalised as $\mathrm{Tr}\,T^a T^b = \frac{1}{2}\delta^{ab}$. We note that in the adjoint representation the elements of $\widetilde{U}$-matrices are real and $\widetilde{U}^{-1} = \widetilde{U}^T$.

The lattice action (2.3) is parametrised with two dimensionless parameters, $\beta_L = 4/g^2_{\mathrm{bare}}$ and $\kappa = 1/[8 + 2am_{q,0}]$. The parameter κ is related to the fermion mass. In the continuum limit $a^4 \sum_x \to \int d^4x$ as $a \to 0$, and the leading order contribution from (2.3) yields the continuum action while the terms of higher order in a will be suppressed; these terms are generically termed "lattice artifacts". Since gauge invariance forbids any contribution from dimension five operators to the gauge action, only the fermion action here is subject to lattice artifacts at $\mathcal{O}(a)$. These are removed (for on-shell quantities) by considering the improved action

$$S_{\mathrm{impr}} = S_0 + \delta S_{\mathrm{sw}}, \tag{2.11}$$

$$\delta S_{\mathrm{sw}} = a^5 \sum_x c_{\mathrm{sw}} \bar{\psi}(x) \frac{i}{4} \sigma_{\mu\nu} F_{\mu\nu}(x) \psi(x) \tag{2.12}$$

and tuning the Sheikholeslami-Wohlert coefficient c_{sw} at each β_L so that the $\mathcal{O}(a)$ effects in on-shell quantities cancel; to lowest order in perturbation theory $c_{\mathrm{sw}} = 1$ [49]. Here $\sigma_{\mu\nu} = i[\gamma_\mu, \gamma_\nu]/2$ and $F_{\mu\nu}(x)$ is the "clover term", lattice field strength tensor in the appropriate representation symmetrized over the four μ, ν-plane plaquettes which include the point x.

Because our aim in future work is to measure the evolution of the gauge coupling constant using the Schrödinger functional method, we also need to consider the improvement of the action at the special Schrödinger functional boundary conditions. Schrödinger functional method is also used in this work for measuring c_{sw}, but for this the boundary improvement is not necessary.

We consider a system of size $L^3 \times T$, with periodic boundary conditions to the spatial directions and with Dirichlet boundary conditions for the gauge fields to the time direction:

$$U_k(x_0 = 0) = W(k), \;\; U_k(x_0 = T) = W'(k), \tag{2.13}$$

where $k = 1, 2, 3$; the explicit form of the boundary fields will be discussed later. For the measurement of the coupling constant the boundary gauge fields are chosen so that they lead to a constant background chromoelectric field. Due to the frozen boundaries there now exists $\mathcal{O}(a)$ contribution to the gauge part of the action, and to account for these we consider

$$S_{G,\mathrm{impr}} = \frac{\beta_L}{4} \sum_p w(p) \mathrm{tr}(1 - U(p)), \tag{2.14}$$

where the weights $w(p)$ are equal to 1 for plaquettes in the bulk, $w(p) = c_s/2$ for spatial plaquettes at $x_0 = 0$ and T and $w(p) = c_t$ for time-like plaquettes attached to a boundary

plane. The parameters c_s and c_t are tuned to reduce the $\mathcal{O}(a)$ boundary contributions.[2] To leading order in perturbation theory $c_t = c_s = 1$. For the electric background field which we consider the terms proportional to c_s do not contribute.

The boundary values of the fermion fields are set as

$$\begin{aligned} P_+\psi(x_0 = 0, \mathbf{x}) &= \rho(\mathbf{x}), \;\; P_-\psi(x_0 = T, \mathbf{x}) + \rho'(\mathbf{x}), \\ P_-\psi(x_0 = 0, \mathbf{x}) &= P_+\psi(x_0 = T, \mathbf{x}) = 0, \end{aligned} \tag{2.15}$$

with similar definitions on the conjugate fields. The projection operators are $P_\pm = \frac{1}{2}(1 \pm \gamma_0)$. The boundary fields ρ, ρ' are source fields for correlation functions, and they are set to zero when generating configurations in simulations. In the spatial directions it is customary to introduce a "twist" for the phase of the fermion fields [42]:

$$\psi(x + L\hat{k}) = e^{i\theta_k}\psi(x), \;\; \bar{\psi}(x + L\hat{k}) = \bar{\psi}(x)e^{-i\theta_k}. \tag{2.16}$$

In this work we use $\theta_k = \pi/5$ throughout. The twist, together with the Dirichlet boundary conditions, regulates the fermion matrix so that simulations at zero fermion masses become possible.

The improved lattice action is now given by

$$S_{\text{impr}} = S_{G,\text{impr}} + S_F + \delta S_{\text{sw}} + \delta S_{F,\text{b}}. \tag{2.17}$$

Now the Sheikholeslami-Wohlert term only accounts for the bulk,

$$\delta S_{\text{cw}} = a^5 \sum_{x_0=a}^{T-a} \sum_{\mathbf{x}} c_{\text{sw}} \bar{\psi}(x) \frac{i}{4} \sigma_{\mu\nu} F_{\mu\nu}(x) \psi(x), \tag{2.18}$$

while the boundary effects are captured by $\delta S_{F,\text{b}}$. This counterterm has two contributions, controlled by parameters denoted by $\tilde{c}_s$ and $\tilde{c}_t$. The term proportional to $\tilde{c}_s$ is

$$\begin{aligned} \delta S_{\tilde{c}_s} = a^4(\tilde{c}_s - 1) \sum_{\mathbf{x}} \Bigg[&\frac{1}{2} \bar{\psi}(0, \mathbf{x}) P_- \gamma_k (\nabla_k^* + \nabla_k) P_+ \psi(0, \mathbf{x}) \\ &+ \frac{1}{2} \bar{\psi}(L, \mathbf{x}) P_+ \gamma_k (\nabla_k^* + \nabla_k) P_- \psi(L, \mathbf{x}) \Bigg] \end{aligned} \tag{2.19}$$

and it clearly vanishes if we set fermionic fields to zero on the boundaries.

So, similarly to the gauge action, only the term proportional to $\tilde{c}_t$ contributes, and this contribution is given by

$$\delta S_{F,\text{b}} = a^4 \sum_x (\tilde{c}_t - 1) \frac{1}{a} \bar{\psi}(x) \psi(x) (\delta(x_0 - a) + \delta(x_0 - (L - a))). \tag{2.20}$$

This can be seen as a correction to the bare mass term at $x_0 = a$ and $x_0 = L - a$, hence accounted for by the modification

$$m_{q,0} \mapsto m_{q,0} + (\tilde{c}_t - 1)(\delta_{t,a} + \delta_{t,L-a}). \tag{2.21}$$

[2] Recall that gauge invariance guarantees that there are no $\mathcal{O}(a)$ contributions to the gauge action in the bulk, and hence the boundary terms controlled by c_s and c_t are the only ones which arise to $\mathcal{O}(a)$ in the gauge action.

It is known that $\tilde{c}_t = 1$ to leading order.[3]

Hence, to obtain $\mathcal{O}(a)$ improvement we need to determine the parameters c_t, $\tilde{c}_t$ and $c_{\rm sw}$ in the action (2.17). The parameters c_t and $\tilde{c}_t$ are determined perturbatively as will be described in the following section. The parameter $c_{\rm sw}$ is determined nonperturbatively, and this will be determined in section 4.

3. Perturbative analysis of the boundary improvement

As explained in the previous section, due to the Dirichlet boundary conditions associated with the Schrödinger functional formalism, we are led to counteract $\mathcal{O}(a)$ lattice artifacts on the boundaries both in the gauge and fermion parts of the action. In this section we describe in detail the analysis of the rquired counterterms. Although we are mostly interested in matter fields in fundamental or adjoint representation of SU(2) gauge group, we will present the results applicable also for higher representations of SU(3) since these are relevant for the current developments in the studies of these theories on the lattice.

In principle there exists four counterterms associated with the spatial links in the boundary and with temporal links connected to the boundary. Due to the specific form of the background field we have chosen, only two of these are needed and these are denoted by c_t and $\tilde{c}_t$. These boundary coefficients have a perturbative expansion of the form

$$c_x = 1 + c_x^{(1)} g_0^2 + \mathcal{O}(g_0^4). \tag{3.1}$$

Our goal is to determine $\tilde{c}_t$ and c_t to one-loop order in perturbation theory.

3.1 Coefficient $\tilde{c}_t^{(1)}$

We follow the analysis performed in [44] for the fundamental representation. The result of [44] is

$$\tilde{c}_t^{(1)} = -0.0135(1) C_F, \tag{3.2}$$

and this generalizes to other fermion representations simply by replacing the fundamental representation Casimir operator C_F with Casimir operator C_R of the representation R under consideration. This is so because the relevant correlations functions are proportional to the diagrams presented in figure 1, which all include the color factor $\sum_a (T^a)^2 = C_R$. Thus it can be shown that also $\tilde{c}_t^{(1)} \propto C_R$.

In the case of fundamental fermions the original result of [44] is directly applicable with $C_F = (N_c^2 - 1)/(2N_c) = 3/4$ for $N_c = 2$. For the other case we have fermions transforming in the adjoint representation of SU(2), for which the Casimir invariant is $C_A = 2$. The results for different gauge groups and fermion representations are shown in table 1.

3.2 Coefficient $c_t^{(1)}$

The coefficient $c_t^{(1)}$ can be split into gauge and fermionic parts

$$c_t^{(1)} = c_t^{(1,0)} + c_t^{(1,1)} N_f. \tag{3.3}$$

[3] This is so because free Wilson fermions are not subject to $\mathcal{O}(a)$ artifacts.

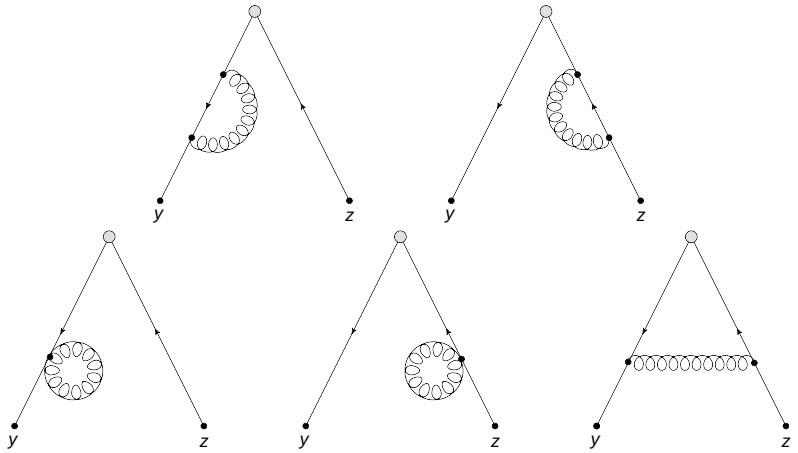

Figure 1: Diagrams contributing to the calculation of $\tilde{c}_t^{(1)}$. The shaded blob on each diagram indicates the insertion of the operator $\Gamma_x = \{\mathbb{1}, \gamma_5\}$.

The contribution $c_t^{(1,0)}$ is entirely due to gauge fields and has been evaluated in [51] for SU(2) and in [52] for SU(3). The fermionic contribution $c_t^{(1,1)}$ to c_t has been evaluated for fundamental fermions in [43] both for SU(2) and SU(3). We have extended these computations for SU(2) and SU(3) gauge theory with higher representation fermions and for SU(4) gauge theory with fundamental representation fermions.

The method we have used is the same as the one presented in [43], with two exceptions. First, the boundary fields have to be transformed to the desired fermion representation. Generally the boundary fields are of the form

$$U(x,k)|_{(x_0=0)} = \exp(aC_k), \quad U(x,k)|_{(x_0=L)} = \exp(aC'_k), \tag{3.4}$$

where

$$C_k = \frac{i}{L}\mathrm{diag}(\phi_1, \ldots, \phi_n), \quad C'_k = \frac{i}{L}\mathrm{diag}(\phi'_1, \ldots, \phi'_n), \tag{3.5}$$

and n is the dimension of the representation. The transformed boundary fields are obtained from the fundamental representation counterparts for adjoint representation via (2.10). After the transformation one simply diagonalizes the resulting matrices and ends up with a matrix of the form

$$\mathrm{diag}\left(\exp[i\phi_1^A], \ldots, \exp[i\phi_n^A]\right), \tag{3.6}$$

where ϕ_i^A give the adjoint representation boundary fields

$$C_k^A = \frac{i}{L}\mathrm{diag}(\phi_1^A, \ldots, \phi_n^A), \quad C'_k = \frac{i}{L}\mathrm{diag}(\phi_1'^A, \ldots, \phi_n'^A). \tag{3.7}$$

For the symmetric representation the components of the boundary fields C_k^S and $C_k'^S$ can be obtained by taking all the symmetric combinations of ϕ_i. For $SU(3)$ sextet repre-

sentation this is

$$\begin{aligned}
\phi_1^S &= \phi_1 + \phi_1, \\
\phi_2^S &= \phi_1 + \phi_2, \\
\phi_3^S &= \phi_1 + \phi_3, \\
\phi_4^S &= \phi_2 + \phi_2, \\
\phi_5^S &= \phi_2 + \phi_3, \\
\phi_6^S &= \phi_3 + \phi_3.
\end{aligned} \tag{3.8}$$

The other crucial note comes from the normalization in the calculation of $c_t^{(1,1)}$. Using the Schrödinger functional scheme and taking the lattice action with constant background field as an effective action Γ_0, the running coupling is defined via

$$\bar{g}^2 = \frac{\partial_\eta \Gamma_0}{\partial_\eta \Gamma}. \tag{3.9}$$

The boundary fields C_k and C'_k are functions of the parameter η so the running coupling is given by the change of the system as the boundary fields are altered. The effective action Γ is to one loop order in perturbation theory

$$\Gamma = g_0^{-2}\Gamma_0 + \Gamma_1 + \mathcal{O}(g_0^2), \tag{3.10}$$

so the running coupling can be written, as a function of the bare coupling g_0, in the form

$$\bar{g}^2 = g_0^2 \left(1 - g_0^2 \frac{\partial_\eta \Gamma_1}{\partial_\eta \Gamma_0}\right) + \mathcal{O}(g_0^6). \tag{3.11}$$

On small lattice spacings a, the one loop correction Γ_1 diverges. This leads to renormalization of the lattice coupling, which is given in terms of the bare coupling as

$$g_{\mathrm{lat}}^2 = g_0^2 + z_1 g_0^4 + \mathcal{O}(g_0^6), \tag{3.12}$$

where $z_1 = 2b_0 \ln(a\mu)$ and

$$b_0 = \frac{1}{(4\pi)^2}\left(\frac{11}{3}C_A - \frac{4}{3}T(R)N_F\right) \tag{3.13}$$

is the coefficient in one loop beta function. Now we can write the running coupling as a function of the renormalized coupling

$$\bar{g}^2 = g_{\mathrm{lat}}^2 \left[1 - g_{\mathrm{lat}}^2 \left(\frac{\partial_\eta \Gamma_1}{\partial_\eta \Gamma_0} + z_1\right)\right] + \mathcal{O}(g_{\mathrm{lat}}^6). \tag{3.14}$$

The one loop correction to the effective action Γ_1 can also be written as

$$\Gamma_1 = \frac{1}{2}\ln\det\Delta_1 - \ln\det\Delta_0 - \frac{1}{2}\ln\det\Delta_2, \tag{3.15}$$

where the operators Δ_0 and Δ_1 are related to the gauge fixing and pure gauge part of the action and the operator $\Delta_2 = [(D_{sw} + m_0)\gamma_5]^2$ is related to the fermionic part of the action. The operator D_{sw} is the lattice Dirac operator that includes the Sheikholeslami-Wohlert term. Now for the calculation of Δ_2 one needs to transform the boundary fields

to the appropriate representation. However in the calculation of Γ_0 one needs to keep the boundary fields in the fundamental representation. This is so becouse the pure gauge part of $c_t^{(1)}$ should be independent of the representation of the fermions and this can only be achived if the boundary fields in Γ_0 are kept in the fundamental representation. Also this produces the expected behavior for the series expansion of

$$\left(\frac{\partial_\eta \Gamma_1}{\partial_\eta \Gamma_0} + z_1\right). \tag{3.16}$$

With these remarks, the numerical calculation is straightforward. The results for the nonzero improvement coefficients are tabulated in table 1. The numbers beyond the fundamental representation are new, while those for the fundamental representation provide a good check on our computations. For the application to minimal walking technicolor, the relevant numbers are the ones on the second line of table 1.

Our results are consistent with the generic formula

$$c_t^{(1,1)} \approx 0.019141(2T(R)), \tag{3.17}$$

where $T(R)$ is the normalization of the representation R, defined as $\mathrm{Tr}(T_R^a T_R^b) = T(R)\delta^{ab}$. For the details of the numerical method used to determine coefficient $c_t^{(1,1)}$, we refer to the original literature where the method was developed and applied first for the pure gauge theory case in [51], and later for fundamental representation fermions in [51, 43].

N_c	rep.	$c_t^{(1,0)}$	$c_t^{(1,1)}$	$\tilde{c}_t^{(1)}$
2	**2**	$-0.0543(5)$	0.0192(2)	$-0.0101(3)$
2	**3**	$-0.0543(5)$	0.075(1)	$-0.0270(2)$
3	**3**	$-0.08900(5)$	0.0192(4)	$-0.0180(1)$
3	**8**	$-0.08900(5)$	0.113(1)	$-0.0405(3)$
3	**6**	$-0.08900(5)$	0.0946(9)	$-0.0450(3)$
4	**4**		0.0192(5)	$-0.0253(2)$

Table 1: The nonzero improvement coefficients for Schrödinger functional boundary conditions with electric background field for various gauge groups and fermion representations.

We have also plotted our results of $c_t^{(1,1)}$ scaled with $1/(2T(R))$ against (3.17) in figure 2. Although we did not achieve the accuracy of the original work [43], our results are fully compatible for fundamental representation fermions. The figure also clearly indicates that $c_t^{(1,1)}$ scales with $2T(R)$.

4. Non-perturbative tuning

The continuum physics we are interested in corresponds to massless fermions, so we need to simulate at zero physical quark mass. With Wilson fermions the bare quark mass is additively renormalized, and the zero of the physical quark mass corresponds to tuning the bare quark mass to a critical value, $m_0 = m_{\mathrm{cr}}$. This tuning is done nonperturbatively and allows for determination of the improvement coefficient c_{sw} simultaneously. Here we describe

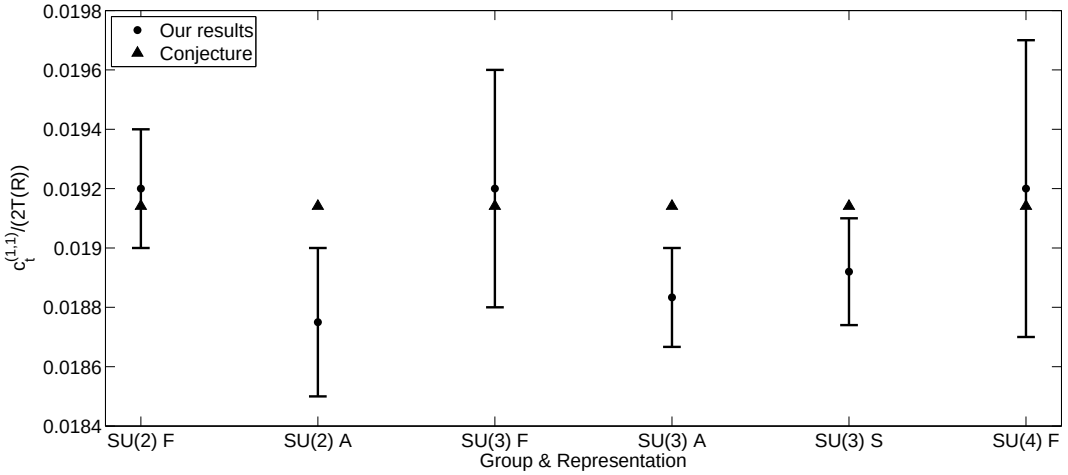

Figure 2: Our results of $c_t^{(1,1)}$ scaled with $2T(R)$ compared with conjectured value of $c_t^{(1,1)}/(2T(R))$.

the calculation of $c_{\rm sw}$ for $N_f = 2$ flavors of SU(2) fundamental and adjoint representation fermions.

In these simulations the fermion fields have the boundary conditions given in Eqs. (2.15,2.16). For the fundamental representation fermons we fix the gauge field Dirichlet boundary conditions at $x_0 = 0$ and $x_0 = T$ [41]:

$$U_k(x_0 = T) = \exp(iC'), \quad C' = -\frac{\pi}{4}\frac{a\sigma^3}{L} \tag{4.1}$$

$$U_k(x_0 = 0) = \exp(iC), \quad C = -\frac{3\pi}{4}\frac{a\sigma^3}{L}, \tag{4.2}$$

for $k = 1, 2, 3$. Because the boundary link matrices commute, we call these boundary conditions Abelian, in contrast to the non-Abelian (non-commuting) ones defined below.

The physical quark mass is defined via the partial conservation of the axial current (PCAC) relation,

$$M(x_0) = \frac{1}{2}\frac{\frac{1}{2}(\partial_0^* + \partial_0)f_A(x_0) + c_A a\partial_0^*\partial_0 f_P(x_0)}{f_P(x_0)} \equiv r(x_0) + c_A s(x_0), \tag{4.3}$$

where

$$A_\mu^a = \bar{\psi}(x)\gamma_5\gamma_\mu\frac{1}{2}\sigma^a\psi(x), \tag{4.4}$$

$$P^a = \bar{\psi}(x)\gamma_5\frac{1}{2}\sigma^a\psi(x), \tag{4.5}$$

$$f_A(x_0) = -a^6\sum_{\mathbf{y},\mathbf{z}}\langle A_0^a(x)\bar{\zeta}(\mathbf{y})\gamma_5\frac{1}{2}\sigma^a\zeta(\mathbf{z})\rangle, \tag{4.6}$$

$$f_P(x_0) = -a^6\sum_{\mathbf{y},\mathbf{z}}\langle P^a(x)\bar{\zeta}(\mathbf{y})\gamma_5\frac{1}{2}\sigma^a\zeta(\mathbf{z})\rangle. \tag{4.7}$$

Another set of correlation functions, f'_A and f'_P is defined via

$$f'_A(T-x_0) = -a^6 \sum_{\mathbf{y},\mathbf{z}} \langle A_0^a(x) \bar{\zeta}(\mathbf{y}) \gamma_5 \frac{1}{2} \sigma^a \zeta(\mathbf{z}) \rangle, \tag{4.8}$$

$$f'_P(T-x_0) = -a^6 \sum_{\mathbf{y},\mathbf{z}} \langle P^a(x) \bar{\zeta}(\mathbf{y}) \gamma_5 \frac{1}{2} \sigma^a \zeta(\mathbf{z}) \rangle. \tag{4.9}$$

The bare mass is tuned so that $M(T/2)$ vanishes. The $c_{\rm sw}$ term is tuned simultaneously using mass measurements at a different point in the bulk looking for variations of the order of the lattice spacing. Defining M' with obvious replacements of primes, it follows that the quantity

$$\Delta M(x_0) = M(x_0) - M'(x_0) \tag{4.10}$$

vanishes up to corrections of $\mathcal{O}(a^2)$ if both $c_{\rm sw}$ and c_A have their proper values. In order to recover the correct tree level behaviour we fix these quantities M and ΔM two their tree level values, measured by from a cold gauge configuration with $\kappa_c = 0.125$. This gives a small correction to the relations:

$$\Delta M(x_0) = M(x_0) - M'(x_0) - \delta = 0, M(x_0) = \delta_M \tag{4.11}$$

However, for the adjoint representation fermions there are complications which significantly reduce the effectiveness of the above method. Using Eq. (2.10) we immediately notice that the Abelian boundary matrices (4.1,4.2) are transformed into form

$$\widetilde{U}_k = \begin{pmatrix} \dots & \dots & 0 \\ \dots & \dots & 0 \\ 0 & 0 & 1 \end{pmatrix} \tag{4.12}$$

Thus, there is a component of the adjoint representation color vector which simply does not see the background field. This feature is independent of the color structure chosen for the boundary conditions. It turns out that regardless of how the fermion sources or the constant boundary conditions are chosen, at long distances the correlation functions behave as if there is no background field. In other words, the adjoint fermion correlation functions "see" the background electric field only at short distances. This significantly reduces the effectiviness of the background field method for tuning $c_{\rm sw}$.

This effect can be improved by using boundary conditions which maximize the difference between the two boundaries. We use the following asymmetric "non-Abelian" boundary conditions: links at the upper $x_0 = T$ boundary are chosen to be trivial

$$U(x_0 = T, k) = I \tag{4.13}$$

and at the lower boundary $x_0 = 0$ we use

$$U(x_0 = 0, k) = \exp(aC_k), \quad C_k = \frac{\pi}{2} \frac{\tau^k}{iL}. \tag{4.14}$$

This creates a strong chromomagnetic field at $x_0 = 0$ boundary. These boundary conditions do not fully cure the problem, but nevertheless provide enough leverage so that the PCAC mass relation can be used to tune $c_{\rm sw}$.

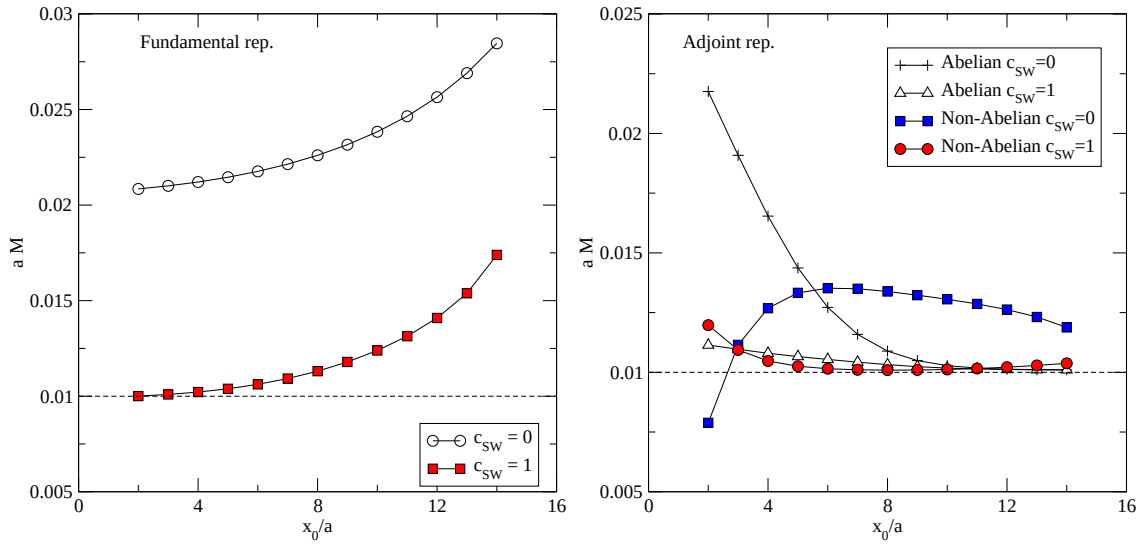

Figure 3: *Left:* Fundamental representation fermion mass $aM(x_0)$ measured from the classical gauge field configuration satisfying the Abelian boundary conditions (4.1, 4.2) on a $8^3 \times 16$-lattice. Bare mass is $am_0 = 0.01$, which is also aM in the continuum limit. Inclusion of the clover term ($c_{\rm sw} = 1$) significantly reduces the cutoff effects. *Right:* $aM(x_0)$ for adjoint representation fermions and for the Abelian boundary conditions (4.1), (4.2), and for the non-Abelian boundary conditions (4.13,4.14). Here the correlation functions between $c_{\rm sw} = 0$ and $c_{\rm sw} = 1$ differ significantly at long distances only for the non-Abelian boundary conditions.

This behaviour can be demonstrated already at the classical level: in figure 3 we show the PCAC fermion mass (4.3), measured using the classical minimum action gauge field configuration which satisfies the appropriate boundary conditions. The bare fermion mass has been set to $am_0 = 0.01$, and, in the absence of the background field or lattice cutoff effects, the PCAC measurement would yield precisely this value. However, with finite lattice spacing the non-trivial classical background field gives rise to cutoff effects, which moves the PCAC mass away from $aM = 0.01$. For the fundamental representation fermions and the Abelian boundary conditions (4.1), (4.2). (left panel in figure 3), we can observe that setting $c_{\rm sw} = 0$ (non-improved standard Wilson fermions) the measured mass values are far from the continuum limit, whereas using $c_{\rm sw} = 1$ (the correct value at the classical level) these effects are strongly reduced.

For the adjoint representation fermions the behaviour is very different, as shown on the right panel of fig. 3: using the Abelian boundary conditions the measured masses $aM(x_0)$ rapidly approach $0.01/a$ as x_0 increases, for both $c_{\rm sw} = 0$ or 1. This indicates that the correlation function lacks the sensitivity to $c_{\rm sw}$ and cannot be used for tuning it to the correct value.

On the other hand, with the non-Abelian boundary conditions (4.13,4.14) the correlation function remains sensitive to the value of $c_{\rm sw}$ to longer distances. The sensitivity remains in the mass asymmetry $\Delta M(x_0)$, (4.10), which can now be used to tune $c_{\rm sw}$. We note that these boundary conditions are useful only for determining $c_{\rm sw}$, not for evaluating the coupling constant.

In order to remove the dependence on c_A, for fundamental fermions, we consider

$$M(x_0, y_0) = r(x_0) - s(x_0)\frac{r(y_0) - r'(y_0)}{s(y_0) - s'(y_0)}, \tag{4.15}$$

which coincides with $M(x_0)$ up to $\mathcal{O}(a^2)$ corrections and is independent of c_A. With adjoint fermions this quantity suffers from large statistical fluctuations and is not useful. Instead we simply consider the quantity $M(x_0)$ and fix c_A to its perturbative value [44]

$$c_A = -0.00567(1)C_R g^2 + \mathcal{O}(g^4). \tag{4.16}$$

We then measure c_A separately to confirm the validity of our choice.

In order to evaluate $c_{\rm sw}$ we used the following routine: we choose lattice volume $L^3 \times T = 8^3 \times 16$ for both fundamental and adjoint representation fermions, and a set of values of the lattice coupling β. For fundamental fermions we measure $M = M(T/2, T/4)$ and $\Delta M = \Delta M(3T/4, T/4)$. For adjoint fermions we measure $M = M(T/2)$ and $\Delta M = \Delta M(3T/4)$ fixing c_A to its perturbative value.

1. For a given β, we choose initial $c_{\rm sw}$ (typically extrapolating from results obtained with previous values of β).

2. We choose a couple of values for κ, and determine by interpolation the critical value $\kappa_c(\beta, c_{\rm sw})$ where the fermion mass M is equal to the tree level value.

3. Once we have an estimate of the critical κ, we choose a new value for $c_{\rm sw}$ and repeat the search of κ_c.

4. At the same time, we measure $\Delta M(c_{\rm sw})$. Now we can linearly interpolate/extrapolate in $c_{\rm sw}$ so that ΔM vanishes, obtaining the desired value of $c_{\rm sw}$. Using simulations at this final $c_{\rm sw}$ we can relocate the critical κ, if desired, and verify the results of the interpolation.

The above tuning is done at small L/a, and the results are applied for all lattice sizes since the L/a dependence is expected to be weak. Furthermore, we only consider a range of β and fit the critical values to an interpolating function to obtain $m^c(\beta_L)$ and $c^c_{\rm sw}(\beta_L)$.

4.1 Measurement of $c_{\rm sw}$

In figures 4 and 5 we show our results for the clover coefficient $c_{\rm sw}$ for both fundamental and adjoint representations. The values of β used are $\beta = 2.5, 3, 4, 5, 6, 8$, and also $\beta = 2.25$ and 10 for the adjoint representation. To clarify the tuning method we provide the measurements of M and ΔM with adjoint fermions in table 2. In tables 3 and 4 we give our results for $c_{\rm sw}$ for fundamental and adjoint fermions respectively.

Finally, the measured values for $c_{\rm sw}$ can be fitted with a rational interpolating expression, which can used in simulations for this range of β-values. For fundamental representation fermions we use the perturbative 1-loop result $c_{\rm sw} = 1 + 0.1551(1)g^2 + O(g^4)$ [44] to constrain the fit:

$$c_{\rm sw} = \frac{1 - 0.090254g^2 - 0.038846g^4 + 0.028054g^6}{1 - (0.1551 + 0.090254)g^2}. \tag{4.17}$$

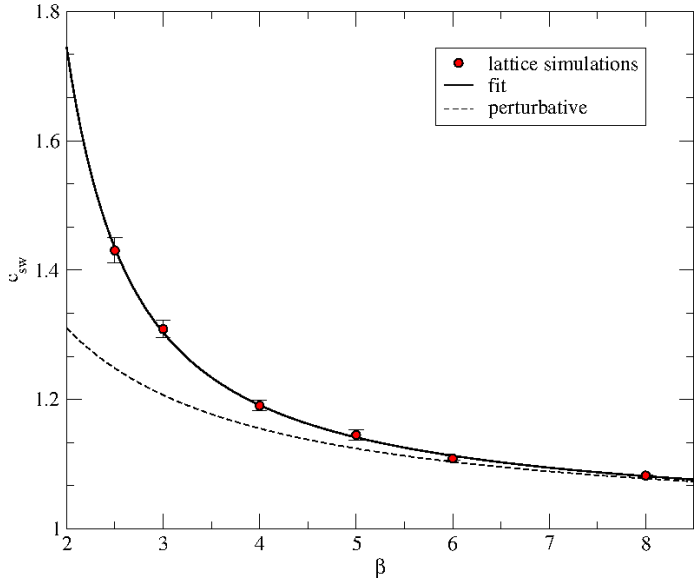

Figure 4: $c_{\rm sw}$ for two flavors of fundamental representation fermions. The solid line is the interpolating fit, Eq. (4.17), and the dashed line is the 1-loop perturbative value

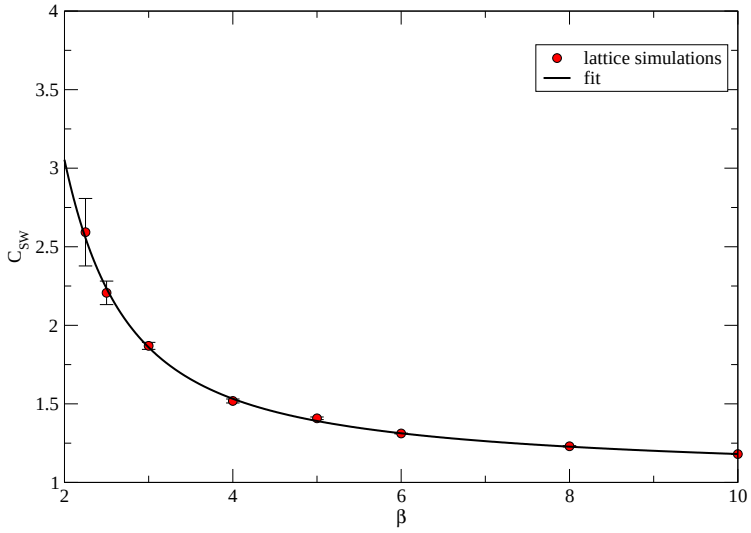

Figure 5: $c_{\rm sw}$ for two flavors of adjoint representation fermions, with the interpolating fit, Eq. (4.18).

For the adjoint representation the perturbative result is not known, and we obtain the fit result

$$c_{\rm sw} = \frac{1 + 0.032653g^2 - 0.002844g^4}{1 - 0.314153g^2}. \tag{4.18}$$

In both cases the interpolating fits are valid for $\beta \gtrsim 2.5$. For the adjoint fermions it is difficult to reach smaller β-values because $c_{\rm sw}$ grows rapidly, and while we were able to reach $\beta = 2.25$ the errors were too large to constrain the fit (4.18) further.

β	$c_{\rm sw}$	κ	aM	$a\Delta M$
10	1.16	0.1302552	0.00020(7)	−0.0004(1)
10	1.17208	0.1301818	0.00114(7)	−0.0002(1)
10	1.1774	0.1301818	0.00050(7)	0.0001(1)
10	1.17915	0.13017157	0.00037(10)	0.0002(2)
8	1.2	0.13171	−0.00156(8)	−0.0004(2)
8	1.225	0.13154	0.00031(8)	−0.0001(2)
8	1.227	0.1315265	0.00035(8)	0.0000(2)
8	1.23	0.1315265	−0.00018(9)	0.0000(2)
8	1.25	0.1315265	0.00003(8)	0.0003(2)
6	1.28	0.1340604	−0.00054(7)	−0.0007(1)
6	1.3	0.133903	0.00034(8)	−0.0003(1)
6	1.3135	0.1338131	0.00055(8)	−0.0001(1)
6	1.3143	0.1338131	0.0002510)	0.0001(1)
6	1.33	0.1338131	−0.00280(8)	0.0005(1)
5	1.3	0.1363278	0.0006(1)	−0.0015(3)
5	1.4	0.1356033	0.0007(1)	−0.0003(3)
5	1.4058	0.136	−0.0130(2)	0.0000(3)
5	1.5	0.1348774	0.0007(1)	0.0014(3)
4	1.45	0.1391039	0.0012(2)	−0.0008(3)
4	1.522	0.1385882	−0.0024(2)	0.0001(2)
4	1.6	0.1378078	0.0004(2)	0.0008(2)
3	1.6	0.145311	0.0002(2)	−0.0022(4)
3	1.75	0.1435289	0.0038(2)	−0.0005(3)
3	1.834	0.1426551	0.0018(2)	−0.0006(4)
3	1.9	0.1419574	0.0009(3)	0.0002(4)
3	2.1	0.1400727	0.0082(2)	0.0016(3)
2.5	1.5	0.1540744	0.0021(4)	−0.023(5)
2.5	2	0.147733	−0.0036(3)	−0.0005(4)
2.5	2.5	0.141683	0.0015(2)	0.0005(4)
2.5	2.7	0.139561	−0.0025(2)	0.0027(9)
2.25	1.5	0.1590893	0.0306(3)	−0.0019(6)
2.25	2.3	0.147733	−0.0004(3)	−0.0004(5)
2.25	2.5	0.141683	0.0033(3)	−0.0002(4)

Table 2: Results for the quark mass M and ΔM with two fermions in the adjoint representation

4.2 Non-Perturbative measurement of c_A

When measuring $c_{\rm sw}$ for adjoint fermions we chose to keep the coefficient c_A at the perturbative value. In figure 6 we show how the choice of c_A affect $\Delta M(3T/4)$ with certain choice of parameters. Typically c_A is between -0.005 and -0.01 at the range of β we explored. We see that even differences of this order have small effect to ΔM.

β	$c_{\rm sw}$	β	$c_{\rm sw}$
8	1.082(2)	4	1.190(8)
6	1.109(3)	3	1.309(13)
5	1.145(8)	2.5	1.430(19)

Table 3: Results for $c_{\rm sw}$ with two flavors of fermions in the fundamental representation

β	$c_{\rm sw}$	β	$c_{\rm sw}$
10	1.159(3)	4	1.476(17)
8	1.197(8)	3	1.805(23)
6	1.291(3)	2.5	2.059(74)
5	1.376(9)	2.25	2.593(215)

Table 4: Results for $c_{\rm sw}$ with two flavors of fermions in the adjoint representation

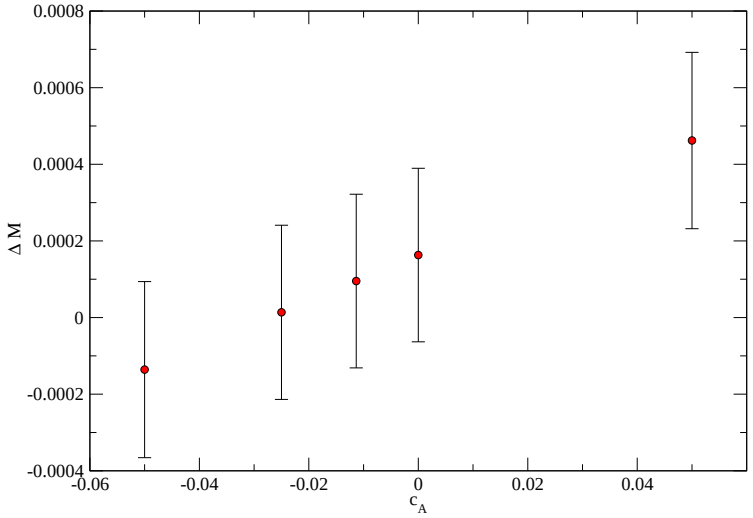

Figure 6: The dependence of $\Delta M(3T/4)$ of c_A. The measurement was done with $\beta = 4$ and $c_{\rm sw} = 1.522$.

To verify the accuracy of our choice we have also estimated a non-perturbative value for c_A. For this we have used the same improvement condition as in [45]. We do simulations with two different values of the fermion phase θ in the boundary conditions 2.16, using the measured values of $c_{\rm sw}$ and κ_c above. Without any discretisation errors the difference in the measured masses should be equal to the tree level value. Requiring that this condition is met, we can find an estimate of c_A.

From two simulations with $\theta = 0$ and $\theta = \pi/2$ we calculated the discretisation effect

$$\Delta M(c_A)' = M\left(x_0 = 8; \theta = 0, c_A\right) - M\left(x_0 = 8; \theta = \pi/2, c_A\right) - \delta, \tag{4.19}$$

where δ is the tree level value of the difference. It is similar to the tree level correction in equation 4.11 and is relatively small. These simulations were done using a trivial boundary condition, where all the boundary matrices were set to unity. Depending on the lattice coupling between 2000 and 35000 trajectories were performed for each value of θ.

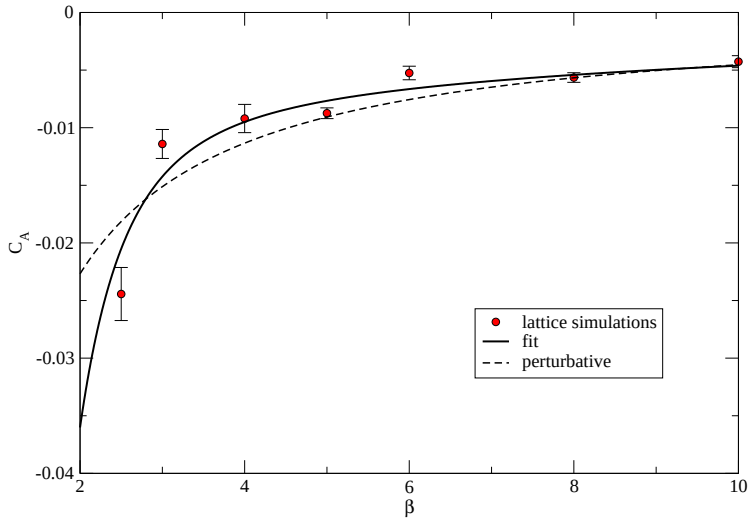

Figure 7: c_A for two flavors of adjoint fermions. The solid line is the interpolating fit, Eq. (4.17), and the dashed line is the 1-loop perturbative value

As the quark mass, and therefore $\Delta M'$ is simply linearly dependent on c_A, we can measure $\Delta M'$ for two of values of c_A to find the correct value where $\Delta M' = 0$.

β	c_A	β	c_A
10	$-0.0043(5)$	4	$-0.0092(12)$
8	$-0.0056(4)$	3	$-0.0114(13)$
6	$-0.0053(6)$	2.5	$-0.0244(23)$
5	$-0.0087(5)$		

Table 5: Results for c_A

The results for c_A are given in table 5 and depicted in figure 7. We see that in the region where we have measured c_{sw} and c_A, it is justified to use the perturbative value for c_A.

5. Conclusions and outlook

We have calculated $\mathcal{O}$-improvement of SU(2) gauge theory with two Wilson fermions in the fundamental or adjoint representation. The main results are the non-perturbative evaluation of the Sheikholeslami-Wohlert clover coefficient $c_{\rm sw}$ and the perturbative calculation of the boundary improvement terms needed for full improvement in the Schrödinger functional formalism. The result for $c_{\rm sw}$ is generally applicable to lattice simulations of these theories. We also verified that the axial current improvement coefficient c_A is well described by the 1-loop perturbative formula in the range of lattice spacings studied. In addition to the perturbative results on SU(2) gauge theory and adjoint fermions, we obtained results also for SU(3) and adjoint or sextet fermions which will be useful also for other groups studying these theories.

The main application for the improved action is more accurate lattice Monte Carlo analyses of the candidate theory for minimal walking technicolor, SU(2) gauge theory with two adjoint representation fermions. The boundary improvement terms permit improved measurement of the evolution of the coupling constant with the Schrödinger functional scheme. Indeed, in earlier unimproved analyses [17, 19] significant cutoff effects were observed at coarse lattices. The measurement of the coupling with the improved action is left for future work.

Acknowledgments

We thank R. Sommer and S. Sint for discussions and comments. This work is supported by the Academy of Finland grant 114371. The simulations were performed at the Finnish IT Center for Science (CSC), Espoo, Finland, and at EPCC, University of Edinburgh. Parts of the simulation program have been derived from the MILC lattice simulation program [53].

References

[1] H. Georgi, *Unparticle Physics*, Phys. Rev. Lett. **98**, 221601 (2007) [arXiv:hep-ph/0703260].

[2] H. Georgi, *Another Odd Thing About Unparticle Physics*, Phys. Lett. B **650**, 275 (2007) [arXiv:0704.2457 [hep-ph]]; K. Cheung, W. Y. Keung and T. C. Yuan, *Collider signals of unparticle physics*, Phys. Rev. Lett. **99**, 051803 (2007) [arXiv:0704.2588 [hep-ph]].

[3] F. Sannino and R. Zwicky, Phys. Rev. D **79** (2009) 015016 [arXiv:0810.2686 [hep-ph]].

[4] S. Weinberg, *Implications Of Dynamical Symmetry Breaking: An Addendum*, Phys. Rev. D **19**, 1277 (1979); L. Susskind, *Dynamics Of Spontaneous Symmetry Breaking In The Weinberg-Salam Theory*, Phys. Rev. D **20**, 2619 (1979).

[5] E. Eichten and K. D. Lane, *Dynamical Breaking Of Weak Interaction Symmetries*, Phys. Lett. B **90**, 125 (1980).

[6] C. T. Hill and E. H. Simmons, Phys. Rept. **381**, 235 (2003) [Erratum-ibid. **390**, 553 (2004)] [arXiv:hep-ph/0203079].

[7] F. Sannino, *Dynamical Stabilization of the Fermi Scale: Phase Diagram of Strongly Coupled Theories for (Minimal) Walking Technicolor and Unparticles*, arXiv:0804.0182 [hep-ph].

[8] B. Holdom, *Raising The Sideways Scale*, Phys. Rev. D **24**, 1441 (1981).

[9] K. Yamawaki, M. Bando and K. i. Matumoto, *Scale Invariant Technicolor Model And A Technidilaton*, Phys. Rev. Lett. **56**, 1335 (1986).

[10] T. W. Appelquist, D. Karabali and L. C. R. Wijewardhana, *Chiral Hierarchies And The Flavor Changing Neutral Current Problem In Technicolor*, Phys. Rev. Lett. **57**, 957 (1986);

[11] T. Appelquist, A. Ratnaweera, J. Terning and L. C. R. Wijewardhana, *The phase structure of an SU(N) gauge theory with N(f) flavors,* Phys. Rev. D **58**, 105017 (1998) [arXiv:hep-ph/9806472].

[12] F. Sannino and K. Tuominen, *Orientifold theory dynamics and symmetry breaking*, Phys. Rev. D **71**, 051901 (2005) [arXiv:hep-ph/0405209]; D. D. Dietrich, F. Sannino and K. Tuominen, *Light composite Higgs from higher representations versus electroweak precision measurements: Predictions for LHC*, Phys. Rev. D **72**, 055001 (2005) [arXiv:hep-ph/0505059]; D. D. Dietrich and F. Sannino, *Conformal window of SU(N) gauge theories with fermions in higher dimensional representations*, Phys. Rev. D **75**, 085018 (2007) [arXiv:hep-ph/0611341].

[13] S. Catterall and F. Sannino, *Minimal walking on the lattice*, Phys. Rev. D **76**, 034504 (2007) [arXiv:0705.1664 [hep-lat]].

[14] A. J. Hietanen, J. Rantaharju, K. Rummukainen and K. Tuominen, *Spectrum of SU(2) lattice gauge theory with two adjoint Dirac flavors,* JHEP **0905**, 025 (2009) [arXiv:0812.1467 [hep-lat]]

[15] L. Del Debbio, A. Patella and C. Pica, *Higher representations on the lattice: numerical simulations. SU(2) with adjoint fermions*, Phys. Rev. D **81** (2010) 094503 [arXiv:0805.2058 [hep-lat]].

[16] S. Catterall, J. Giedt, F. Sannino and J. Schneible, *Phase diagram of SU(2) with 2 flavors of dynamical adjoint quarks,* JHEP **0811**, 009 (2008) [arXiv:0807.0792 [hep-lat]].

[17] A. J. Hietanen, K. Rummukainen and K. Tuominen, *Evolution of the coupling constant in SU(2) lattice gauge theory with two adjoint fermions,* Phys. Rev. D **80**, 094504 (2009) [arXiv:0904.0864 [hep-lat]].

[18] F. Bursa, L. Del Debbio, L. Keegan, C. Pica and T. Pickup, *Mass anomalous dimension in SU(2) with two adjoint fermions,* Phys. Rev. D **81**, 014505 (2010) [arXiv:0910.4535 [hep-ph]];

[19] L. Del Debbio, B. Lucini, A. Patella, C. Pica and A. Rago, *Conformal vs confining scenario in SU(2) with adjoint fermions,* Phys. Rev. D **80**, 074507 (2009) [arXiv:0907.3896 [hep-lat]].

[20] L. Del Debbio, B. Lucini, A. Patella, C. Pica and A. Rago, *The infrared dynamics of Minimal Walking Technicolor,* Phys. Rev. D **82** (2010) 014510 [arXiv:1004.3206 [hep-lat]].

[21] L. Del Debbio, B. Lucini, A. Patella, C. Pica and A. Rago, *Mesonic spectroscopy of Minimal Walking Technicolor,* Phys. Rev. D **82** (2010) 014509 [arXiv:1004.3197 [hep-lat]].

[22] E. Kerrane *et al.*, *Improved Spectroscopy of Minimal Walking Technicolor,* arXiv:1011.0607 [hep-lat].

[23] Y. Shamir, B. Svetitsky and T. DeGrand, *Zero of the discrete beta function in SU(3) lattice gauge theory with color sextet fermions*, Phys. Rev. D **78**, 031502 (2008) [arXiv:0803.1707 [hep-lat]];

[24] T. DeGrand, Y. Shamir and B. Svetitsky, *Phase structure of SU(3) gauge theory with two flavors of symmetric-representation fermions,* Phys. Rev. D **79**, 034501 (2009) [arXiv:0812.1427 [hep-lat]];

[25] T. DeGrand, Y. Shamir and B. Svetitsky, *Running coupling and mass anomalous dimension of SU(3) gauge theory with two flavors of symmetric-representation fermions,* Phys. Rev. D **82**, 054503 (2010) [arXiv:1006.0707 [hep-lat]].

[26] Z. Fodor, K. Holland, J. Kuti, D. Nogradi and C. Schroeder, *Chiral properties of SU(3) sextet fermions,* JHEP **0911**, 103 (2009) [arXiv:0908.2466 [hep-lat]].

[27] J. B. Kogut and D. K. Sinclair, *Thermodynamics of lattice QCD with 2 flavours of colour-sextet quarks: A model of walking/conformal Technicolor,* Phys. Rev. D **81**, 114507 (2010) [arXiv:1002.2988 [hep-lat]].

[28] P. H. Damgaard, U. M. Heller, A. Krasnitz and P. Olesen, *On lattice QCD with many flavors,* Phys. Lett. B **400**, 169 (1997) [arXiv:hep-lat/9701008].

[29] T. Appelquist, G. T. Fleming and E. T. Neil, *Lattice Study of the Conformal Window in QCD-like Theories*, Phys. Rev. Lett. **100**, 171607 (2008) [arXiv:0712.0609 [hep-ph]].

[30] T. Appelquist, G. T. Fleming and E. T. Neil, *Lattice Study of Conformal Behavior in SU(3) Yang-Mills Theories,* Phys. Rev. D **79**, 076010 (2009) [arXiv:0901.3766 [hep-ph]].

[31] Z. Fodor, K. Holland, J. Kuti, D. Nogradi and C. Schroeder, *Nearly conformal gauge theories in finite volume,* Phys. Lett. B **681**, 353 (2009) [arXiv:0907.4562 [hep-lat]];

[32] A. Deuzeman, M. P. Lombardo and E. Pallante, *The physics of eight flavours*, Phys. Lett. B **670**, 41 (2008) [arXiv:0804.2905 [hep-lat]];

[33] A. Deuzeman, M. P. Lombardo and E. Pallante, *Evidence for a conformal phase in SU(N) gauge theories,* Phys. Rev. D **82**, 074503 (2010) [arXiv:0904.4662 [hep-ph]];

[34] E. Itou *et al.*, *Search for the IR fixed point in the Twisted Polyakov Loop scheme (II)* arXiv:1011.0516 [hep-lat].

[35] X. Y. Jin and R. D. Mawhinney, *Evidence for a First Order, Finite Temperature Phase Transition in 8 Flavor QCD,* PoS **LATTICE2010**, 055 (2010) [arXiv:1011.1511 [hep-lat]].

[36] M. Hayakawa, K. I. Ishikawa, Y. Osaki, S. Takeda, S. Uno and N. Yamada, *Running coupling constant of ten-flavor QCD with the Schródinger functional method*, arXiv:1011.2577 [hep-lat].

[37] A. Hasenfratz, *Conformal or Walking? Monte Carlo renormalization group studies of SU(3) gauge models with fundamental fermions,* Phys. Rev. D **82**, 014506 (2010) [arXiv:1004.1004 [hep-lat]].

[38] A. Hasenfratz, *Investigating the critical properties of beyond-QCD theories using Monte Carlo Renormalization Group matching,* Phys. Rev. D **80**, 034505 (2009) [arXiv:0907.0919 [hep-lat]].

[39] F. Bursa, L. Del Debbio, L. Keegan, C. Pica and T. Pickup, *Mass anomalous dimension and running of the coupling in SU(2) with six fundamental fermions*, arXiv:1010.0901 [hep-ph].

[40] H. Ohki *et al.*, *Study of the scaling properties in SU(2) gauge theory with eight flavors,* arXiv:1011.0373 [hep-lat].

[41] M. Luscher, R. Sommer, U. Wolff and P. Weisz, *Computation Of The Running Coupling In The SU(2) Yang-Mills Theory,* Nucl. Phys. B **389**, 247 (1993) [arXiv:hep-lat/9207010].

[42] S. Sint, *One Loop Renormalization Of The QCD Schrodinger Functional,* Nucl. Phys. B **451**, 416 (1995) [arXiv:hep-lat/9504005].

[43] S. Sint and R. Sommer, *The Running coupling from the QCD Schrodinger functional: A One loop analysis,* Nucl. Phys. B **465** (1996) 71 [arXiv:hep-lat/9508012].

[44] M. Luscher and P. Weisz, *O(a) improvement of the axial current in lattice QCD to one-loop order of perturbation theory,* Nucl. Phys. B **479** (1996) 429 [arXiv:hep-lat/9606016].

[45] M. Luscher, S. Sint, R. Sommer, P. Weisz and U. Wolff, *Non-perturbative O(a) improvement of lattice QCD,* Nucl. Phys. B **491**, 323 (1997) [arXiv:hep-lat/9609035].

[46] K. Jansen, *Lattice QCD: a critical status report*, arXiv:0810.5634 [hep-lat].

[47] T. Karavirta, A. M. Mykkanen, J. Rantaharju, K. Rummukainen and K. Tuominen, *Perturbative improvement of SU(2) gauge theory with two Wilson fermions in the adjoint representation,* arXiv:1011.2057 [hep-lat];

[48] A. Mykkanen, J. Rantaharju, K. Rummukainen, T. Karavirta and K. Tuominen, *Non-perturbatively improved clover action for SU(2) gauge + fundamental and adjoint representation fermions,* arXiv:1011.1781 [hep-lat].

[49] B. Sheikholeslami and R. Wohlert, *Improved Continuum Limit Lattice Action For QCD With Wilson Fermions,* Nucl. Phys. B **259** (1985) 572.

[50] Y. Shamir, B. Svetitsky and E. Yurkovsky, *Improvement via hypercubic smearing in triplet and sextet QCD,* arXiv:1012.2819 [hep-lat].

[51] M. Luscher, R. Narayanan, P. Weisz and U. Wolff, *The Schrodinger functional: A Renormalizable probe for nonAbelian gauge theories,* Nucl. Phys. B **384**, 168 (1992) [arXiv:hep-lat/9207009].

[52] M. Luscher, R. Sommer, P. Weisz *et al.*, *A Precise determination of the running coupling in the SU(3) Yang-Mills theory,* Nucl. Phys. **B413** (1994) 481-502. [hep-lat/9309005].

[53] http://physics.utah.edu/∼detar/milc.html

HIP-2012-05/TH
NSF-KITP-12-013

Casimir scaling and renormalization of Polyakov loops in large-N gauge theories

Anne Mykkänen[a], Marco Panero[a,b] and Kari Rummukainen[a]

[a] *Department of Physics and Helsinki Institute of Physics*
P.O. Box 64, FI-00014 University of Helsinki, Finland

[b] *Kavli Institute for Theoretical Physics*
University of California, Santa Barbara, CA 93106, USA

E-mail: anne-mari.mykkanen@helsinki.fi, marco.panero@helsinki.fi, kari.rummukainen@helsinki.fi

Abstract

We study Casimir scaling and renormalization properties of Polyakov loops in different irreducible representations in SU(N) gauge theories; in particular, we investigate the approach to the large-N limit, by performing lattice simulations of Yang-Mills theories with an increasing number of colors, from 2 to 6. We consider the twelve lowest irreducible representations for each gauge group, and find strong numerical evidence for nearly perfect Casimir scaling of the bare Polyakov loops in the deconfined phase. Then we discuss the temperature dependence of renormalized loops, which is found to be qualitatively and quantitatively very similar for the various gauge groups. In particular, close to the deconfinement transition, the renormalized Polyakov loop increases with the temperature, and its logarithm reveals a characteristic dependence on the inverse of the square of the temperature. At higher temperatures, the renormalized Polyakov loop overshoots one, reaches a maximum, and then starts decreasing, in agreement with weak-coupling predictions. The implications of these findings are discussed.

PACS numbers: 12.38.Gc, 11.15.Ha, 11.10.Wx, 11.15.Pg, 12.38.Aw

1 Introduction and motivation

The change of state to a deconfined phase at high temperatures or densities is a very important phenomenon in quantum chromodynamics (QCD) and in other non-Abelian gauge theories. While at zero and low temperatures the physical states are color-singlet hadronic states, in the high-temperature limit the physical running coupling becomes small, due to asymptotic freedom, and one expects that the physics should be described in terms of a gas of weakly interacting quarks and gluons [1]: the quark-gluon plasma (QGP) [2]. These two qualitatively different phases should be separated by a phase transition or a crossover, which has been searched for in an extensive experimental heavy-ion collision programme since the 1980's. The results obtained at SPS, RHIC and LHC during the last decade show, indeed, convincing evidence for the creation of a new state of matter at temperatures about 160 MeV, which behaves as an almost ideal fluid [3]. The experimental research on the QCD phase diagram will be continued and extended at FAIR and NICA.

On the theoretical side, however, the quantitative understanding of the QCD plasma is still an open problem. One of the reasons for this is that the deconfined plasma retains some non-perturbative features even in the limit of high temperatures T. In particular, the presence of severe infrared divergences in weak-coupling expansions for thermal gauge theories leads to non-analytical properties of the perturbative series for various physical observables, and to a break-down of the correspondence between loop expansions and expansions in powers of the coupling [4]. As a consequence, the long-wavelength modes of the QGP are strongly coupled at all temperatures, and thus cannot be treated perturbatively—see ref. [5] for a review. Finally, at the typical temperatures probed in experiments, the physical coupling of QCD turns out to be relatively small, but not extremely so, and perturbative predictions fail close to the deconfinement temperature [6].

For these reasons, the theoretical study of the QGP at temperatures close to the deconfining transition is usually addressed with non-perturbative methods, including, in particular, numerical simulations on the lattice [7]. During the last decade, lattice computations of the equation of state in QCD with light dynamical quarks have reached high levels of precision, and showed that the deconfinement at finite temperature and vanishing quark chemical potential (for physical values of the quark masses) is a crossover, rather than a genuine phase transition. In fact, in QCD with quarks of finite mass there is no exact symmetry-breaking pattern to characterize the deconfinement.

By contrast, pure SU(N) Yang-Mills theories (which capture most of the qualitative features of the physics of deconfinement) provide much a cleaner theoretical setup: in the Euclidean formulation, it is easy to see that the Lagrangian of SU(N) Yang-Mills theories at finite temperature is invariant under a global symmetry associated with the center of the gauge group $\mathbb{Z}_N$ [8]. The order parameter for this symmetry is the trace of the temporal Wilson line, or Polyakov loop [9]:

$$L = \langle \mathrm{Tr}\, L(\vec{x}) \rangle = \left\langle \mathrm{Tr}\, \mathcal{P} \exp \left[i g_0 \int_0^{1/T} \mathrm{d}\tau A_0(\tau, \vec{x}) \right] \right\rangle . \tag{1}$$

In the thermodynamic limit, the ground-state expectation value of L is exactly vanishing in the

low-temperature phase, while it becomes non-zero above the critical deconfinement temperature T_c, signaling the spontaneous breakdown of center symmetry. Although L, *per se*, is not a physical observable, it can be interpreted as the trace of the propagator of an external, infinitely massive probe color charge located at $\vec{x}$: a vanishing L in the $\mathbb{Z}_N$-symmetric ground state at low temperatures $T < T_c$ means that the expectation value of a static color charge is zero, and hence the system is confined. On the contrary, L is non-zero in the high-temperature phase at $T > T_c$, corresponding to a finite free energy for the probe color charge in the deconfined phase. Thus, L has the meaning of an order parameter for the finite-temperature deconfinement transition in Yang-Mills theory. Another possible order parameter for the transition is given by the two-point Polyakov loop correlation function: across the phase transition, it changes from confining to exponentially screened. The Polyakov loop correlation function extracted from lattice simulations at finite temperature is often used as an input for effective potential models for quarkonia [10]; however, certain subtleties related to the connection between the real- and the imaginary-time formalism, and to the spectral decomposition into singlet and octet contributions to the corresponding free energies have recently been pointed out in the literature [11].

Note that the free energy associated with the *bare* Polyakov loop defined by eq. (1) is a divergent quantity, and hence needs to be renormalized [12].

In general, in SU(N) Yang-Mills theory the Polyakov loop is an order parameter for a probe charge in a generic irreducible representation of the gauge group with non-zero N-ality (i.e., a representation transforming non-trivially under the center of the group). The free energy associated with charges in different irreducible representations is expected to be proportional to the eigenvalue of the corresponding quadratic Casimir operator $\langle C_2 \rangle$ [13]. This property is called "Casimir scaling": it is not specific to Polyakov loops, and indeed it has been studied for various other observables [14] (see also ref. [15] for a discussion). For the Polyakov loop, perturbative calculations predict Casimir scaling to hold at the lowest orders [16] (deviations from Casimir scaling are predicted to occur only at $O(g^6)$).

In this work, we study the behavior of bare and renormalized Polyakov loops in non-Abelian gauge theories with a different number of colors, from 2 to 6, discussing various renormalization methods, and comparing our results to those of recent, similar studies for SU(3) [17–19] and SU(2) [20–22] Yang-Mills theories. In particular, we investigate the features that emerge when N is large. The motivations for looking at the limit of a large number of colors are manifold. First of all, the large-N limit of QCD at fixed 't Hooft coupling $\lambda = g^2 N$ and fixed number of flavors N_f is known to lead to dramatic mathematical simplifications [23]. For the phase diagram of QCD-like theories, the large-N limit has also interesting implications for new phases at high density [24]. Furthermore, it plays a technically crucial rôle in holographic computations, inspired by the conjectured equivalence of maximally supersymmetric Yang-Mills theory with $\mathcal{N} = 4$ supercharges in four dimensions and supersymmetric type IIB string theory in a 10-dimensional $AdS_5 \times S^5$ spacetime [25]. This conjecture relates the large-N limit of the strongly coupled gauge theory to the classical gravity limit of string theory in a five-dimensional anti-de Sitter spacetime, which can be studied analytically. While at zero temperature the $\mathcal{N} = 4$ theory is qualitatively very different from QCD, there are arguments suggesting that at finite temperature the two theories should share at least some qualitative (or semi-quantitative) physical features [26].

Calculations based on the gauge/string duality have also been extended to various other models, which mimic the features of QCD either by breaking explicitly some of the symmetries of the $\mathcal{N} = 4$ theory using some additional ingredients ("top-down" approach), or by constructing some *ad hoc* five-dimensional gravity model, which should reproduce the properties of QCD ("bottom-up" approach). These models are often used to study analytically certain features of the strongly coupled quark-gluon plasma [27].

One important technical aspect in all holographic computations is that they are based on the approximation of an infinite number of colors in the gauge theory: this limit allows one to neglect loop effects in the dual string theory, i.e. to reduce it to its classical limit. Recent lattice studies have showed that the large-N limit is indeed a good approximation for the physical SU(3) case, both as it concerns spectral and thermal observables [28]; remarkably, this also holds for theories in $2+1$ spacetime dimensions [29]. However, the validity of the infinite-N approximation is, in general, a non-trivial issue, which can depend on the observable considered, and should be studied on a case-by-case basis.

In the context of gauge/string duality, the behavior of the renormalized Polyakov loop as a function of the temperature has been recently discussed in refs. [30–32]. In particular, in ref. [30] it was argued that, in strongly coupled theories with a holographic dual, the renormalized Polyakov loop should be monotonically increasing with T. This is in contrast with perturbative computations [16], which predict that the leading-order correction to the free limit is positive, and hence that the renormalized loop $L^{\rm ren}$ should tend to unity *from above* in the high-temperature limit. However, it should be noted that these two theoretical predictions are expected to hold in the strong- and in the weak-coupling regime, respectively. A holographic prediction for the renormalized Polyakov loop was worked out analytically in ref. [31], using a simple holographic model with one deformation parameter [33]. This work found that, at the leading order in a high-temperature expansion, the logarithm of the Polyakov loop in the strong coupling regime should be given by the sum of a constant plus a term proportional to $(T_c/T)^2$, an effect which has also been observed and discussed in refs. [34–36].

The properties of renormalized Polyakov loops in theories based on different gauge groups are also of interest for effective models of the quark-gluon plasma in the region near T_c, see refs. [18,37,38] and references therein. In particular, the behavior in the large-N limit may reveal analogies with the third-order transition that one finds in $1 + 1$ dimensions [39]. Moreover, at large N one expects that different irreducible representations become equivalent, up to $O(1/N)$ corrections: for example, the two-index symmetric and antisymmetric representations are expected to be equivalent for $N \to \infty$. Furthermore, using the group theoretical tools of composite representations [40] (see the appendix A for details), it is possible to show that in the large-N limit the eigenvalue of the quadratic Casimir remains $O(N)$.

Finally, the finite-temperature properties of strongly coupled gauge theories based on different gauge groups and with *dynamical* fermions in various representations are also interesting for extended technicolor models [41].

With this motivation, in this work we address a first-principle lattice study of Polyakov loops at finite temperature in SU(N) gauge theories with a different number of colors N, and for several irreducible representations. In particular, we consider the twelve lowest non-trivial irreducible

representations of each gauge group, and investigate the Casimir scaling at temperatures close to the deconfinement transition. Then we define non-perturbatively renormalized Polyakov loops, discussing various renormalization methods that have recently been proposed in the literature. While all our computations are performed in the setup of the pure Yang-Mills theory, it is worth remarking that, in the 't Hooft limit, the dynamics of gluons dominates, with the contributions from virtual quark loops suppressed by powers of $1/N$: the large-N limit of QCD is a unitary quenched theory, and by virtue of this, in this limit it is legitimate to consider only the glue sector of the theory on the lattice. This allows one to avoid the complications arising from lattice fermions, and to achieve a smoother approach to the planar limit (the leading-order finite-N corrections in the glue sector are proportional to $1/N^2$).

In section 2 we define the setup of our lattice computations and the method to extract the renormalized Polyakov loop free energies. Our results are presented in section 3, while in section 4 we discuss their implications, and summarize our findings. Some useful group-theoretical formulæ are listed in the appendix A.

Preliminary results of this study were presented in ref. [42].

2 Lattice simulation setup

Our numerical simulations are based on the regularization of SU(N) Yang-Mills theories with $N =$ 2, 3, 4, 5 and 6 colors on a four-dimensional Euclidean hypercubic, isotropic lattice Λ of spacing a, with periodic boundary conditions in all directions. We use natural units ($\hbar = c = k_{\rm B} = 1$), so that the temperature equals the inverse of the size of the system in the compactified Euclidean time direction: $T = 1/(aN_t)$, and denote the spatial volume of the lattice as $V = (aN_s)^3$. For most of our simulations at finite temperature, we used lattices characterized by an aspect ratio $N_s/N_t \geq 4$, which provides a good approximation of the thermodynamic limit [43]. The fundamental degrees of freedom in the lattice regularization of the theory are a discrete (and finite, if one considers a finite hypervolume) set of $U_\mu(x)$ matrices in the $N \times N$ representation of the group, which are defined on (and represent parallel transporters along) the oriented bonds between nearest-neighbor sites on the lattice. The functional integral defining the continuum partition function of the system is traded for a well-defined, finite, multi-dimensional ordinary integral:

$$Z = \int \prod_{x \in \Lambda} \prod_{\alpha=1}^{4} \mathrm{d}U_\alpha(x) e^{-S_{\rm L}^{\rm E}}, \tag{2}$$

where $\mathrm{d}U_\alpha(x)$ is the Haar measure for each $U_\alpha(x) \in \mathrm{SU}(N)$ link matrix, and $S_{\rm L}^{\rm E}$ denotes a gauge-invariant lattice action. The simplest choice for $S_{\rm L}^{\rm E}$ is given by the Wilson gauge action [44]:

$$S_{\rm W} = \beta \sum_{x \in \Lambda} \sum_{1 \leq \mu < \nu \leq 4} \left[1 - \frac{1}{N} \mathrm{Re}\,\mathrm{Tr}\, U_{\mu,\nu}^{1,1}(x) \right], \tag{3}$$

with $\beta = 2N/g_0^2$ and:

$$U_{\mu,\nu}^{1,1}(x) = U_\mu(x) U_\nu(x + a\hat{\mu}) U_\mu^\dagger(x + a\hat{\nu}) U_\nu^\dagger(x). \tag{4}$$

However, in our study we used the tree-level improved gauge action [45, 46]:

$$S_{\rm imp} = \beta \sum_{x\in\Lambda} \sum_{1\le\mu<\nu\le 4} \left\{ \frac{3}{2} - \frac{1}{N} {\rm Re\,Tr} \left[\frac{5}{3} U^{1,1}_{\mu,\nu}(x) - \frac{1}{12} U^{1,2}_{\mu,\nu}(x) - \frac{1}{12} U^{1,2}_{\nu,\mu}(x) \right] \right\}, \tag{5}$$

where:

$$U^{1,2}_{\mu,\nu}(x) = U_\mu(x) U_\nu(x + a\hat{\mu}) U_\nu(x + a\hat{\mu} + a\hat{\nu}) U^\dagger_\mu(x + 2a\hat{\nu}) U^\dagger_\nu(x + a\hat{\nu}) U^\dagger_\nu(x). \tag{6}$$

Assuming that the $U_\mu(x)$ group variables are related to the continuum gauge fields $A^a_\mu(x)t_a$ via: $U_\mu(x) = \exp[iag_0 A^a_\mu(x + a\hat{\mu}/2)t_a]$, it is straightforward to show that both $S_{\rm W}$ and $S_{\rm imp}$ tend to the Yang-Mills action in the continuum limit $a \to 0$, but the tree-level improved action defined by eq. (5) is characterized by smaller discretization effects than those of the Wilson action. Expectation values of gauge-invariant physical observables $\mathcal{O}$ on the lattice are defined by:

$$\langle \mathcal{O} \rangle = \frac{1}{Z} \int \prod_{x\in\Lambda} \prod_{\mu=1}^{4} {\rm d}U_\mu(x)\ \mathcal{O}\ e^{-S^{\rm E}_{\rm L}} \tag{7}$$

and can be estimated numerically by Monte Carlo sampling over a finite set of $\{U_\alpha(x)\}$ configurations; in the following, we denote the number of configurations used in our computations as $n_{\rm conf}$. The algorithm we used to generate the configurations is based on a $3 + 1$ combination of local overrelaxation [47] and heat-bath [48] updates on $N(N-1)/2$ SU(2) subgroups of SU(N) [49]. The parameters of our lattice simulations are shown in tab. 1.

N	N_s	N_t	$\beta_{\rm min}$	$\beta_{\rm max}$	n_β	$n_{\rm conf}$
2	20	5	1.5	16.5	46	2.5×10^4
3	20	5	4	7.8	20	1.8×10^4
4	20	5	7	7.45	4	2.5×10^4
	20	5	7.6	15.03	40	3×10^4
	24	5	7	9.85	20	2×10^4
	16	16	7.25	9.05	11	3×10^3
5	20	5	12	16.6	30	2×10^4
	16	16	12.1	13.7	9	8×10^3
6	20	5	17	25.6	40	2×10^4

Table 1: Parameters of the lattice simulations used in this work. N denotes the number of colors, N_s and N_t are the number of sites along the space-like and time-like sizes of the lattice, n_β is the number of β-values that were simulated, in the $\beta_{\rm min} \le \beta \le \beta_{\rm max}$ interval. For each set of parameters, the number of thermalized configurations, that we used in our numerical estimates, is shown in the last column.

Converting the simulation results to physical units requires a definition of the lattice scale. In order to set the scale for our simulations with the improved action, we calculated the $T = 0$ static potential in lattice units from expectation values of Wilson loops $\langle W(r, L)\rangle$:

$$V(r) = a^{-1} \lim_{L\to\infty} \ln \frac{\langle W(r, L - a)\rangle}{\langle W(r, L)\rangle}. \tag{8}$$

In particular, we extracted the potential from Wilson loops defined from smeared links, using five levels of smearing for the spacelike links (leaving the timelike links unsmeared). The values of $V(r)$ thus obtained are then fitted to the Cornell potential:

$$V(r) = \sigma r + V_0 + \frac{\gamma}{r}, \tag{9}$$

enabling one to extract σ (as well as V_0 and γ) in lattice units; statistical errors are estimated with a jackknife analysis. All fits give $\chi^2_{\rm red}$ values close to 1, and the γ parameter is always very close to the bosonic string prediction: $\gamma = -\pi/12$ [50] (see fig. 1 in ref. [42]).

Note that this non-perturbative definition of the scale is not unique: in general, it would be equally legitimate to define the value of a (for a given β), using the lattice results for a different dimensionful physical observable—for example, the critical temperature T_c [51]. On a finite-spacing lattice, different physical observables are generally affected by different discretization artifacts, and hence lead to slightly different definitions of the scale. This ambiguity is a systematic effect in the scale determination, but the associated relative uncertainty is numerically small, and vanishes in the continuum limit $a \to 0$.

On the lattice, the trace of the bare Polyakov loop in the irreducible representation r can be defined as:

$$\mathrm{Tr} \prod_{n_t=1}^{N_t} U_t^{(r)}(\vec{x}, an_t) \ , \tag{10}$$

where $g^{(r)}$ denotes the value of the group element g in the irreducible representation r. Note that the matrix elements of a generic $g^{(r)}$ can be easily obtained from those of g in the defining representation, by means of basic relations of representation theory. In particular, the characters of group elements in different irreducible representations can be easily expressed using Young calculus and the Weyl formula [52] (see the appendix A for details).

Note, however, that, due to the finiteness of the number of degrees of freedom on any finite lattice, the expectation value of the operator defined in eq. (10) would always be vanishing, both in the confining and in the deconfined phase. In the latter, in particular, the barriers separating different center sectors in the phase space are always finite for a finite lattice, so that any (sufficiently long, ergodic) simulation would probe all center sectors, leading to a vanishing expectation value for the average Polyakov loop. Since all numerical simulations are necessarily performed on finite lattices, it is more convenient to compute the expectation value of the *modulus* of the average Polyakov loop on each gauge configuration:

$$\left| \frac{1}{N_s^3} \sum_{\vec{x}} \mathrm{Tr} \prod_{n_t=1}^{N_t} U_t^{(r)}(\vec{x}, an_t) \right| \ . \tag{11}$$

Although this quantity is not an exact order parameter, it is an efficient probe of the deconfinement transition (for any irreducible representation r of non-zero N-ality), since its expectation value tends to zero in the confining phase, while it remains finite in the deconfined phase. Henceforth, we use eq. (11) to define the expectation values of bare Polyakov loops in our lattice simulations.

3 Results

3.1 Setting the scale

To determine the scale for our simulations with the tree-level improved lattice action, we fit our results for $a^2\sigma$ (as extracted from Cornell fits of the $T = 0$ potential using smeared Wilson loops) at the largest couplings to the functional form:

$$a^2\sigma = \exp\{-[A_0 + A_1(\beta - \beta_0) + A_2(\beta - \beta_0)^2 + A_3(\beta - \beta_0)^3]\}, \tag{12}$$

where $\beta = 2N/g_0^2$, and β_0 is an arbitrary reference value in the β-range of our simulations.

As an example, fitting the SU(3) data taken from ref. [46] to eq. (12) (choosing $\beta_0 = 4.3$) yields:

$$a^2\sigma = \exp\left\{-2.660(12) - 3.145(66)\cdot(\beta - 4.3) + 0.97(11)\cdot(\beta - 4.3)^2 - 0.33(26)\cdot(\beta - 4.3)^3\right\}, \tag{13}$$

with $\chi^2_{\rm red} = 0.34$. The corresponding data, together with the fitted curve, are shown in the top panel of fig. 1.

Similarly, our data for the SU(4) gauge group yield:

$$a^2\sigma = \begin{cases} \exp\left\{-3.894(38) - 1.21(14)(\beta - 9) - 0.41(16)(\beta - 9)^2 - 0.320(55)(\beta - 9)^3\right\} & \text{for } \beta < 8 \\ \exp\{-1.165(29)\beta + 6.54(23)\} & \text{for } \beta \geq 8 \end{cases}, \tag{14}$$

with $\chi^2_{\rm red} = 1.22$, and are shown in the central panel of fig. 1, while for SU(5) we obtain:

$$a^2\sigma = \begin{cases} \exp\left\{-3.021(15) - 0.682(17)(\beta - 13) + 0.214(30)(\beta - 13)^2\right\} & \text{for } \beta < 12.7 \\ \exp\{-0.636(35)\beta + 5.28(45)\} & \text{for } \beta \geq 12.7 \end{cases}, \tag{15}$$

with $\chi^2_{\rm red} = 3.41$, see the bottom panel in fig. 1.

3.2 Casimir scaling

The first issue that we investigated is Casimir scaling of bare Polyakov loops, i.e., whether the free energy associated to bare Polyakov loops in a given irreducible representation r is proportional to the eigenvalue of the quadratic Casimir $\langle C_2\rangle$ of that representation. To study this problem, we rescaled the loop free energies by the ratio of the Casimir in the given representation over the one in the fundamental representation f. This corresponds to raising the values of the loops to the power $1/d$, where:

$$d = \langle C_2\rangle_r / \langle C_2\rangle_f \tag{16}$$

(the values of d are reported in the appendix A).

Our results for the SU(4) gauge theory are displayed in fig. 2, which shows the values of $L^{1/d}$ for the twelve different representations, as obtained from simulations with the tree-level improved action on a lattice with $N_t = 5$ and $N_s = 20$ sites along the Euclidean time and spatial directions,

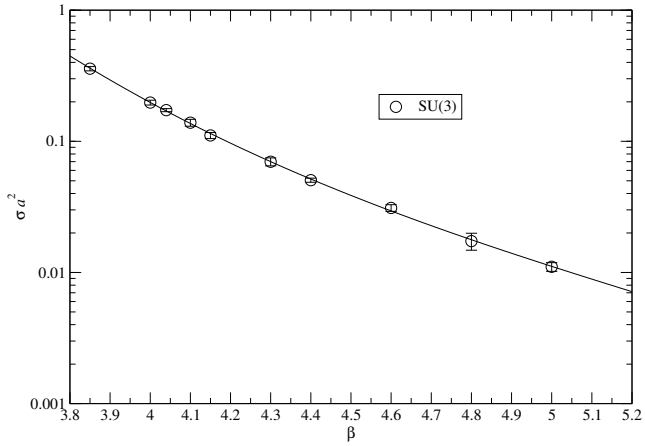

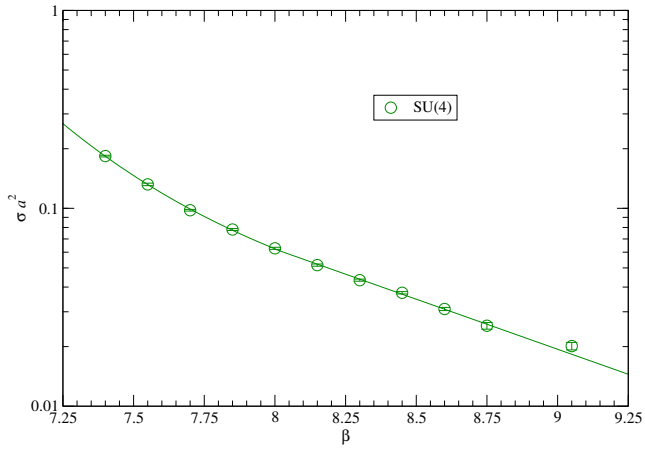

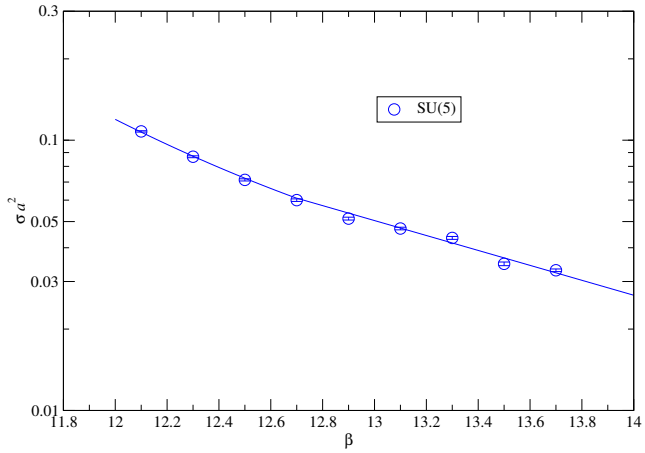

Figure 1: The top panel shows a fit of the results for the string tension in lattice units in the SU(3) gauge theory, taken from ref. [46], to the functional form in eq. (13). The central and bottom panels display the fits of our results for the string tension in lattice units to eq. (14) in SU(4) and SU(5) Yang-Mills theories, respectively.

respectively. If Casimir scaling holds, then this rescaling should make the values corresponding to higher representations collapse onto those of the fundamental representation (for which $d = 1$). Note that, in this plot, the data are displayed as a function of $\beta = 2N/g_0^2$: since the bare loops do not depend only on the temperature T, but also on the bare coupling g_0, it is natural to display these values (from simulations at fixed N_t) as a function of β. This also allows one to avoid introducing any potential ambiguity related to the definition of the temperature scale. In any case, the mapping between β and T at fixed N_t is just a scale redefinition, which, for the parameters of interest, can be directly obtained combining eq. (14) with the relation: $T = 1/(aN_t)$. In order to give an idea of the temperatures involved, we also display tick marks corresponding to a few reference temperatures along the upper horizontal axis.

Our results show an approximately perfect Casimir scaling in the deconfined phase, for all the representations that we considered. Although the bare values of loops in different representations vary by orders of magnitude, rescaling their free energies according to the corresponding quadratic Casimir eigenvalues makes them fall onto the same, universal curve. Our data show that the only significant deviations from this behavior (apart from the obvious ones in the confined phase, where Casimir scaling is *not* expected to hold) are visible for strongly suppressed high representations, which are most sensitive to finite-volume effects. For example, the rescaled bare loops in the representations denoted as **20′**, **35**, **50** and **56** show significant deviations from the curve of the other data for temperatures $T \lesssim 1.75\ T_c$, while they collapse on that curve at higher temperatures (for $L^{1/d} \gtrsim 0.2$). This is simply due to the fact that, for these representations, for $T \lesssim 1.75\ T_c$ the expectation value of the corresponding loops in the thermodynamic limit is smaller than the (non-vanishing) average value of $|L|$ computed on a lattice of finite volume. This is the same effect that, on any finite lattice, is responsible for the non-vanishing values of $|L|$ in the confining phase.

Fig. 3 gives evidence of this: the left panel shows our results for bare Polyakov loops in the fundamental representation of SU(4), obtained from lattices of two different spatial volumes, $V = (20a)^3$ and $V = (24a)^3$. The results of the two sets of simulations are compatible with each other in the deconfined phase (signaling that finite-volume corrections to the critical value of β are small for both ensembles), whereas the data obtained from the larger lattice are strongly suppressed in the confining phase, in agreement with the expectation that the average Polyakov loop is exactly zero in the thermodynamic limit. The right panel shows the same comparison, for loops in the representation of size **56**: for high-dimensional representations like this, the thermodynamic limit value of the Polyakov loop is very small, even in large regions of the deconfined phase, and thus it is overwhelmed by finite-size artifacts on the lattices that we considered. As fig. 2 shows, for such representations it is only at very large values of β (i.e., at very high temperatures) that the contribution surviving the thermodynamic limit becomes dominant over finite-volume artifacts.

In principle, one could perform an extrapolation to the thermodynamic limit, by repeating the simulations on a series of lattices of increasing volume. However, it should be pointed out that this would require a non-trivial computational effort for higher representations, especially at temperatures close to the deconfinement region. While this task is beyond the scope of the present work, we emphasize that the results displayed in the right panel of fig. 3 give strong support to the interpretation of the deviation from Casimir scaling for high representations close to the

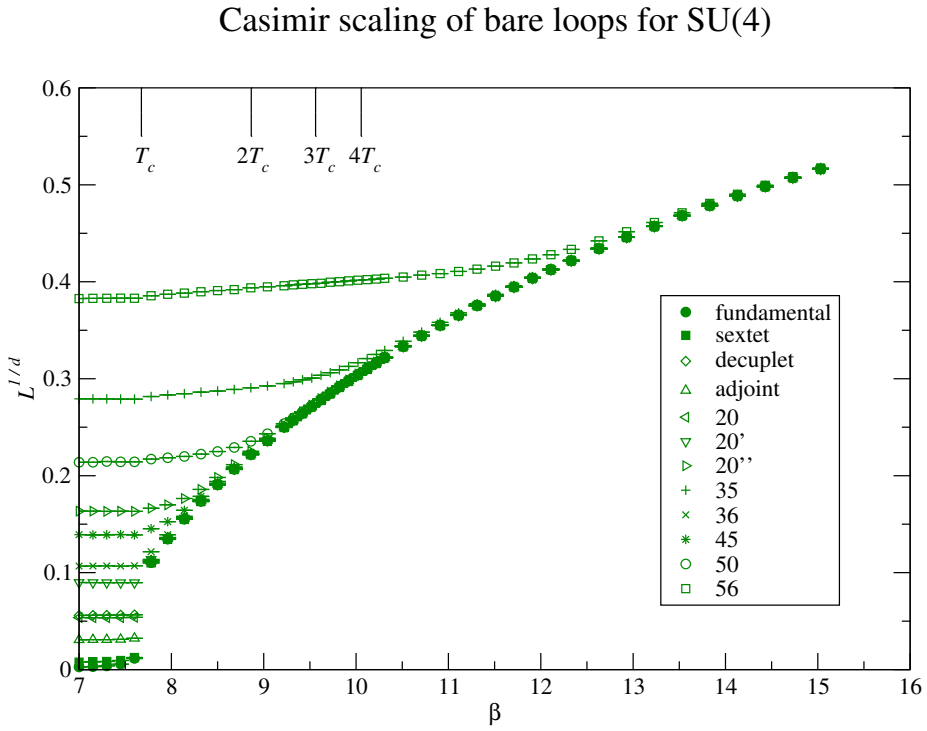

Figure 2: Temperature dependence of bare SU(4) Polyakov loops in different representations, after dividing their free energies by (a quantity proportional to) the eigenvalue of the corresponding quadratic Casimir $\langle C_2 \rangle_r$. This plot displays the results we obtained from simulations with the tree-level improved action, on lattices with $N_t = 5$ and $N_s = 20$ sites along the compactified time and spatial directions, respectively. The deviations from Casimir scaling observed for high representations close to the deconfinement transition are, likely, due to finite-volume effects (see the text for a detailed discussion).

deconfinement region in our data as a phenomenon which is (at least partially) due finite-volume artifacts. In particular, this plot (in which the scale on the vertical axis is logarithmic) shows that, for this high representation, an increase of the lattice volume by a factor approximately equal to 1.73leads to a nearly uniform shift of all data towards smaller values, and that this happens both in the confined and in the deconfined phase. The comparison with the left panel, which shows that in the same range of couplings (i.e., of temperatures) and for the same values of V, our numerical results for the fundamental representation are sensitive to this shift only in the confined phase, is strongly suggestive that, at temperatures close to T_c, the numerical data for high representations are dominated by finite-volume effects, and, hence, that the deviations from Casimir scaling observed in fig. 2 do not necessarily survive in the thermodynamic limit.

Our results for bare Polyakov loops in different representations (rescaled by dividing the respective free energies by the factor d, proportional to the quadratic Casimir eigenvalue of the

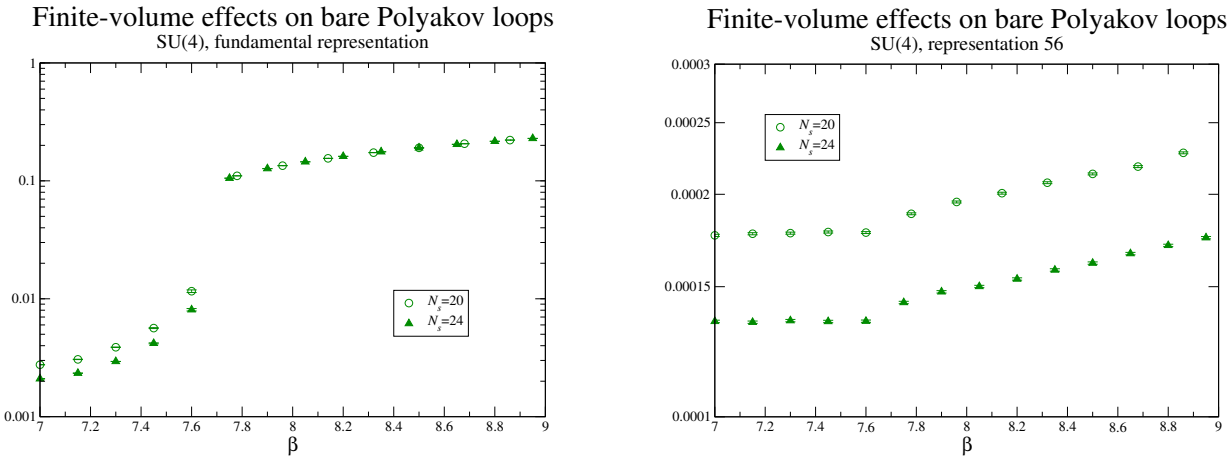

Figure 3: Left-hand side panel: Comparison of bare SU(4) Polyakov loops in the fundamental representation, obtained from lattices of different volumes: in the confined phase, the results tend to zero in the thermodynamic limit. Right-hand side panel: Loops in high-dimensional representations (such as the **56**, displayed in this plot), whose expectation values are strongly suppressed, are particularly sensitive to finite-volume artifacts.

corresponding representation) for the SU(2), SU(3), SU(5) and SU(6) theories are displayed in fig. 4: they reveal the same behavior observed for the SU(4) gauge group. Furthermore, comparing the plots of the rescaled bare loops for different groups, one also observes that, when N grows, the numerical study of higher representations simplifies, in the sense that they tend to be less sensitive to finite-volume effects. This is related to the fact that, in general, for $N \to \infty$ the quadratic Casimir grows only linearly with N, and with the number of fundamental and anti-fundamental indices out of which a generic representation is built (see the appendix A for a discussion). For example, while the d factor for the highest SU(2) representation considered here (i.e., for the twelfth lowest, non-trivial) is equal to 56, its value for the twelfth SU(6) representation is less than 6. As a consequence, from this point of view, the study of higher representations at large N actually becomes *simpler* than for smaller gauge groups.

Note that, deep in the weak-coupling region, one could compare the simulation results with the predictions from lattice perturbation theory. In particular, for the Wilson action the latter have been known for many years [53]. However, since our simulations are based on the tree-level improved action, rather than the Wilson action, we did not perform such a comparison.

3.3 Renormalized Polyakov loops

Finally, we present our results for the renormalized Polyakov loops, restricting our attention to loops in the fundamental representation. Our renormalization procedure is based on the determination of the constant term V_0 in the $T = 0$ interquark potential extracted from the lattice, at each value of the bare coupling. More precisely, we define the renormalized Polyakov

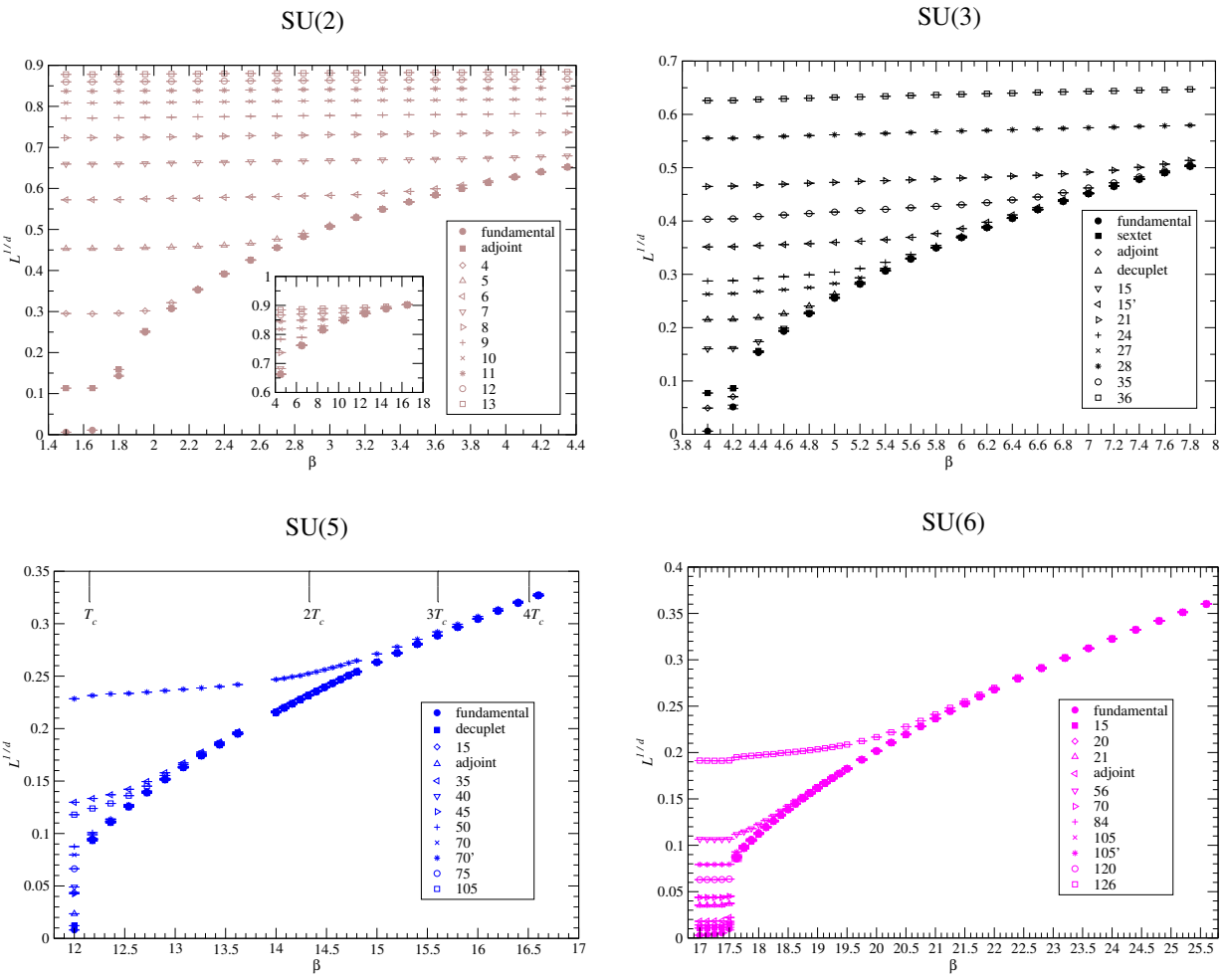

Figure 4: The top left panel shows results analogous to those in fig. 2, but for the SU(2) Yang-Mills theory. The inset shows the convergence to a universal curve, in a parameter range where finite-volume effects cease to dominate the results for higher representations. Similarly, the top right panel shows the corresponding results for the SU(3) gauge group, whereas the bottom left and bottom right plots display the results for the SU(5) and SU(6) theories, respectively.

loop as:

$$\langle L^{\rm ren}\rangle = Z^{N_t}\langle L\rangle, \qquad \text{with: } Z = e^{aV_0/2}, \tag{17}$$

where aV_0 is obtained from our fits of the interquark potential. Note that, in the expression above, the renormalized loop $L^{\rm ren}$ is expected to depend only on the physical temperature T, while the bare one L depends both on g_0^2 and on N_t. On the other hand, Z depends only on g_0^2.

Note that, since eq. (17) defines $\langle L^{\rm ren}\rangle$ in the fundamental representation through the charge renormalization factor Z, it follows that the corresponding factors for any higher representation can be defined as Z^d, with d defined in eq. (16).[1] As a consequence, with this renormalization procedure, it follows that renormalized Polyakov loops in higher representations obey Casimir scaling, if the corresponding bare ones do. This is no longer necessarily true, if a different renormalization prescription is used (see below for a discussion). However, previous studies of the SU(3) gauge theory revealed that renormalized loops still obey Casimir scaling to very high accuracy, even when different renormalization methods (involving renormalization factors which are, a priori, independent for each representation) are used—see, e.g., ref. [19]. Since these alternative renormalization methods are, typically, quite noisy and not ideally suited for computationally demanding simulations of SU($N > 3$) gauge theories, in the present work we restricted our analysis to the renormalization prescription defined by eq. (17), focusing our attention on the fundamental representation.

For SU(4), in the temperature region that we are most interested in (i.e., in the deconfined phase, close to T_c), our fits show that an accurate parameterization of $Z(g_0^2)$ is of the form:

$$Z(g_0^2) = \exp[-0.166(21)g_0^2 + 0.259(28)g_0^4], \tag{18}$$

for $g_0^2 \leq 0.8$; the quoted errors are conservative. Using eq. (18) to renormalize the bare loops obtained from our simulations with $N_t = 5$, $N_s = 20$, we obtain the renormalized Polyakov loop values displayed in the top panel of fig. 5, in which the displayed errorbars also include an estimate of the systematic uncertainties related to scale setting and renormalization prescription choice (which are discussed below). The inset shows a comparison of our data over a broader range (with extrapolation in the scale setting and in the parameterization of the renormalization constant) with the perturbative prediction for this gauge group, taken from ref. [16]. In particular, the upper solid curve is obtained using one-loop estimates for the coupling and Debye mass, whereas the lower dashed curve is obtained from two-loop estimates of these quantities [54]. The figure shows that the renormalized loop takes a value close to 1/2 for $T \to T_c^+$, and increases with the

[1] One could also imagine to define the renormalization factor for a higher representation r, by extracting the constant term of the potential between static sources in that representation. However, this procedure would be very tricky, for several reasons. In particular, sources in representations of vanishing N-ality at $T = 0$ get completely screened at large distances, while for representations of non-zero N-ality it is well-known that the confining behavior at asymptotically large distances is characterized by the string tension of the smallest representation with the same N-ality (although, at intermediate distances, the slope of the confining potential can be different). Moreover, extracting the confining potential from lattice calculations of Wilson loops in higher representations is computationally very demanding, due to the strong suppression of the signal-to-noise ratio, which is exponentially damped with the loop sizes and with the string tension. These features make a proper definition of aV_0 for high representations subtle, and its extraction from lattice simulations particularly challenging.

temperature, overshooting 1 at $T \simeq 3.4 T_c$. Extrapolating our parameterizations for the scale and for Z to a range of small coupling values (in which we have not performed non-perturbative computations of the $T = 0$ interquark potential), we find that the renormalized fundamental loop in the SU(4) theory reaches a maximum (about 1.07) at temperatures around $30 T_c$, then starts decreasing and approaching the next-to-next-to-leading order perturbative prediction, which, for the SU(N) Yang-Mills theory, reads [16]:

$$L^{\rm ren} = 1 + \frac{g^2 m_E \langle C_2 \rangle_f}{8\pi T} + \frac{g^4 N \langle C_2 \rangle_f}{(4\pi)^2} \left(\ln \frac{m_E}{T} + \frac{1}{4} \right) + O(g^5), \tag{19}$$

where g denotes the physical coupling, and m_E is the Debye mass. The behavior we observe in our SU(4) data is consistent with the results obtained for SU(3) in previous studies [17–19].

Similarly, our results for the SU(5) gauge group are based on the following parameterization of $Z(g_0^2)$:

$$Z(g_0^2) = \exp[0.4115(26) g_0^2], \tag{20}$$

for $g_0^2 \leq 0.8$, and are displayed in the bottom panel of fig. 5. Similarly to the case of four colors, also in the SU(5) theory the renormalized loop has a value close to 1/2 for $T \to T_c^+$, and increases up to values larger than 1.

Finally, in fig. 6, we show (minus twice) the logarithm of the renormalized fundamental loops for the SU(4) and SU(5) gauge groups, as a function of the inverse of the square of the temperature. As it was already observed in the case of the SU(3) theory [35], at temperatures between T_c and a few times T_c, the logarithm of the renormalized Polyakov loop appears to be of the form:

$$-2 \ln L^{\rm ren} = m \left(\frac{T_c}{T} \right)^2 + q. \tag{21}$$

In fig. 6, the straight lines are fits (in the temperature ranges shown in the plot legends) to eq. (21), which yield $m = 1.1166(55)$, $q = -0.0959(11)$, with $\chi^2_{\rm red} = 0.004$ for SU(4) and $m = 1.4283(62)$, $q = -0.3056(15)$, with $\chi^2_{\rm red} = 0.003$ for SU(5). The small $\chi^2_{\rm red}$ values are due to the fact that the errorbars affecting our numerical results are dominated by the systematic uncertainties, for which we could only provide a crude, but conservative, estimate.

Note, however, that the statement, that the logarithm of the renormalized Polyakov loop is of the form appearing on the right-hand side of eq. (21), is a scheme-dependent one. For example, redefining the renormalized Polyakov loop free energy with the addition of a constant, would introduce an additive contribution $O(T^{-1})$ to the logarithm of the renormalized loop. We find that the statement holds for the renormalization scheme that we discussed here (see also ref. [17]).

In view of this observation, one may wonder, whether there are arguments supporting our scheme choice, rather than others. As discussed above, our renormalization scheme for the Polyakov loop is based on the subtraction of the constant term appearing in the $T = 0$ potential between two static sources. This reduces the form of the renormalized confining potential to:

$$V(r) = \sigma r + \frac{\gamma}{r} + O(r^{-2}). \tag{22}$$

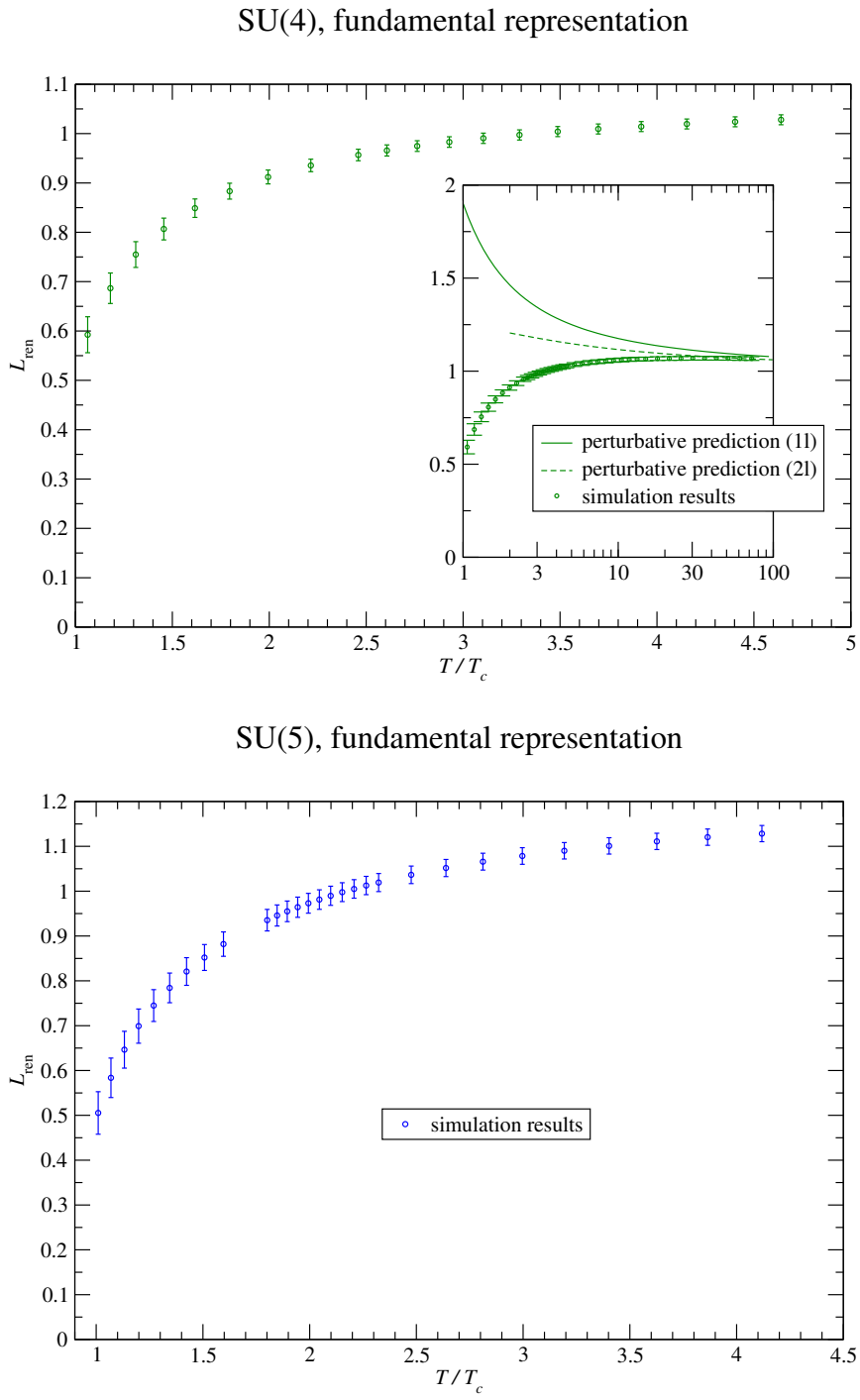

Figure 5: Top panel: Renormalized SU(4) Polyakov loop in the fundamental representation, as a function of the temperature (in units of T_c), in comparison with one- and two-loop perturbative predictions. Bottom panel: Renormalized fundamental loop, as a function of T/T_c, in the SU(5) theory.

The functional form appearing on the right-hand side of eq. (22) can be derived (at the leading order in an expansion around the large-distance limit) from an effective bosonic string model for confinement [50]. Various recent works (see, e.g., ref. [55] and references therein) show that Lorentz-Poincaré symmetries constrain the first few terms in the expansion of the effective string action to equal those that are obtained expanding the Nambu–Goto action [56], while corrections only appear at high orders in $1/r$. The fact that the Nambu–Goto string provides a good effective model for the confining potential is also confirmed by extensive numerical evidence from lattice simulations, both for SU(N) Yang-Mills theories [57] and for theories based on smaller gauge groups [58]. Following ref. [59], it is then natural to define a renormalization scheme yielding a $T = 0$ interquark potential with a vanishing constant term, eq. (22), and to apply it to the renormalization of the Polyakov loop.

In ref. [31], a holographic prediction for the renormalized Polyakov loop was computed, using a model with one deformation parameter [33]. The result reads:

$$L^{\mathrm{ren}}(T) = b_1 \exp\left\{-b_2\left[\sqrt{\pi}\frac{T_c}{T}\mathrm{Erfi}\left(\frac{T_c}{T}\right) - \exp\left(\frac{T_c}{T}\right)^2\right]\right\}, \tag{23}$$

where b_1 and b_2 are two coefficients that can be fitted, and Erfi denotes the imaginary error function. At the leading order in a high-temperature expansion, eq. (23) predicts that the logarithm of the Polyakov loop would be given by the sum of a constant plus a $(T_c/T)^2$ term, as observed in the numerical data.

More recently, a holographic computation of the Polyakov loop was also performed in ref. [32], finding good agreement with the SU(3) lattice data from ref. [19], and a numerical value of $L^{\mathrm{ren}}(T)$ very close to $1/2$ for $T \to T_c^+$.

In the literature, it was suggested that the dependence of $\ln L^{\mathrm{ren}}$ on T^{-2} could be due to a non-perturbative contribution from a gluon condensate [35, 36]. Similar arguments have been invoked to explain the behavior of the interaction measure Δ at temperatures of the order of a few times T_c [33,34,37,60]: in all SU(N) gauge theories, both in $D = 3+1$ [28] and in $D = 2+1$ [29] spacetime dimensions, Δ appears to be proportional to T^2.

3.4 Systematic uncertainties

Apart from the precision limits related to the finiteness of our statistical samples, the main systematic uncertainties affecting our study include: ambiguities in the scale determination, renormalization prescription dependence, effects due to the volume finiteness, and finite-cutoff effects. Let us discuss each of them in turn.

In the temperature range of interest in this study, a reliable definition of the temperature scale is necessarily non-perturbative, and—as discussed above—requires the choice of a dimensionful physical observable of reference. As different observables are generally affected by different lattice artifacts, this leads to slight ambiguities in the definition of the scale; however, this systematic effect becomes negligible at small lattice spacings. A potentially more severe ambiguity is related to the functional form that one can choose to parameterize the data to be fitted. Rather than interpolating our simulation results with arbitrary, arbitrarily complicated functions, in the

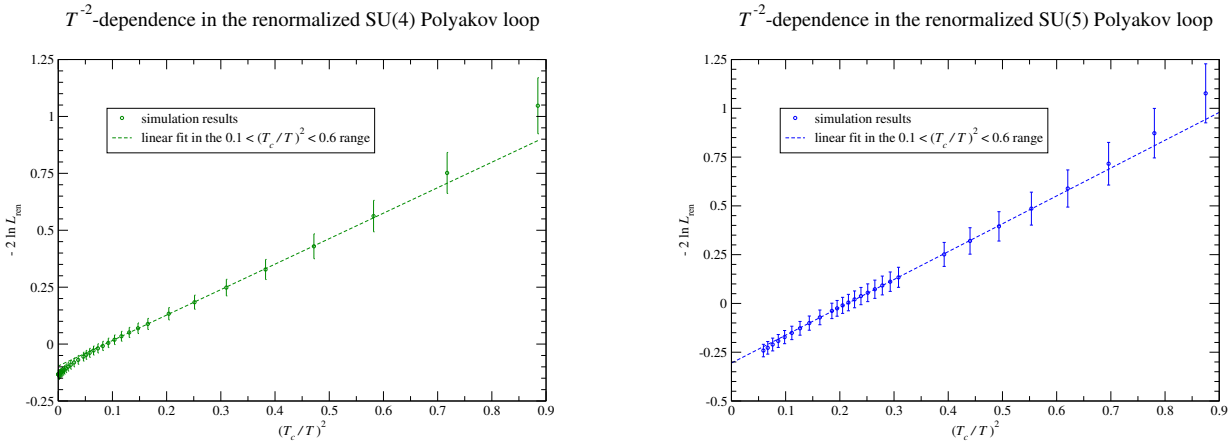

Figure 6: Similarly to what was observed for the SU(3) theory [35], also the logarithm of the SU(4) (left-hand side panel) and SU(5) (right-hand side panel) renormalized Polyakov loops exhibits a characteristic T^{-2}-dependence in the deconfined phase, up to temperatures of a few times T_c. Note that the errorbars include conservative estimates of the systematic uncertainties (see subsection 3.4).

present study we tried to use physically motivated functional forms, with a minimal number of parameters, and estimated the systematic uncertainty related to scale setting by comparing the results with different parameterizations, at various values of the lattice gauge coupling.

A potentially large systematic ambiguity in our computation is related to the choice of the Polyakov loop renormalization method. In the present work, we followed the approach already used in a similar study for the SU(2) gauge theory [21]. Other related studies discuss different renormalization methods, which lead to roughly compatible results. In particular, the authors of ref. [19] discussed a comparison of a renormalization method based on the $Q\bar{Q}$ potential (similar to our prescription) with an iterative renormalization (based on simulations on lattices of different spacing and at the same temperatures): these two methods appear to be compatible with each other, although the latter has the drawback of leading to an accumulation of statistical errors, particularly at temperatures close to T_c. A different renormalization method was suggested in ref. [18]: there, the idea is to extract the free energy of the renormalized Polyakov loop at a given temperature T, by identifying the N_t-independent contributions to the free energy F of bare loops extracted from simulations on lattices of different spacing:

$$F = N_t F^{\rm div} + F^{\rm ren} + F^{\rm lat}/N_t + \ldots , \tag{24}$$

where $F^{\rm div}$ and $F^{\rm lat}$ respectively denote the coefficient of the contribution to the bare free energy that diverges in the continuum limit, and the coefficient of the leading term due to lattice artifacts. A problem with this method, however, is that, in order to keep the temperature $T = 1/(aN_t)$ fixed, the lattice spacing a is obviously different for each simulation at a different N_t. Since a is tuned by varying the bare coupling g_0, this implies that $F^{\rm div}$, $F^{\rm ren}$ and $F^{\rm lat}$, which generically depend

on g_0, are *not* held fixed when T is fixed. Yet another renormalization method was proposed in ref. [22], following the fixed-scale approach [61]: the idea is to fix Z at only one value of the bare coupling g_0, and then to vary the temperature in the lattice simulations by varying N_t at fixed spacing a (i.e., at fixed bare coupling). A potential drawback of this method, however, is that it does not allow one to vary the temperature continuously. Aspects related to the renormalization of Wilson lines have also been discussed in ref. [59]. To get a rough estimate of the systematic uncertainty associated with the choice of a renormalization method, we compared the difference between various methods, at different temperatures, both in our data and in the results available in the literature.

Finally, finite-volume and finite-cutoff effects appear to be under control in our study. In particular, the results of our simulations show that, for $N \geq 4$, deviations from the thermodynamic limit in the deconfined phase are clearly visible only for high representations, whereas they appear to be negligible for the fundamental representation (see fig. 3). In fact, the lattices used in the present study are characterized by an aspect ratio $N_s/N_t \geq 4$, which is known to provide a good approximation of the thermodynamic limit in the temperature range of interest [43]. As for finite-cutoff effects, unfortunately we could not repeat all of our calculations on finer lattices, hence we are unable to perform a continuum extrapolation of our results. The systematic error due to cutoff effects on lattices with $N_t = 5$, however, is expected to be rather small for simulations with the improved action that we used: previous studies for the SU(3) gauge group [19] showed no significant discrepancies between $N_t = 4$ and $N_t = 8$.

Adding up the various sources of systematic uncertainties in quadrature, the total relative errors on our renormalized Polyakov loops are in the range between 1% and 5% for SU(4), and between 1.5% and 8% for SU(5).

4 Discussion and conclusions

Our main findings can be summarized as follows.

1. For all gauge groups, and for all the representations considered in this work, the bare Polyakov loops show excellent Casimir scaling, for all values of the coupling (or, equivalently, of the temperature), down to the deconfining transition. The only deviations, that our data reveal, can be explained in terms of finite-volume artifacts: they especially affect the high representations, particularly close to T_c (while they become negligible at sufficiently high temperatures), and can be reduced by increasing the spatial volume of the system. As we mentioned, in the literature, several works have reported evidence for Casimir scaling in SU(N) Yang-Mills theories, including, in particular, for the $T = 0$ string tension associated to the potential between two static sources in a given representation [14]. This observation has an interesting implication related to the large-N limit. As it is well-known, for pure SU(N) Yang-Mills theories, the expansion around the $N \to \infty$ limit can be organized in a series of powers of $1/N^2$, i.e. it does not contain odd powers of $1/N$. As discussed in ref. [62], this expectation seems to be at odds with the numerical evidence of Casimir scaling of k-string tension from lattice simulations [14], since, in general, if Casimir scaling

holds, then the leading finite-N corrections are $O(1/N)$. The resolution of this apparent paradox, however, was recently pointed out in ref. [63], and is based on a cancellation of terms involving odd $1/N$ powers in the spectrum of open string states. Similar arguments were also discussed in ref. [64].

2. In the thermodynamic limit the renormalized fundamental Polyakov loop is vanishing in the confined phase, and jumps to a finite value at the critical temperature, compatibly with the first-order nature of the deconfining transition. The limit of $L^{\rm ren}$ for $T \to T_c^+$ is a number close to 1/2, which, interestingly, is the value that is obtained analytically for $N \to \infty$ in $1+1$ spacetime dimensions [39]. For $T > T_c$, the renormalized Polyakov loop is at first growing with the temperature (in the regime in which the plasma is most strongly coupled), it overshoots the value 1 at temperatures around $3T_c$, reaches a maximum, and then eventually starts decreasing, in agreement with the perturbative predictions [16].

3. In the deconfined phase, for temperatures up to approximately $3T_c$ or $4T_c$, the logarithm of the renormalized Polyakov loop (in the renormalization scheme that we considered here) is described well by the sum of a term inversely proportional to the square of the temperature, plus a constant.

4. The finite-temperature behavior of gauge theories based on different SU(N) gauge groups appears to be qualitatively and quantitatively very similar (confirming previous studies both in $3+1$ [28] and in $2+1$ dimensions [29]). The precision and accuracy limits in this study do not allow us to extract a reliable estimate of the (small) differences between the various groups.

In conclusion, our study shows that, in the deconfined phase, the Polyakov loop satisfies Casimir scaling, and is only mildly dependent on the number of colors N. The independence on the rank of the gauge group (which has also been observed for the equation of state per gluon d.o.f. [28]) supports analytical approaches based on the large-N limit, including, in particular, holographic computations. Our results for the renormalized Polyakov loop show that this quantity interpolates between a regime (possibly dominated by contributions of non-perturbative nature) in which it is increasing with T, and one in which it tends to the perturbative prediction, and decreases with the temperature, approaching 1 from above in the weak-coupling limit for $T \to \infty$.

For the future, we plan to extend the present study of large-N gauge theories at finite temperature, by looking at other observables, which could potentially reveal a stronger dependence on the rank of the gauge group. Of particular phenomenological interest are transport and diffusion coefficients—see, e.g., ref. [65] for a review.

Acknowledgements.

This work is supported by the Academy of Finland, project 1134018, and in part by the National Science Foundation under Grant No. PHY11-25915. A.M. acknowledges support from the Magnus Ehrnrooth Foundation. M.P. gratefully acknowledges the Kavli Institute for Theoretical

Physics in Santa Barbara, USA, for support and hospitality during the "Novel Numerical Methods for Strongly Coupled Quantum Field Theory and Quantum Gravity" program, during which part of this work was done. The simulations were performed at the Finnish IT Center for Science (CSC), Espoo, Finland. We thank F. Gliozzi, O. Kaczmarek, M. Laine, D. Nógrádi, R. Pisarski, K. Tuominen and M. Vepsäläinen for helpful comments and discussions.

A Irreducible representations of the algebra of generators of SU(N)

In the following, we discuss the classification of irreducible representations of the algebra of generators of a generic special unitary group of degree N. Further details can be found, e.g., in ref. [66].

A generic irreducible representation of the algebra of generators of SU(N) can be labelled by $N-1$ non-negative integers $\lambda_1, \lambda_2, \lambda_3, \ldots, \lambda_{N-1}$, with:

$$\lambda_1 \geq \lambda_2 \geq \lambda_3 \geq \cdots \geq \lambda_{N-1} \geq 0. \tag{A.1}$$

The $[\lambda_1, \lambda_2, \lambda_3, \ldots, \lambda_{N-1}]$ sequence can be uniquely associated to a Young diagram with rows of lengths $\lambda_1, \ldots, \lambda_{N-1}$. An alternative way to identify an irreducible representation is in terms of its canonical label $(m_1, m_2, \ldots, m_{N-1})$, where the m_i's represent the differences in lengths of subsequent rows in the corresponding Young diagram: $m_i = \lambda_{i+1} - \lambda_i$ for $i < N-1$, and $m_{N-1} = \lambda_{N-1}$.

Particularly interesting irreducible representations of SU(N) include the fundamental one $[1, 0, 0, \ldots, 0]$, of dimension N, the trivial one $[0, 0, 0, \ldots, 0]$ of dimension 1, and the adjoint one $[2, 1, 1, \ldots, 1]$, of dimension $N^2 - 1$.

More in general, the dimension of an irreducible representation is given by the formula:

$$\prod_{i=1}^{N-1} \prod_{j=i+1}^{N} \frac{l_i - l_j}{l_i^0 - l_j^0}, \quad l_i = \lambda_i + N - i, \quad l_i^0 = N - i, \tag{A.2}$$

with $\lambda_N = 0$ or, equivalently:

$$\frac{1}{\mathcal{N}_N} \prod_{l=1}^{N-1} \prod_{i=1}^{N-l} \sum_{k=i}^{i+l-1} (m_k + 1), \quad \text{with:} \quad \mathcal{N}_N = \prod_{t=1}^{N-1} (t!). \tag{A.3}$$

A common way to denote irreducible representations is via their dimension; note, however, that this may be ambiguous (except for SU(2)), since in general there can be inequivalent irreducible representations of the same dimension. For example, SU(4) has three inequivalent irreducible representations of dimension 20, which can be denoted as **20**, **20′** and **20″**. In such cases, our convention is to use the notation with the least primes for the representation with the smallest λ_i for the minimum value of i (namely, for the representation described by a Young diagram with the smallest number of boxes in the top row, or in the highest row which is different from the

other representations of the same dimension). So, for instance, for SU(3) the $[3,1]$ irreducible representation is denoted as **15**, while the $[4,0]$ will be denoted as $\mathbf{15'}$; for SU(4), the $[2,1,0]$ is denoted as **20**, the $[2,2,0]$ is denoted as $\mathbf{20'}$, and the $[3,0]$ is denoted as $\mathbf{20''}$.

The N-ality of an SU(N) representation defines its transformation properties under the center of the group, $\mathbb{Z}_N$, and is given by the total number of boxes appearing in the Young diagram, modulo N. Representations of vanishing N-ality (such as the trivial representation and the adjoint one) are blind to the action of the transformations in the group center.

Given an irreducible representation $r = [\lambda_1, \lambda_2, \ldots, \lambda_{N-1}]$, its conjugate representation is: $\bar{r} = [\lambda_1, \lambda_1 - \lambda_{N-1}, \lambda_1 - \lambda_{N-2}, \ldots, \lambda_1 - \lambda_2]$, so that its Young diagram is obtained by fitting the diagram of the representation r in a rectangle of N rows and λ_1 columns, removing all the boxes belonging to the Young diagram of r, and turning the diagram with the remaining boxes by an angle π.

Obviously, two mutually conjugated representations have the same dimension, and, given that their respective characters are obtained from each other by complex conjugation, we only include one of them in our lists of irreducible representations. It is most natural to use the "barred" notation for the representation with the Young diagram with more boxes, so that, for example the $[1,0]$ representation of SU(3) is denoted as **3**, while its conjugate representation $[1,1]$ is denoted as $\bar{\mathbf{3}}$.

Representations which are self-conjugate have real characters; in particular, this is always the case for the trivial and for the adjoint representations. Also, note that, for a self-conjugate irreducible representation, the canonical label is a palindrome.

In order to discuss the large-N scaling of the size and quadratic Casimir of an irreducible representation r, it is convenient to introduce the non-negative integers l and m, which represent the minimum number of fundamental and anti-fundamental factors from which the representation r can be constructed (by tensor products). l and m can be easily obtained from the Young diagram of r: l is given by the sum of the number of boxes in all columns of length not larger than $N/2$, while m is given by the sum of the number of missing boxes in all columns of length larger than $N/2$. The N-ality of a representation is given by $(l - m)$ modulo N. In the large-N limit, it is possible to show [40] that characters of different representations only depend on l and m, and that, although the dimension of the representation r grows like N^{l+m}, the eigenvalue of the quadratic Casimir is linear in N:

$$\langle C_2 \rangle_r = \frac{N}{2} \left[l + m + O(1/N) \right]. \tag{A.4}$$

For SU(2), *all* irreducible representations are self-conjugate. The Young diagram of a generic irreducible representation of spin $j = n/2$ consists of one horizontal row of n boxes; bosonic representations correspond to even values of n, and have vanishing N-ality, while fermionic representations correspond to odd values of n, and their N-ality is 1. The associated canonical label is (n) (with $l = n$, $m = 0$), the dimension is $n+1$, the eigenvalue of the quadratic Casimir (defined according to our conventions) is $\langle C_2 \rangle = n(n+2)/4$, and its ratio with respect to the fundamental representation is $d = n(n+2)/3$.

For larger SU(N) groups (up to $N = 8$), the lowest irreducible representations are listed in tables 2–7.

Young diagram	N-ality	canonical label	dimension	notes	$\langle C_2 \rangle$	d
	1	$(1,0)$	**3**	fundamental	4/3	1
	2	$(2,0)$	**6**		10/3	5/2
	0	$(1,1)$	**8**	adjoint	3	9/4
	0	$(3,0)$	**10**		6	9/2
	1	$(2,1)$	**15**		16/3	4
	1	$(4,0)$	**15′**		28/3	7
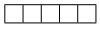	2	$(5,0)$	**21**		40/3	10
	2	$(3,1)$	**24**		25/3	25/4
	0	$(2,2)$	**27**	self-conjugate	8	6
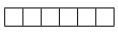	0	$(6,0)$	**28**		18	27/2
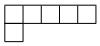	0	$(4,1)$	**35**		12	9
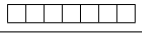	1	$(7,0)$	**36**		70/3	35/2

Table 2: The irreducible representations of the SU(3) gauge group studied in this work. For this group, the integers l and m of each representation are respectively equal to the first and second index in the canonical label.

Generically, the eigenvalues of a group element g in the fundamental representation of SU(N) lie on the unit circle in the complex plane, and their product is 1:

$$g_f = U \cdot \mathrm{diag}(e^{i\alpha_1}, e^{i\alpha_2}, e^{i\alpha_3}, \ldots, e^{i\alpha_N}) \cdot U^\dagger, \quad \text{with: } \sum_{i=1}^{N} \alpha_i = 0 \bmod 2\pi. \tag{A.5}$$

Knowing the eigenvalues of g_f, it is possible to calculate explicitly the character of g in *any* irreducible representation $r = [\lambda_1, \lambda_2, \ldots, \lambda_{N-1}]$ by means of the Weyl formula [52]:

$$\mathrm{Tr}\, g_r = \frac{\det F(\vec{\lambda})}{\det F(\vec{0})}, \tag{A.6}$$

where $F(\vec{\lambda})$ is an $N \times N$ matrix with entries defined as: $F_{kl}(\vec{\lambda}) = \exp\left[i\,(N + \lambda_l - l)\,\alpha_k\right]$, with $\lambda_N = 0$, and $e^{i\alpha_1}$, $e^{i\alpha_2}$, … $e^{i\alpha_N}$ are the eigenvalues of g in the fundamental representation.

In many cases, however, the characters in high-dimensional irreducible representations can be more expediently calculated, using the laws of representation composition encoded in Young calculus, and using the well-known fact that the character in a representation which can be expressed as the tensor sum (product) of two representations is equal to the sum (product) of the characters in the summand (factor) representations.

Young diagram	N-ality	canonical label	dimension	l	m	notes	$\langle C_2 \rangle$	d
	1	$(1,0,0)$	**4**	1	0	fundamental	15/8	1
	2	$(0,1,0)$	**6**	2	0	self-conjugate	5/2	4/3
	2	$(2,0,0)$	**10**	2	0		9/2	12/5
	0	$(1,0,1)$	**15**	1	1	adjoint	4	32/15
	3	$(1,1,0)$	**20**	3	0		39/8	13/5
	0	$(0,2,0)$	**20′**	4	0	self-conjugate	6	16/5
	3	$(3,0,0)$	**20″**	3	0		63/8	21/5
	0	$(4,0,0)$	**35**	4	0		12	32/5
	1	$(2,0,1)$	**36**	2	1		55/8	11/3
	0	$(2,1,0)$	**45**	4	0		8	64/15
	2	$(0,3,0)$	**50**	6	0	self-conjugate	21/2	28/5
	1	$(5,0,0)$	**56**	5	0		135/8	9

Table 3: Same as in table 2 (with the addition of the l and m indices), but for the SU(4) gauge group.

A.1 Casimir operators

A Casimir operator of a Lie algebra g is a homogeneous polynomial of order p, lying in the enveloping algebra of g, $T(g)$, and commuting with all elements of g. Given a Casimir operator C_p, any product of it by an arbitrary scalar factor aC_p, as well as any integer power of it C_p^q, are also Casimir operators; however, the number of *independent* Casimir operators of a given algebra g is equal to the rank l of the algebra. In particular, the algebra of generators of the special unitary group SU(N) has $N-1$ independent Casimir operators C_2, C_3, $\dots C_N$, whose eigenvalues $\langle C_p \rangle$ can be used to classify the irreducible representations of the algebra.

Explicit expressions for the C_p's can be obtained as follows. Starting from a basis $\{E_{i,j}\}_{i,j=1\dots N}$ of generators of U(N):

$$[E_{a,b}, E_{c,d}] = \delta_{b,c} E_{a,d} - \delta_{a,d} E_{c,b}, \tag{A.7}$$

introduce a basis for the algebra of generators, denoted as $\left\{\tilde{E}_{i,j}\right\}$ (where both i and j run from 1 to N, but the element $\tilde{E}_{N,N}$ element is not defined), through:

$$\tilde{E}_{i,j} = \begin{cases} E_{i,j} & \text{if } i \neq j, \\ E_{i,i} - \frac{1}{N} \sum_{k=1}^{N} E_{k,k} & \text{if } i = j. \end{cases} \tag{A.8}$$

For the generators of SU(N), the Casimir operator of order p can then be defined as:

$$C_p = \frac{1}{p} \sum_{i_1, i_2, \dots i_p = 1}^{N} \tilde{E}_{i_1 i_2} \tilde{E}_{i_2 i_3} \dots \tilde{E}_{i_{p-1} i_p} \tilde{E}_{i_p i_1}. \tag{A.9}$$

Young diagram	N-ality	canonical label	dimension	l	m	notes	$\langle C_2 \rangle$	d
	1	$(1,0,0,0)$	**5**	1	0	fundamental	12/5	1
	2	$(0,1,0,0)$	**10**	2	0		18/5	3/2
	2	$(2,0,0,0)$	**15**	2	0		28/5	7/3
	0	$(1,0,0,1)$	**24**	1	1	adjoint	5	25/12
	3	$(3,0,0,0)$	**35**	3	0		48/5	4
	3	$(1,1,0,0)$	**40**	3	0		33/5	11/4
	4	$(1,0,1,0)$	**45**	1	2		32/5	8/3
	4	$(0,2,0,0)$	**50**	4	0		42/5	7/2
	1	$(2,0,0,1)$	**70**	2	1		42/5	7/2
	4	$(4,0,0,0)$	**70′**	4	0		72/5	6
	0	$(0,1,1,0)$	**75**	2	2	self-conjugate	8	10/3
	4	$(2,1,0,0)$	**105**	4	0		52/5	13/3

Table 4: Same as in table 3, but for the SU(5) gauge group.

Note that, by construction, the linear Casimir operator C_1 is identically vanishing on the algebra of generators of SU(N), as they are all traceless.

The eigenvalue of C_p in the generic irreducible representation labelled by $[\lambda_1, \lambda_2, \ldots \lambda_{N-1}]$ can be obtained in the following way (taking $\lambda_N = 0$) [67]:

1. define $\lambda = \sum_{i=1}^{N} \lambda_i$;
2. define $m_i = \lambda_i - \lambda/N$ for all $i = 1, 2, \ldots N$;
3. define $\rho_i = N - i$ and $l_i = m_i + \rho_i$ for all $i = 1, 2, \ldots N$;
4. for all $k \geq 2$, construct the quantities: $S_k = \sum_{i=1}^{N} \left(l_i^k - \rho_i^k\right)$;
5. for all $k \geq 2$, define the coefficients: $a_k = \sum_{j=1}^{k-1} \frac{(k-1)!}{j!(k-j)!} S_j$;
6. construct the function: $\varphi(z) = \sum_{k=2}^{\infty} a_k z^k$;
7. calculate the B_p coefficients from the following Taylor expansion around $z = 0$:

$$\frac{1 - \exp\left[-\varphi(z)\right]}{z} = \sum_{p=0}^{\infty} B_p z^p \tag{A.10}$$

Young diagram	N-ality	canonical label	dimension	l	m	notes	$\langle C_2 \rangle$	d
	1	$(1,0,0,0,0)$	**6**	1	0	fundamental	35/12	1
	2	$(0,1,0,0,0)$	**15**	2	0		14/3	8/5
	3	$(0,0,1,0,0)$	**20**	3	0	self-conjugate	21/4	9/5
	2	$(2,0,0,0,0)$	**21**	2	0		20/3	16/7
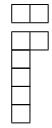	0	$(1,0,0,0,1)$	**35**	1	1	adjoint	6	72/35
	3	$(3,0,0,0,0)$	**56**	3	0		45/4	27/7
	3	$(1,1,0,0,0)$	**70**	3	0		33/4	99/35
	5	$(1,0,0,1,0)$	**84**	1	2		95/12	19/7
	4	$(1,0,1,0,0)$	**105**	4	0		26/3	104/35
	4	$(0,2,0,0,0)$	**105′**	4	0		32/3	128/35
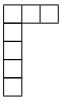	1	$(2,0,0,0,1)$	**120**	2	1		119/12	17/5
	4	$(4,0,0,0,0)$	**126**	4	0		50/3	40/7

Table 5: Same as in table 3, but for the SU(6) gauge group.

(note that $B_0 = 0$);

8. compute the eigenvalue of C_p from the formula:

$$\langle C_p \rangle = \frac{B_p - N B_{p-1}}{p}. \tag{A.11}$$

This gives, in particular, the following relations:

$$\langle C_2 \rangle = \frac{S_2}{2}, \tag{A.12}$$

$$\langle C_3 \rangle = \frac{1}{3}\left[S_3 + \left(\frac{3}{2} - N\right) S_2\right], \tag{A.13}$$

$$\langle C_4 \rangle = \frac{1}{4}\left[S_4 + (2-N)\, S_3 + \left(2 - \frac{3}{2}N\right) S_2\right], \tag{A.14}$$

$$\langle C_5 \rangle = \frac{1}{5}\left[S_5 + \left(\frac{5}{2} - N\right) S_4 + \left(\frac{10}{3} - 2N\right) S_3 + \left(\frac{5}{2} - 2N\right) S_2 - \frac{1}{2} S_2^2\right], \tag{A.15}$$

Young diagram	N-ality	canonical label	dimension	l	m	notes	$\langle C_2 \rangle$	d
	1	$(1,0,0,0,0,0)$	**7**	1	0	fundamental	24/7	1
	2	$(0,1,0,0,0,0)$	**21**	2	0		40/7	5/3
	2	$(2,0,0,0,0,0)$	**28**	2	0		54/7	9/4
	3	$(0,0,1,0,0,0)$	**35**	3	0		48/7	2
	0	$(1,0,0,0,0,1)$	**48**	1	1	adjoint	7	49/24
	3	$(3,0,0,0,0,0)$	**84**	3	0		90/7	15/4
	3	$(1,1,0,0,0,0)$	**112**	3	0		69/7	23/8
	6	$(1,0,0,0,1,0)$	**140**	1	2		66/7	11/4
	1	$(2,0,0,0,0,1)$	**189**	2	1		80/7	10/3
	4	$(0,2,0,0,0,0)$	**196**	4	0		90/7	15/4
	4	$(1,0,1,0,0,0)$	**210**	4	0		76/7	19/6
	4	$(4,0,0,0,0,0)$	**210′**	4	0		132/7	11/2

Table 6: Same as in table 3, but for the SU(7) gauge group.

$$\langle C_6 \rangle = \frac{1}{6}\left[S_6 + (3-N)\,S_5 + \left(5-\frac{5}{2}N\right)S_4 + \left(5-\frac{10}{3}N\right)S_3 + \left(3-\frac{5}{2}N\right)S_2 - S_2S_3 + \left(\frac{N}{2}-\frac{3}{2}\right)S_2^2\right], \tag{A.16}$$

$$\langle C_7 \rangle = \frac{1}{7}\left[S_7 + \left(\frac{7}{2}-N\right)S_6 + (7-3N)\,S_5 + \left(\frac{35}{4}-5N\right)S_4 + (7-5N)\,S_3 + \left(\frac{7}{2}-3N\right)S_2 - S_4S_2 - \frac{1}{2}S_3^2 + \left(-\frac{7}{2}+N\right)S_3S_2 + \left(-\frac{25}{8}+\frac{3}{2}N\right)S_2^2\right], \tag{A.17}$$

$$\langle C_8 \rangle = \frac{1}{8}\left[S_8 + (4-N)\,S_7 + \left(\frac{28}{3}-\frac{7}{2}N\right)S_6 + (14-7N)\,S_5 + \left(14-\frac{35}{4}N\right)S_4 + \left(\frac{28}{3}-7N\right)S_3 + \left(4-\frac{7}{2}N\right)S_2 - S_5S_2 - S_4S_3 + (-4+N)\,S_4S_2 + \left(-2+\frac{N}{2}\right)S_3^2 + \left(-\frac{25}{3}+\frac{7}{2}N\right)S_3S_2 + \left(-\frac{11}{2}+\frac{25}{8}N\right)S_2^2 + \frac{1}{6}S_2^3\right]. \tag{A.18}$$

Young diagram	N-ality	canonical label	dimension	l	m	notes	$\langle C_2 \rangle$	d
	1	$(1,0,0,0,0,0,0)$	**8**	1	0	fundamental	63/16	1
	2	$(0,1,0,0,0,0,0)$	**28**	2	0		27/4	12/7
	2	$(2,0,0,0,0,0,0)$	**36**	2	0		35/4	20/9
	3	$(0,0,1,0,0,0,0)$	**56**	3	0		135/16	15/7
	0	$(1,0,0,0,0,0,1)$	**63**	1	1	adjoint	8	128/63
	4	$(0,0,0,1,0,0,0)$	**70**	4	0	self-conjugate	9	16/7
	3	$(3,0,0,0,0,0,0)$	**120**	3	0		231/16	11/3
	3	$(1,1,0,0,0,0,0)$	**168**	3	0		183/16	61/21
	7	$(1,0,0,0,0,1,0)$	**216**	1	2		175/16	25/9
	1	$(2,0,0,0,0,0,1)$	**280**	2	1		207/16	23/7
	4	$(4,0,0,0,0,0,0)$	**330**	4	0		21	16/3
	4	$(0,2,0,0,0,0,0)$	**336**	4	0		15	80/21

Table 7: Same as in table 3, but for the SU(8) gauge group.

In turn, the equations above lead to the following expressions for the quadratic Casimir eigenvalues $\langle C_2 \rangle$:

$$\langle C_2 \rangle = \frac{1}{4}\lambda_1 \left(\lambda_1 + 2\right) \quad \text{for SU(2)}, \tag{A.19}$$

$$\langle C_2 \rangle = \frac{1}{3}\left(\lambda_1^2 + 3\lambda_1 - \lambda_1\lambda_2 + \lambda_2^2\right) \quad \text{for SU(3)}, \tag{A.20}$$

$$\langle C_2 \rangle = \frac{1}{8}\left[3\lambda_1^2 + \lambda_2\left(4 + 3\lambda_2\right) - 2\lambda_3\left(\lambda_2 + 2\right) + 3\lambda_3^2 - 2\lambda_1\left(\lambda_2 + \lambda_3 - 6\right)\right] \quad \text{for SU(4)}, \tag{A.21}$$

$$\begin{aligned} \langle C_2 \rangle \;\; = \;\; & \frac{1}{5}\left[2\left(\lambda_1^2 + \lambda_2^2 + \lambda_3^2 + \lambda_4^2\right) - \left(5 + \lambda_3\right)\lambda_4 + \lambda_2\left(5 - \lambda_3 - \lambda_4\right)\right. \\ & \left. + \lambda_1\left(10 - \lambda_2 - \lambda_3 - \lambda_4\right)\right] \quad \text{for SU(5)}, \end{aligned} \tag{A.22}$$

$$\langle C_2\rangle = \frac{1}{12}\left[5\left(\lambda_1^2+\lambda_2^2+\lambda_3^2+\lambda_4^2+\lambda_5^2\right)+6\left(\lambda_3-\lambda_4\right)-2\lambda_3\lambda_4-2\left(9+\lambda_3+\lambda_4\right)\lambda_5 \right.$$
$$\left.+2\lambda_2\left(9-\lambda_3-\lambda_4-\lambda_5\right)+2\lambda_1\left(15-\lambda_2-\lambda_3-\lambda_4-\lambda_5\right)\right] \quad \text{for SU(6)}, \tag{A.23}$$

$$\langle C_2\rangle = \frac{1}{7}\left[3\left(\lambda_1^2+\lambda_2^2+\lambda_3^2+\lambda_4^2+\lambda_5^2+\lambda_6^2\right)+7\left(3\lambda_1+2\lambda_2+\lambda_3-\lambda_5-2\lambda_6\right)-\lambda_4\lambda_5 \right.$$
$$-\lambda_3\left(\lambda_4+\lambda_5\right)-\left(\lambda_3+\lambda_4+\lambda_5\right)\lambda_6-\left(\lambda_3+\lambda_4+\lambda_5+\lambda_6\right)\lambda_2$$
$$\left.-\lambda_1\left(\lambda_2+\lambda_3+\lambda_4+\lambda_5+\lambda_6\right)\right] \quad \text{for SU(7)}, \tag{A.24}$$

$$\langle C_2\rangle = \frac{1}{16}\left[7\left(\lambda_1^2+\lambda_2^2+\lambda_3^2+\lambda_4^2+\lambda_5^2+\lambda_6^2+\lambda_7^2\right)+24\lambda_3+8\lambda_4-2\lambda_3\lambda_4-8\lambda_5-2\lambda_3\lambda_5 \right.$$
$$-2\lambda_4\lambda_5-24\lambda_6-2\lambda_3\lambda_6-2\lambda_4\lambda_6-2\lambda_5\lambda_6-2\left(20+\lambda_3+\lambda_4+\lambda_5+\lambda_6\right)\lambda_7$$
$$-2\lambda_2\left(-20+\lambda_3+\lambda_4+\lambda_5+\lambda_6+\lambda_7\right)$$
$$\left.-2\lambda_1\left(-28+\lambda_2+\lambda_3+\lambda_4+\lambda_5+\lambda_6+\lambda_7\right)\right] \quad \text{for SU(8)}. \tag{A.25}$$

Note that the Casimir operators are defined up to a multiplicative constant; with the conventions fixed by the construction above, the eigenvalue of the SU(N) quadratic Casimir operator in the fundamental representation is $(N^2-1)/(2N)$, while in the adjoint representation it is N.

References

[1] N. Cabibbo and G. Parisi, Phys. Lett. B **59** (1975) 67. J. C. Collins and M. J. Perry, Phys. Rev. Lett. **34**, 1353 (1975).

[2] E. V. Shuryak, Phys. Lett. B **78** (1978) 150 [Sov. J. Nucl. Phys. **28** (1978) 408] [Yad. Fiz. **28** (1978) 796].

[3] U. W. Heinz and M. Jacob, arXiv:nucl-th/0002042. M. Gyulassy and L. McLerran, Nucl. Phys. A **750** (2005) 30 [arXiv:nucl-th/0405013]. K. Adcox *et al.* [PHENIX Collaboration], Nucl. Phys. A **757**, 184 (2005) [arXiv:nucl-ex/0410003]. I. Arsene *et al.* [BRAHMS Collaboration], Nucl. Phys. A **757**, 1 (2005) [arXiv:nucl-ex/0410020]. B. B. Back *et al.*, Nucl. Phys. A **757**, 28 (2005) [arXiv:nucl-ex/0410022]. J. Adams *et al.* [STAR Collaboration], Nucl. Phys. A **757**, 102 (2005) [arXiv:nucl-ex/0501009]. T. K. Nayak, arXiv:1201.4264 [nucl-ex].

[4] A. D. Linde, Phys. Lett. B **96**, 289 (1980). D. J. Gross, R. D. Pisarski and L. G. Yaffe, Rev. Mod. Phys. **53**, 43 (1981).

[5] J.-P. Blaizot, arXiv:1108.3482 [hep-ph].

[6] P. B. Arnold and C.-X. Zhai, Phys. Rev. **D50** (1994) 7603 [hep-ph/9408276]; Phys. Rev. **D51** (1995) 1906 [hep-ph/9410360]. C.-X. Zhai and B. M. Kastening, Phys. Rev. **D52** (1995) 7232 [hep-ph/9507380]. J. O. Andersen, E. Braaten and M. Strickland, Phys. Rev. Lett. **83** (1999) 2139 [hep-ph/9902327]. J.-P. Blaizot, E. Iancu and A. Rebhan, Phys. Rev. **D63** (2001) 065003

[hep-ph/0005003]. K. Kajantie, M. Laine, K. Rummukainen and Y. Schröder, Phys. Rev. **D67** (2003) 105008 [hep-ph/0211321]. A. Hietanen, K. Kajantie, M. Laine, K. Rummukainen and Y. Schröder, Phys. Rev. **D79** (2009) 045018 [arXiv:0811.4664 [hep-lat]]. J. O. Andersen, M. Strickland and N. Su, Phys. Rev. Lett. **104** (2010) 122003 [arXiv:0911.0676 [hep-ph]]. J. O. Andersen, L. E. Leganger, M. Strickland and N. Su, Phys. Lett. **B696** (2011) 468 [arXiv:1009.4644 [hep-ph]].

[7] C. DeTar and U. M. Heller, Eur. Phys. J. **A41** (2009) 405 [arXiv:0905.2949 [hep-lat]]. M. Laine, PoS **LAT2009** (2009) 006 [arXiv:0910.5168 [hep-lat]]. K. Kanaya, PoS **LATTICE2010** (2010) 012 [arXiv:1012.4247 [hep-lat]]. C. DeTar, [arXiv:1101.0208 [hep-lat]]. L. Levkova, PoS **LATTICE2011** (2011) 012.

[8] G. 't Hooft, Nucl. Phys. B **138** (1978) 1.

[9] A. M. Polyakov, Phys. Lett. B **72** (1978) 477. L. D. McLerran and B. Svetitsky, Phys. Rev. D **24**, 450 (1981). J. Kuti, J. Polónyi and K. Szlachányi, Phys. Lett. B **98**, 199 (1981).

[10] T. Matsui and H. Satz, Phys. Lett. B **178** (1986) 416. S. Digal, P. Petreczky and H. Satz, Phys. Lett. B **514** (2001) 57 [hep-ph/0105234]. Á. Mócsy and P. Petreczky, Phys. Rev. D **73** (2006) 074007 [hep-ph/0512156]. L. Kluberg and H. Satz, arXiv:0901.3831 [hep-ph].

[11] O. Jahn and O. Philipsen, Phys. Rev. D **70** (2004) 074504 [hep-lat/0407042]. O. Philipsen, Nucl. Phys. A **820** (2009) 33C [arXiv:0810.4685 [hep-ph]]. J. Ghiglieri, arXiv:1201.2920 [hep-ph].

[12] V. S. Dotsenko and S. N. Vergeles, Nucl. Phys. B **169** (1980) 527.

[13] J. Ambjørn, P. Olesen and C. Peterson, Nucl. Phys. B **240** (1984) 189.

[14] L. Del Debbio, M. Faber, J. Greensite and Š. Olejník, Phys. Rev. D **53** (1996) 5891 [hep-lat/9510028]. M. Faber, J. Greensite and Š. Olejník, Phys. Rev. D **57** (1998) 2603 [hep-lat/9710039]. G. S. Bali, Phys. Rev. D **62** (2000) 114503 [hep-lat/0006022]. C. Piccioni, Phys. Rev. D **73** (2006) 114509 [hep-lat/0503021]. F. Bursa and M. Teper, JHEP **0508** (2005) 060 [hep-lat/0505025]. J. Greensite, K. Langfeld, Š. Olejník, H. Reinhardt and T. Tok, Phys. Rev. D **75** (2007) 034501 [hep-lat/0609050]. M. Döring, K. Hübner, O. Kaczmarek and F. Karsch, Phys. Rev. D **75** (2007) 054504 [hep-lat/0702009 [HEP-LAT]]. P. Bicudo, M. Cardoso and O. Oliveira, Phys. Rev. D **77** (2008) 091504 [arXiv:0704.2156 [hep-lat]]. B. Bringoltz and M. Teper, Phys. Lett. B **663** (2008) 429 [arXiv:0802.1490 [hep-lat]]. L'u. Lipták and Š. Olejník, Phys. Rev. D **78** (2008) 074501 [arXiv:0807.1390 [hep-lat]]. B. H. Wellegehausen, A. Wipf and C. Wozar, Phys. Rev. D **83** (2011) 016001 [arXiv:1006.2305 [hep-lat]].

[15] V. I. Shevchenko and Y. A. Simonov, Phys. Rev. Lett. **85** (2000) 1811 [hep-ph/0001299]; hep-ph/0104135. Y. A. Simonov, arXiv:1003.3608 [hep-ph].

[16] Y. Burnier, M. Laine and M. Vepsäläinen, JHEP **1001** (2010) 054 [arXiv:0911.3480 [hep-ph]]. N. Brambilla, J. Ghiglieri, P. Petreczky and A. Vairo, Phys. Rev. D **82** (2010) 074019 [arXiv:1007.5172 [hep-ph]].

[17] O. Kaczmarek, F. Karsch, P. Petreczky and F. Zantow, Phys. Lett. B **543** (2002) 41 [hep-lat/0207002].

[18] A. Dumitru, Y. Hatta, J. Lenaghan, K. Orginos and R. D. Pisarski, Phys. Rev. D **70** (2004) 034511 [hep-th/0311223].

[19] S. Gupta, K. Hübner, O. Kaczmarek, Phys. Rev. **D77** (2008) 034503 [arXiv:0711.2251 [hep-lat]].

[20] S. Digal, S. Fortunato and P. Petreczky, Phys. Rev. D **68**, 034008 (2003) [hep-lat/0304017].

[21] K. Hübner and C. Pica, PoS LATTICE **2008** (2008) 197 [arXiv:0809.3933 [hep-lat]].

[22] R. V. Gavai, Phys. Lett. B **691** (2010) 146 [arXiv:1001.4977 [hep-lat]].

[23] G. 't Hooft, Nucl. Phys. **B72** (1974) 461. E. Witten, Nucl. Phys. **B160** (1979) 57. L. G. Yaffe, Rev. Mod. Phys. **54** (1982) 407. A. V. Manohar, arXiv:hep-ph/9802419. E. E. Jenkins, Ann. Rev. Nucl. Part. Sci. **48** (1998) 81 [hep-ph/9803349]. Y. Makeenko, arXiv:hep-th/0001047.

[24] L. McLerran and R. D. Pisarski, Nucl. Phys. A **796** (2007) 83 [arXiv:0706.2191 [hep-ph]]. S. Lottini and G. Torrieri, Phys. Rev. Lett. **107** (2011) 152301 [arXiv:1103.4824 [nucl-th]].

[25] J. M. Maldacena, Adv. Theor. Math. Phys. **2**, 231 (1998) [Int. J. Theor. Phys. **38**, 1113 (1999)] [arXiv:hep-th/9711200]. S. S. Gubser, I. R. Klebanov and A. M. Polyakov, Phys. Lett. B **428**, 105 (1998) [arXiv:hep-th/9802109]. E. Witten, Adv. Theor. Math. Phys. **2**, 253 (1998) [arXiv:hep-th/9802150].

[26] E. Witten, Adv. Theor. Math. Phys. **2** (1998) 505 [hep-th/9803131].

[27] D. T. Son and A. O. Starinets, Ann. Rev. Nucl. Part. Sci. **57**, 95 (2007) [arXiv:0704.0240 [hep-th]]. D. Mateos, Class. Quant. Grav. **24**, S713 (2007) [arXiv:0709.1523 [hep-th]]. S. S. Gubser and A. Karch, Ann. Rev. Nucl. Part. Sci. **59**, 145 (2009) [arXiv:0901.0935 [hep-th]]. J. Casalderrey-Solana, H. Liu, D. Mateos, K. Rajagopal and U. A. Wiedemann, arXiv:1101.0618 [hep-th]. U. Gürsoy, E. Kiritsis, L. Mazzanti, G. Michalogiorgakis and F. Nitti, Lect. Notes Phys. **828** (2011) 79 [arXiv:1006.5461 [hep-th]].

[28] M. J. Teper, hep-th/9812187. B. Lucini and M. Teper, Phys. Rev. D **64** (2001) 105019 [hep-lat/0107007]; JHEP **0106** (2001) 050 [hep-lat/0103027]. B. Lucini, M. Teper and U. Wenger, Phys. Lett. B **545**, 197 (2002) [arXiv:hep-lat/0206029]; JHEP **0401**, 061 (2004) [arXiv:hep-lat/0307017]; Nucl. Phys. B **715**, 461 (2005) [arXiv:hep-lat/0401028]; JHEP **0502**, 033 (2005) [arXiv:hep-lat/0502003]; JHEP **0406** (2004) 012 [hep-lat/0404008]. H. Meyer and M. Teper, JHEP **0412** (2004) 031 [hep-lat/0411039]. B. Bringoltz and M. Teper, Phys. Lett. B **628**

(2005) 113 [arXiv:hep-lat/0506034]; Phys. Rev. D **73** (2006) 014517 [arXiv:hep-lat/0508021]; L. Del Debbio, B. Lucini, A. Patella and C. Pica, JHEP **0803** (2008) 062 [arXiv:0712.3036 [hep-th]]. G. S. Bali and F. Bursa, JHEP **0809** (2008) 110 [arXiv:0806.2278 [hep-lat]]. M. Panero, Phys. Rev. Lett. **103**, 232001 (2009) [arXiv:0907.3719 [hep-lat]]; PoS **LAT2009**, 172 (2009) [arXiv:0912.2448 [hep-lat]]. S. Datta and S. Gupta, Phys. Rev. D **80** (2009) 114504 [arXiv:0909.5591 [hep-lat]]; Phys. Rev. D **82** (2010) 114505 [arXiv:1006.0938 [hep-lat]].

[29] M. J. Teper, Phys. Rev. D **59**, 014512 (1999) [arXiv:hep-lat/9804008]. R. W. Johnson and M. J. Teper, Phys. Rev. D **66** (2002) 036006 [arXiv:hep-ph/0012287]. H. B. Meyer and M. J. Teper, Nucl. Phys. **B668** , 111 (2003) [hep-lat/0306019]. A. Athenodorou, B. Bringoltz and M. Teper, Phys. Lett. B **656** (2007) 132 [arXiv:0709.0693 [hep-lat]]. M. Caselle, L. Castagnini, A. Feo, F. Gliozzi and M. Panero, JHEP **1106** (2011) 142 [arXiv:1105.0359 [hep-lat]]. M. Caselle, L. Castagnini, A. Feo, F. Gliozzi, U. Gürsoy, M. Panero and A. Schäfer, arXiv:1111.0580 [hep-th].

[30] J. Noronha, Phys. Rev. D **81** (2010) 045011 [arXiv:0910.1261 [hep-th]].

[31] O. Andreev, Phys. Rev. Lett. **102** (2009) 212001 [arXiv:0903.4375 [hep-ph]].

[32] E. Megías, H. J. Pirner and K. Veschgini, Phys. Rev. D **83** (2011) 056003 [arXiv:1009.2953 [hep-ph]].

[33] O. Andreev, Phys. Rev. D **76** (2007) 087702 [arXiv:0706.3120 [hep-ph]].

[34] E. Megías, E. Ruiz Arriola and L. L. Salcedo, JHEP **0601** (2006) 073 [hep-ph/0505215].

[35] E. Megías, E. Ruiz Arriola and L. L. Salcedo, Phys. Rev. **D81** (2010) 096009 [arXiv:0912.0499 [hep-ph]].

[36] F. Xu and M. Huang, arXiv:1111.5152 [hep-ph].

[37] P. N. Meisinger, T. R. Miller and M. C. Ogilvie, Phys. Rev. D **65** (2002) 034009 [hep-ph/0108009].

[38] R. D. Pisarski, hep-ph/0101168. A. Dumitru and R. D. Pisarski, Nucl. Phys. A **698** (2002) 444 [hep-ph/0102020]. O. Scavenius, A. Dumitru and A. D. Jackson, Phys. Rev. Lett. **87** (2001) 182302 [hep-ph/0103219]. A. Dumitru and R. D. Pisarski, Phys. Lett. B **525** (2002) 95 [hep-ph/0106176]; Phys. Rev. D **66** (2002) 096003 [hep-ph/0204223]. A. Dumitru, J. Lenaghan and R. D. Pisarski, Phys. Rev. D **71** (2005) 074004 [hep-ph/0410294]. A. Dumitru, Y. Guo, Y. Hidaka, C. P. K. Altes and R. D. Pisarski, Phys. Rev. D **83** (2011) 034022 [arXiv:1011.3820 [hep-ph]]. Á. Mócsy, F. Sannino and K. Tuominen, Phys. Rev. Lett. **92** (2004) 182302 [hep-ph/0308135].

[39] D. J. Gross and E. Witten, Phys. Rev. D **21** (1980) 446. S. Wadia, EFI-79/44-CHICAGO.

[40] D. J. Gross and W. Taylor, Nucl. Phys. B **400** (1993) 181 [hep-th/9301068]; Nucl. Phys. B **403** (1993) 395 [hep-th/9303046]. S. Samuel, Nucl. Phys. B **205** (1982) 221.

[41] K. Rummukainen, AIP Conf. Proc. **1343** (2011) 51 [arXiv:1101.5875 [hep-lat]]. L. Del Debbio, arXiv:1102.4066 [hep-lat].

[42] A. Mykkänen, M. Panero and K. Rummukainen, PoS LATTICE **2011** (2011) 211 [arXiv:1110.3146 [hep-lat]].

[43] F. Gliozzi, J. Phys. A A **40** (2007) F375 [hep-lat/0701020]. M. Panero, PoS LATTICE **2008** (2008) 175 [arXiv:0808.1672 [hep-lat]].

[44] K. G. Wilson, Phys. Rev. **D10** (1974) 2445.

[45] P. Weisz, Nucl. Phys. B **212** (1983) 1. P. Weisz and R. Wohlert, Nucl. Phys. B **236** (1984) 397 [Erratum-ibid. B **247** (1984) 544].

[46] B. Beinlich, F. Karsch, E. Laermann and A. Peikert, Eur. Phys. J. **C6** (1999) 133 [arXiv:hep-lat/9707023 [hep-lat]].

[47] S. L. Adler, Phys. Rev. D **23** (1981) 2901. F. R. Brown and T. J. Woch, Phys. Rev. Lett. **58** (1987) 2394.

[48] M. Creutz, Phys. Rev. D **21**, 2308 (1980). A. D. Kennedy and B. J. Pendleton, Phys. Lett. B **156**, 393 (1985).

[49] N. Cabibbo and E. Marinari, Phys. Lett. B **119**, 387 (1982).

[50] M. Lüscher, Nucl. Phys. B **180** (1981) 317. M. Lüscher, K. Symanzik and P. Weisz, Nucl. Phys. B **173** (1980) 365. J. Polchinski and A. Strominger, Phys. Rev. Lett. **67** (1991) 1681.

[51] M. Caselle, M. Panero and S. Piemonte, in preparation.

[52] H. Weyl, *The Classical Groups. Their Invariants and Representations* (Princeton University Press, Princeton, 1997), ISBN 978-0-691-05756-9. C. Itzykson and M. Nauenberg, Rev. Mod. Phys. **38** (1966) 95.

[53] U. M. Heller and F. Karsch, Nucl. Phys. B **251** (1985) 254.

[54] M. Laine and Y. Schröder, JHEP **0503** (2005) 067 [hep-ph/0503061]. M. Laine and M. Vepsäläinen, JHEP **0909** (2009) 023 [arXiv:0906.4450 [hep-ph]].

[55] O. Aharony and E. Karzbrun, JHEP **0906** (2009) 012 [arXiv:0903.1927 [hep-th]]. F. Gliozzi, Phys. Rev. D **84** (2011) 027702 [arXiv:1103.5377 [hep-th]]. O. Aharony and M. Dodelson, arXiv:1111.5758 [hep-th].

[56] T. Goto, Prog. Theor. Phys. **46** (1971) 1560. Y. Nambu, Phys. Rev. D **10** (1974) 4262.

[57] M. Teper, Acta Phys. Polon. B **40** (2009) 3249 [arXiv:0912.3339 [hep-lat]].

[58] K. J. Juge, J. Kuti and C. Morningstar, Phys. Rev. Lett. **90** (2003) 161601 [hep-lat/0207004]. M. Caselle, M. Hasenbusch and M. Panero, JHEP **0301** (2003) 057 [hep-lat/0211012]. M. Panero, JHEP **0505** (2005) 066 [hep-lat/0503024]; Nucl. Phys. Proc. Suppl. **140** (2005) 665 [hep-lat/0408002]. F. Gliozzi, S. Lottini, M. Panero and A. Rago, Nucl. Phys. B **719** (2005) 255 [cond-mat/0502339]. P. Giudice, F. Gliozzi and S. Lottini, JHEP **0903** (2009) 104 [arXiv:0901.0748 [hep-lat]].

[59] Y. Hidaka and R. D. Pisarski, Phys. Rev. D **80** (2009) 074504 [arXiv:0907.4609 [hep-ph]].

[60] E. Megías, E. Ruiz Arriola and L. L. Salcedo, Phys. Rev. **D80** (2009) 056005 [arXiv:0903.1060 [hep-ph]]. O. Andreev, Phys. Rev. **D73** (2006) 107901 [hep-th/0603170]. R. D. Pisarski, Prog. Theor. Phys. Suppl. **168** (2007) 276 [hep-ph/0612191].

[61] T. Umeda, S. Ejiri, S. Aoki, T. Hatsuda, K. Kanaya, Y. Maezawa and H. Ohno, Phys. Rev. D **79** (2009) 051501 [arXiv:0809.2842 [hep-lat]].

[62] A. Armoni and M. Shifman, Nucl. Phys. B **664** (2003) 233 [hep-th/0304127]; Nucl. Phys. B **671** (2003) 67 [hep-th/0307020].

[63] J. Greensite, B. Lucini and A. Patella, Phys. Rev. D **83** (2011) 125019 [arXiv:1101.5344 [hep-th]].

[64] C. P. Korthals Altes and H. B. Meyer, hep-ph/0509018.

[65] H. B. Meyer, Eur. Phys. J. A **47** (2011) 86 [arXiv:1104.3708 [hep-lat]].

[66] F. Iachello, *Lie Algebras and Applications*, Lect. Notes Phys. **708** (Springer, Berlin, Heidelberg 2006), DOI 10.1007/b11785361.

[67] A. M. Perelomov and V. S. Popov, Sov. J. Nucl. Phys. **3** (1966) 676.

HIP-2012-18/TH

The static quark potential from a multilevel algorithm for the improved gauge action

Anne Mykkänen

Department of Physics and Helsinki Institute of Physics,
P.O. Box 64, FI-00014 University of Helsinki, Finland
email: anne-mari.mykkanen@helsinki.fi

Abstract

We generalize the multilevel algorithm of Lüscher and Weisz to study SU(N) Yang-Mills theories with the tree-level improved gauge action. We test this algorithm, comparing its results with those obtained using the Wilson action, in SU(3) and SU(4) Yang-Mills theories in $2+1$ and $3+1$ dimensions. We measure the static quark potential and extract the Lüscher term, predicted by the bosonic string theory.

1 Introduction

An efficient lattice gauge theory algorithm proposed by Lüscher and Weisz, the multilevel algorithm, has been shown to provide an exponential reduction of the statistical errors in calculations of the Polyakov loop correlation function [1]. Multilevel algorithms are useful in many contexts, in which one has to cope with an exponentially decaying signal-to-noise ratio, for example in the computation of the glueball spectrum [2] and in the computation of the correlation functions, which are related to the transport coefficients of the quark-gluon plasma [3, 4]. In [5], a multilevel algorithm was used to study the localization properties of gauge fields on domain wall defects. In this paper, we generalize the multilevel algorithm to study the static quark potential.

In a confining theory, the static quark potential has the large distance asymptotic expansion [6]

$$V(r) = \sigma r + \mu + \gamma/r + O(1/r^2), \tag{1}$$

where σ is the string tension, μ a constant (a regularization-dependent mass), and γ is the Lüscher term

$$\gamma = -\frac{\pi}{24}(D-2) \tag{2}$$

with D as the dimension of the space-time [7, 8]. The interaction between the static quark-antiquark pair can be described by an effective string theory. It has been suggested that the expectation values of large Wilson loops have a correspondence with amplitudes of an effective bosonic string theory [6, 9]. The Polyakov loop correlator can be used similarly to the Wilson loop to study string effects [10, 11, 12].

One of the consequences of the effective string description at zero temperature is the presence of the term proportional to $1/r$, i.e. the Lüscher term (2), in the long distance inter-quark potential. The Lüscher term includes a coefficient that depends only on the dimension of the space-time and is not influenced by higher order corrections of the effective string action. The aim of this paper is to study the potential, namely compute the Lüscher term, in pure glue SU(N) Yang-Mills theory, using numerical simulations.

Although the validity of the asymptotic expansion (1) can be checked by means of numerical simulations, the problem in these lattice computations, is that the signal-to-noise ratio decays quickly at large distances. This makes it difficult to clearly separate the γ/r correction from the other terms. Still, lattice gauge theory can offer support for the string model. For example, the data for the potential in a range of distances from 0.4 to 0.8 fm has been noted to agree with (1) within small errors [13]. Also, using highly efficient simulation techniques it was confirmed [14] that the expectation values of large rectangular Wilson loops are matched by the string theory amplitudes to a precision where the subleading string effects can be observed. However, a more recent study [15] on string effects at large-N using Wilson loops seemed to differ from the effective string prediction, contrary to previous studies [16, 17].

In this paper, all simulations are performed utilizing the multilevel algorithm, and besides the standard Wilson action, we will also conduct simulations with the tree level improved action [18, 19, 20, 21]. The improved action can strongly reduce the lattice artifacts, and hence give better results also on relatively small lattices. Examples of "success stories" of the improved action for the gauge action include computations of the SU(3) equation of state [22, 23] and the studies of renormalized Polyakov loops [24, 25]. Similarly, improved actions for the quarks are particularly useful when it comes to computationally challenging problems, like, e.g. lattice studies of walking technicolor models (see, for example, [26]).

The string-like features of the interquark 'flux tube' have already been studied with calculations in $\mathbb{Z}_2$ [14, 27, 28], $\mathbb{Z}_4$ [29], U(1) [30, 31, 32], SU(2) [33, 34, 28, 35], SU(3) [6, 36, 37], as well as with SU($N > 3$) [16, 17, 38, 39], and even in a random percolation model (with an appropriate definition of the observables) [40, 41]. By extending the research also to bigger gauge groups we pursue two main subjects of interest. First of all, since large-N studies are largely motivated by the fact that they can provide a mathematically simplified frame for studying QCD, we want to see whether the numerical results for the flux tube obtained with a large-N theory agree with SU(3) results. A second motivation comes from the conjectured con-

nection between large-N conformal gauge theories and string theory (see for example the review [42] and [43]), affiliating with the Maldacena conjecture and AdS/CFT. In this paper, the groups SU(3) and SU(4) are studied.

This paper is organized as follows: In section 2, as an extended introduction on the topic of this paper, we will discuss some basic issues on bosonic string theory, namely the Nambu-Goto string and how it can model the behavior of the flux tube in a confining gauge theory, and also some earlier lattice results relevant to this topic. Then, in section 3 we discuss the Polyakov loop correlation function on the lattice and the actions used in this work, and in section 4 we describe the multilevel algorithm in more detail. In sections 5 and 6 we present the results of this work and the conclusions.

2 Bosonic string theory

2.1 Nambu-Goto string

The simplest effective action for a bosonic string is simply the string tension σ times the area of the string world sheet, i.e. the Nambu-Goto action [44, 45, 46]

$$S_{\text{eff}} = \sigma \int d^2\xi \sqrt{\det g_{\alpha\beta}}. \tag{3}$$

In the so called "physical gauge" the integrand reads

$$\sqrt{1 + (\partial_0 h)^2 + (\partial_1 h)^2 + (\partial_0 h \times \partial_1 h)^2} \tag{4}$$

where h is the displacement of the world sheet surface in the transverse directions. Expanding this in a perturbative series in $1/(\sigma r^2)$, at leading order we get the following expression for the Polyakov loop correlation function (see, e.g. [30] for a discussion)

$$\langle P^\star(r) P(0)\rangle = \frac{e^{-\sigma r L - \mu L}}{\left(\eta\left(i\frac{L}{2r}\right)\right)^{D-2}}, \tag{5}$$

where we have used Dedekind's η function

$$\eta(\tau) = q^{\frac{1}{24}} \prod_{n=1}^{\infty}(1-q^n), \qquad q = e^{2\pi i \tau}. \tag{6}$$

When $\frac{L}{2r} \gg 1$, eq. (5) gives the Lüscher term in the quark-antiquark potential.

The spectrum of the Nambu-Goto string can be obtained by canonical quantization [47, 48]: the energy levels for a string with fixed ends are

$$E_n(r) = \sigma r \sqrt{1 + \frac{2\pi}{\sigma r^2}\left(n - \frac{D-2}{24}\right)}, \qquad n \in \mathbb{N}, \tag{7}$$

$$= \sigma r - \frac{(D-2-24n)\pi}{24r} + O(1/r^3). \tag{8}$$

As a consequence, the partition function describing the string with fixed ends reads

$$Z = \sum_{n=0}^{\infty} \omega_n e^{-E_n(r)L} \tag{9}$$

where ω_n are the number of states.

As mentioned, one of the outcomes of the effective string description at zero temperature is the presence of the Lüscher term in the long distance inter-quark potential. One should not confuse this with a Coulomb term originating from the one-gluon exchange process. The Lüscher term is a Casimir effect, which is due to the finiteness of the interquark distance r. As a heuristic argument for the term, let us consider the string-like tube created by two color sources separated by distance r. Due to quantum fluctuations, the string can vibrate, and we can express its wavelength through

$$r = \lambda\Big(\frac{1+n}{2}\Big) \tag{10}$$

where $n = 0, 1, 2, 3, \ldots$. If we consider each of these modes as quantum mechanical harmonic oscillators, then their energies are

$$E_n^k = \hbar\omega_n\Big(k + \frac{1}{2}\Big) \tag{11}$$

and if we just consider the ground state, $k = 0$, we can write

$$\begin{aligned} E_n &= \sum_{n=0}^{\infty} \frac{1}{2}\hbar\omega_n = \frac{1}{2}\sum_{n=0}^{\infty} \frac{2\pi}{\lambda_n} = \pi \sum_{n=0}^{\infty} \frac{1}{\lambda_n} \\ &= \frac{\pi}{r}\Big(\frac{1}{2} + 1 + \frac{3}{2} + 2 + \frac{5}{2} + \ldots\Big) \\ &= \frac{\pi}{2r}\Big(1 + 2 + 3 + 4 + 5 + \ldots\Big) \\ &= -\frac{1}{2}\frac{\pi}{12r} \end{aligned} \tag{12}$$

where we have used the Riemann zeta regularization. This is just for one transverse direction; in D dimensions there are $D-2$ transverse directions, so in four dimensions, we have

$$E_n = -\frac{\pi}{12r}. \tag{13}$$

Finally, the effective string model also gives a prediction for the form of the inter-quark potential in finite temperature gauge theories [35, 33, 49].

2.2 QCD string

In a pure gauge theory the ground state interquark potential $V(r)$ of a heavy $Q\bar{Q}$ pair can be expressed in terms of the two-point correlation function $G(r)$ of Polyakov lines

$$V(r) = -\frac{1}{L}\log G(r) = -\frac{1}{L}\log\langle P^\star(r)P(0)\rangle, \tag{14}$$

where r is the interquark distance and L the system size in the time-like direction [30].

In the confining regime of SU(N) gauge theories, the asymptotic behavior of $V(r)$ at large distances is a linear rise, and the flux lines between the well separated color sources are expected to be squeezed in a thin, string-like tube [7, 8, 50]. This "confining string" can be considered as a basic object, in particular when it cannot break, i.e. when there is no matter in representations of non-zero N-ality. By studying the low-energy effective action on the string we pursue to understand the low-energy dynamics of long strings. In large-N gauge theories the confining string can be thought of as a weakly coupled fundamental string subject to some effective action which, if known, can be used to study the low-energy properties of the model. Unfortunately, in general the effective string action is not known, but Monte Carlo computations on a lattice may offer a way to study the low energy effective action of a confining string and give insights of its properties. Furthermore, the general properties of the effective string can be derived based on the symmetries it should have [51, 52, 53, 54, 55].

Even though the interquark potential $V(r)$ and related quantities have been studied extensively on the lattice for many years (see, for example, [37, 56, 57] for references), the question whether the picture given by effective string models is quantitatively satisfactory, is still under investigation. Previous results [37, 56] have shown prominent support for the bosonic string prediction, in particular, the Lüscher term has been shown to be a universal feature of the IR regime of confined gauge theories. However, results from recent, high precision Monte Carlo simulations [32, 58, 6, 27, 59, 34, 60, 33, 61, 62] suggest that higher order corrections to $V(r)$ might not be universal. In fact, there are theoretical arguments suggesting that the effective string action is different from the Nambu-Goto one at higher orders.

Another aspect of interest, is the excitation spectrum description. According to the bosonic string picture, the excitations are expected to be described by the spectrum of harmonic oscillator energies

$$E = E_0 + \frac{\pi}{r} n, \qquad n \in \mathbb{N}. \tag{15}$$

In the ground state potential the Lüscher term is supported by numerical evidence down to very short distances, but for the excited states the lattice results are not in such a good agreement with the theoretical expectations, as discussed in [30]. Mismatches between effective string predictions [10] and numerical results have been found in [63, 36, 64, 28].

In this paper however, we shall focus the attention onto the ground state interquark potential. Assuming that the low energy dynamics of the pure gauge model is described by the effective string, and assuming that decays of excited states do not play a significant role, we can write the Polyakov loop two-point correlation function as a string partition function

$$\langle P^\star(r) P(0) \rangle = \int \mathcal{D}h e^{-S_{\text{eff}}}, \tag{16}$$

where $S_{\rm eff}$ is the effective action for the world sheet spanned by the string.

The dynamics of the confining string is not known, but it should respect the expected rotational symmetries. This implies that only the terms that are rotationally symmetric can be part of the effective string action. In fact these constraints are more general and they restrict the form of the effective action (at least at the lowest orders) to be the Nambu-Goto one. Lattice simulations for pure Yang-Mills theories in $D = 3$ and $D = 4$ show the effective action being very well approximated by this form. However, deviations from Nambu-Goto can be derived at higher orders (see [65] and references therein).

Different approaches allow one to constrain the effective action of a confining string. Polchinski and Strominger [66, 67, 68] proposed to consider the degrees of freedom in the effective action as the embedding coordinates of the string in a conformal gauge world sheet. Requiring the effective action to have the correct critical central charge, one is left with constraints that have been shown to imply the four-derivative effective action to agree with the Nambu-Goto form. Unfortunately, generalizing this approach to higher orders appears to be challenging.

Another approach [7, 8, 69] is to write the effective action in static gauge, such that the degrees of freedom are only the $(D-2)$ transverse fluctuations of the string world sheet. Essentially, the action should non-linearly realize the Lorentz symmetry rotating the direction in which the string propagates, and the transverse directions. Following the suggestion of Lüscher and Weisz in [69], the effective action is constrained by computing the partition function of long closed strings, winding around a periodic size of the system, and writing it in terms of a sum over string states. In [69] it was shown that in $D = 3$ the partition function on the annulus constrains the four-derivative terms to be of Nambu-Goto form.

2.3 Some earlier lattice results

In recent years the effective action of confining strings has been studied on the lattice with higher and higher precision (see [57] for a review of results). Studies of the three dimensional pure Yang-Mills theory have produced very accurate results of the spectrum of confining flux tubes in large-N SU(N) gauge theories [38, 39]. Considering torelons of length L, it has been found that the ground state energy agrees with the Nambu-Goto result at order $1/L$, and is consistent with it at order $1/L^3$. Also, a possible deviation at order $1/L^5$ comes with a very small coefficient. The excitation spectrum has also been found to agree with Nambu-Goto at orders $1/L$ and $1/L^3$, however at higher orders there are deviations. The lattice data are now reaching high precision, so that it is becoming possible to determine at which order the deviation occurs, which could be already at order $1/L^5$ [70, 51].

Similarly, in simulations of large-N gauge theories done in $3+1$ dimensions, there is agreement with Nambu-Goto for large L, but the order in which the deviations arise is not clear. Such is the case also in simulations

of interfaces in the 2 + 1-dimensional Ising model, in which one can also see a good agreement with Nambu-Goto [71], but still more precision would be needed in order to tell at what order deviations from Nambu-Goto arise [70].

$2+1$ dimensional confining strings in higher representations, called "k-strings", have also been studied [72, 73] at large N. Comparison to Nambu-Goto showed large deviations for all states, including the ground state, possibly starting already at order $1/L^5$. However, there are some technical aspects to be taken into account. In the large-N limit, assuming k to be fixed, the binding energy of k fundamental strings to form a k-string may vanish as $1/N^2$ or as $1/N$ [74], implying that in the large-N limit there are at least $(k-1)(D-2)$ light modes on the worldvolume of a k-string, whose mass goes to zero in the large-N limit as $1/N$ or as $1/N^{1/2}$, respectively. The relevant length scales concerning the form of the effective action are larger than $N/\sqrt{T}$ (or $N^{1/2}/\sqrt{T}$).

Finally, we mention that the ground state potential of a confining string in the continuum limit of a percolation model in 2+1 dimensions was studied in [41], and again agreement was found with Nambu-Goto at orders $1/L$ and $1/L^3$, however deviations were seen at order $1/L^5$. As discussed in [70], this model is interesting in itself, as it is not necessarily expected to correspond to a weakly coupled string theory.

3 Polyakov loop correlation function on the lattice

We discretize the SU(N) Yang-Mills theory on an isotropic 4-dimensional, or alternatively, 3-dimensional lattice with spacing a, time-like extent aN_t and spatial size aN_s. Apart from providing precise results more quickly, simulations in 3 dimensions are interesting because there the $1/r$ term is certain to be the Lüscher term; in $4D$ it could get mixed with a Coulomb interaction. In $3D$ the Coulomb interaction is of the form $\log(r)$, rather than $1/r$.

In all directions of the lattice we impose periodic boundary conditions. For the gauge field action we take the usual Wilson plaquette action

$$S = \beta \sum_{x,\mu<\nu} \Big(1 - \frac{1}{N}\mathrm{Re}\,\mathrm{Tr}\, U_{\mu\nu}(x)\Big), \tag{17}$$

where $U_{\mu\nu}$ is the plaquette oriented along the $\mu\nu$-plane and located at the lattice site x, and $\beta = 2N/g^2$. We also carry out the simulations using the tree-level improved action [18, 19, 20, 21]

$$S = \beta \sum_{x,\mu<\nu} \left\{1 - \frac{1}{N}\mathrm{Re}\,\mathrm{Tr}\left[\frac{5}{3}U^{1,1}_{\mu\nu}(x) - \frac{1}{12}U^{1,2}_{\mu\nu}(x) - \frac{1}{12}U^{1,2}_{\nu\mu}(x)\right]\right\}. \tag{18}$$

For any given gauge field configuration $U(x,\mu)$, the (trace of the) Polyakov loop is defined as

$$P(x) = \mathrm{Tr}\, U(x,\mu)U(x+\hat{a}\mu,\mu)\ldots U(x+(T-a)\hat{\mu},\mu)_{\mu=0} \tag{19}$$

and the correlation function

$$\langle P(x)^\star P(y)\rangle = \frac{1}{Z}\int \prod_{x,\mu} dU(x,\mu) P(x)^\star P(y) e^{-S[U]}. \tag{20}$$

The ground state inter-quark potential $V(r)$ of a heavy $\bar{Q}Q$ pair in a pure gauge theory can be expressed with the two-point correlators of the Polyakov loop [6]

$$V(r) = -\frac{1}{aN_t}\log\langle P(x)^\star P(y)\rangle + \epsilon, \tag{21}$$

where

$$\epsilon = \frac{1}{aN_t}(\omega_1 e^{-\Delta E T} + \dots), \qquad \Delta E = E_1 - E_0. \tag{22}$$

4 The Multilevel algorithm

Like mentioned in the introduction, the lattice data is obtained using the multilevel algorithm of Lüscher and Weisz [1]. In this algorithm, using the locality of the theory, the lattice is split into sublattices that do not communicate with one another, and the final observables are built combining the independent measurements of each sublattice. Of course, from time to time the boundaries between the sublattices are updated, so that the final results are the same as in the usual theory.

Following the discussion in [33], suppose we measure an observable $\mathcal{O}$ by combining the results of averages $\mathcal{O}_{sub}$ computed in $\mathcal{N}$ different sublattices. With $\mathcal{N}$ sublattice measurements, the combination of the sublattice averages $\mathcal{O}_{sub}$ corresponds to $(N)^{\mathcal{N}}$ measurements of $\mathcal{O}$, i.e. we get an estimate of $\mathcal{O}$ as if $(N)^{\mathcal{N}}$ measurements would have been performed. However, due to the links that have been kept frozen at the boundaries of the sublattices, this estimate is biased by a background field, but this bias is removed by averaging over the boundary configurations.

Using the notation of [33], consider the correlation function of two Polyakov loops

$$\begin{aligned}\langle P(\vec{0})P(\vec{x})^*\rangle &= \frac{1}{Z}\int\prod_{y,\mu} dU_{y,\mu}\,\mathrm{Tr}\left[U_{(\vec{0},0),4}\dots U_{(\vec{0},L-1),4}\right] \\ &\times \mathrm{Tr}\left[U^*_{(\vec{x},0),4}\dots U^*_{(\vec{x},L-1),4}\right] e^{-S[U]}.\end{aligned} \tag{23}$$

Next, we slice the lattice along the temporal direction into $\mathcal{N} = N_t/n_t$ sublattices, i.e. n_t is the temporal thickness of each sublattice in units of the lattice spacing a. Now, to obtain sublattices isolated from each other, we fix the set V^s_k of all spatial links with time coordinates kn_t, $k = 0,\dots,(\mathcal{N}-1)$. This way, the dynamics of every sublattice depends only on the background field of the two frozen time slices, and hence are totally independent from one another.

As in [33], we rewrite (23) as

$$\begin{aligned}\langle P(\vec{0})P(\vec{x})^*\rangle &= \int\prod_k dU_k^{(s)} T^{\alpha\gamma\beta\delta}_{\vec{0},(\vec{x})}[V_0^{(s)},V_1^{(s)}] \\ &\ldots\ T^{\epsilon\alpha\rho\beta}_{\vec{0},(\vec{x})}[V_{\mathcal{N}-1}^{(s)},V_0^{(s)}]\mathcal{P}[V_k^{(s)}] \end{aligned} \tag{24}$$

where

$$\begin{aligned} T^{\alpha\gamma\beta\delta}_{\vec{0},\vec{(x)}}[V_i^{(s)},V_j^{(s)}] &\equiv \int\prod_{y,\mu} dU_{y,\mu}\Big[U_{(\vec{0},0),4}\ldots U_{(\vec{0},n_t-1),4}\Big]_{\alpha\gamma} \\ &\times \Big[U^*_{(\vec{x},0),4}\ldots U^*_{(\vec{x},n_t-1),4}\Big]_{\beta\delta}\frac{e^{-S[U;V_i^{(s)},V_j^{(s)}]}}{Z[V_i^{(s)},V_j^{(s)}]}. \end{aligned} \tag{25}$$

The partition function of the sublattice with fixed temporal boundaries reads

$$Z[V_i^{(s)},V_j^{(s)}] \equiv \int\prod_{y,\mu} dU_{y,\mu} e^{-S[U;V_i^{(s)},V_j^{(s)}]} \tag{26}$$

in which $S[U;V_i^{(s)},V_j^{(s)}]$ is the action in the sublattice with fixed temporal boundaries $V_i^{(s)}$ and $V_j^{(s)}$. α, β, γ and δ are color indices and $T^{\alpha\gamma\beta\delta}$ are gauge-invariant quantities under sublattice gauge transformations. $\mathcal{P}[V_k^{(s)}]$ is the probability for the spatial links with time coordinates kn_t, $k = 0,\ldots,(\mathcal{N}-1)$, to be $V_k^{(s)}$, and can be written

$$\mathcal{P}[V_k^{(s)}] = \frac{1}{Z}\int\prod_{y,\mu} dU_{y,\mu}\prod_k \delta(U_k^{(s)} - V_k^{(s)})e^{-S[U]} \tag{27}$$

Iterating this procedure and averaging the background field according to the probability distribution of eq. (27) gives a numerical estimate for the integral (24) [33]. This technique is the so-called single level algorithm. A more general "multilevel algorithm by Lüscher and Weisz involves a feature, that the updating frequency of the background field $V_k^{(s)}$ is not the same for the various time slices k. However, for many purposes the single level algorithm seems to be more efficient [6, 33].

In numerical simulations with the single level algorithm, three parameters have to be fixed: the temporal sublattice thickness n_t, the number N of sublattice measurements and the number M of background field configurations to integrate over $V^{(s)}$. These parameters are dependent on each other as well as on the temporal extension N_t of the whole lattice and on the distance between the two Polyakov loops. Finding the optimal choice for them is thus not trivial. Some results on the optimization step can be found in [59, 2].

When measuring the Polyakov loop correlation function $\langle P(\vec{0})P(\vec{x})^*\rangle$ the final error bar is the combination of the uncertainties of the sublattice averages and their fluctuations, due to different background fields. With n_t

fixed, a large distance between two loops requires both N and M to be large. N is typically order of several thousands and M of few hundreds. It should be noted that N does not depend on N_t whereas M does. With the Lüscher and Weisz algorithm, exponential gain in the accuracy of the numerical estimation of $\langle P(\vec{0})P(\vec{x})^* \rangle$ is possible only in the temporal direction. Every sublattice estimate decreases exponentially with the distance, but it is still estimated with an error reduction proportional to $1/\sqrt{N}$ [33].

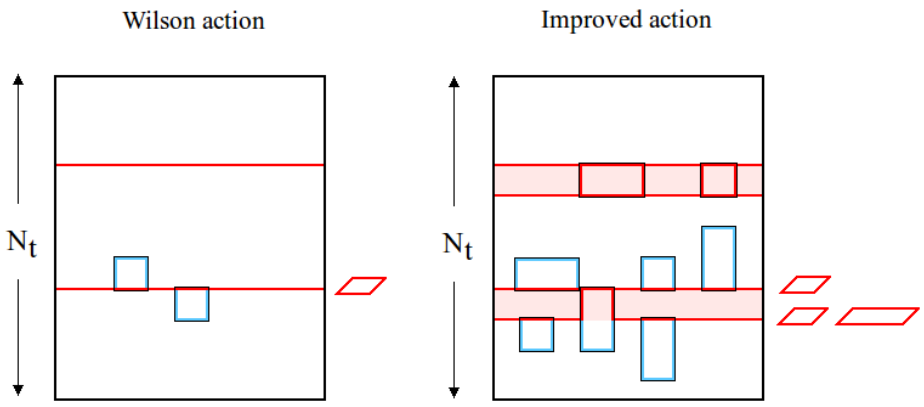

Figure 1: For an example on how the multilevel algorithm works, i.e. which links are updated during the sublattice updates, consider a lattice divided into three sublattices. On the left, a presentation of the Wilson action, and on the right, the improved action. On the borders of a sublattice, the red links are the ones kept fixed, whereas the blue links are updated. The improved action is slightly less local than the Wilson action, because it involves not only plaquettes but also rectangles. However, like the Wilson action, the improved action is still "ultralocal", namely, in the action, each link is coupled directly to other links only up to a finite distance.

5 Results

The simulations were performed with gauge groups SU(3) and SU(4), in $2+1$ and $3+1$ dimensions, with the general Wilson action (17) and with the tree-level improved action (18). The totalling 8 different cases (up to 4 different values of β for each) were studied using the multilevel algorithm with sublattice size of 4 lattice spacings. In $3D$ with SU(3) the lattice size was $N_t = 48$, $N_s = 24$, in the other cases $N_t = 24$, $N_s = 16$. The first 1000 updates were used for thermalization, and the following $1000-5000$ updates were used for the actual measurements of the Polyakov correlation function.

In addition to considering the correlators measured with an "on-axis" increasing distance between the sources, we also measure the correlators in "off-axis" points, i.e. where the sources have "vertical" distance in addition.

In general, the lattice breaks rotational symmetry, so off-axis correlators of Polyakov loops are not expected to lie exactly aligned with the on-axis ones. The full continuum rotational symmetry is however restored when the lattice spacing tends to zero [75]. In the off-axis points one could expect to see a difference between the results obtained using the general Wilson action and the tree-level improved action; when calculating the potential, the off-axis points are expected to fall further from the expected curve with the non-improved action. This makes measuring the off-axis points a valid test to assess the "goodness" of the improved action.

For each value of β, the static quark potential was calculated according to (21), see figures 2-9. In $4D$ cases, a function of the form

$$V(r) = \sigma r + V_0 + \gamma/r \tag{28}$$

was fitted to the data, thus giving estimates for σ, V_0, and γ.

In $3D$ cases the fitted function could basically include also a logarithmic term, i.e. the Coulomb term, which would play a role on small distances. However, including this term makes the fit very unstable on larger distances, as seen also in [76]. Instead, following the conclusions of [69], in $3D$ cases we add a $1/r^3$ term in the fitting function,

$$V(r) = \sigma r + V_0 + \gamma/r + b/r^3. \tag{29}$$

Compared to (28), this form gives us better a fit and better estimates for the Lüscher term γ.

In $3D$ the bosonic string prediction for the Lüscher term is $\gamma \simeq 0.1309$, and in $4D$ $\gamma \simeq 0.2618$. As we can see from the tables 1, 2, in both $3D$ and $4D$, the Lüscher term extracted from our lattice data follows these predictions.

All statistical uncertainties affecting the results were computed using standard statistical analysis methods. In particular, the error bars on the values of the average correlators were computed with the jackknife method, while those on the potential were calculated by Gaussian propagation of the latter.[1]

5.1 Systematic uncertainties

As always with results from lattice studies, there are some systematic uncertainties that need to be taken in account. Finite volume effects, finite cut-off effects and systematic effects in the choice of the fitting function are all sources of such uncertainties in our calculations.

[1] This procedure turns out to be reliable for our data; computing the uncertainties on the potential using the jackknife method leads to comparable results: the small differences between the results obtained with the two methods do not have a really significant impact on the findings of the study, and we include them among the possible sources of systematic uncertainties that we discuss in subsection 5.1

The finite volume effects are exponentially suppressed as $e^{-m_G L}$, where m_G is the mass of the lightest glueball, and L the shortest lattice size. $e^{-m_G L}$ is already very small when $m_G L \gtrsim 4$, so what we want is

$$L \gtrsim \frac{4}{m_G}. \tag{30}$$

The lattice sizes chosen in this work meet this requirement.

As usual, the finite cut-off effects can be controlled by performing simulations at several values of the lattice spacing. The calculations in this paper involve a few different values of β in each studied case, and the results indicate the impact from cut-off effects to be very small. As can be seen from figure 10, the results are clearly already quite close to the continuum, because the points obtained from simulations at different lattice spacing fall on the same curve and because there is no significant difference between points obtained from on-axis versus off-axis correlators (hence the full rotational symmetry is approximately restored).

The systematic effects in the choice of the fitting function can be studied by extending it with an extra term, c/r^α with $\alpha = 2$ or 3, and seeing how the fit parameters behave. With SU(3) in $3D$ and $4D$, adding the extra term with $\alpha = 2$ changes σa^2 and $V_0 a$ only slightly (for example in $3D$ with $\beta = 18.0$, σa^2 changes from 0.04482(40) to 0.0470(59) and $V_0 a$ from 0.2255(23) to 0.202(61)), but gives very poor estimates for γ. With SU(3) in $4D$ adding the extra term with $\alpha = 3$ gives poor estimates for all the parameters; with $\beta = 5.9$, σa^2 changes from 0.0904(70) to 0.08(13), $V_0 a$ from 0.670(21) to 0.72(69), and γ from $-0.236(14)$ to $-0.31(97)$.

The quality of the fit and, more precisely, the χ^2 are heavily influenced by the choice of points that are included in the fitting process. Small distance off-axis points have a huge impact; for example with SU(3), $\beta = 18.5$ in $3D$, we get $\chi^2 = 1.04$ when the small distance off-axis points are neglected in the fitting, but when included, the χ^2 grows to a staggering 4445.21. Obviously, this is due to systematic effects related to lattice artifacts at short distances. Already removing just a couple of these points brings the χ^2 down to 107.028. In another example, with SU(4), $\beta = 23.0$ in $3D$, we get $\chi^2 = 0.91$ with the small distance off-axis points neglected, and $\chi^2 = 3627.49$ when they are included. For reliable results, all fits in this paper are done excluding the small distance off-axis points. The points are however included in the figures 2-9.

6 Conclusions

In this work, we have generalized the Lüscher and Weisz multilevel algorithm for the tree-level improved gauge action to study SU(N) Yang-Mills theories. Applying this efficient lattice gauge theory algorithm, we computed the static quark potential in SU(3) and SU(4) Yang-Mills theories in $2+1$ and $3+1$ dimensions. The calculated Lüscher term was shown to satisfy the predictions of bosonic string theory, more or less equally well with the

N_C	D	β	σa^2	$V_0 a$	γ	b
3	3	18.0	0.043927(57)	0.23041(32)	−0.11434(47)	0.02313(23)
		18.5	0.041339(58)	0.22689(33)	−0.11276(48)	0.02306(21)
		19.0	0.039042(62)	0.22313(36)	−0.11069(53)	0.02276(23)
	4	5.9	0.0904(70)	0.670(21)	−0.236(14)	
		6.0	0.0649(21)	0.6788(63)	−0.2412(42)	
4	3	32.0	0.04716(15)	0.31280(90)	−0.1230(13)	0.02528(60)
		33.5	0.04244(25)	0.3070(15)	−0.1210(23)	0.0255(10)
		34.0	0.04106(27)	0.3050(16)	−0.1202(25)	0.0254(11)
		30.0	0.054518(76)	0.32240(44)	−0.12795(64)	0.02581(28)
	4	11.0	0.0680(14)	0.737(19)	−0.255(12)	

Table 1: fit results with Wilson action

N_C	D	β	σa^2	$V_0 a$	γ	b
3	3	18.0	0.034971(85)	0.20028(48)	−0.10488(68)	0.02115(29)
		18.5	0.03320(14)	0.19695(76)	−0.1025(11)	0.02061(48)
		19.0	0.031427(70)	0.19493(40)	−0.10222(58)	0.02106(25)
	4	4.5	0.0536(22)	0.6686(66)	−0.2478(44)	
4	3	23.0	0.07118(38)	0.3191(21)	−0.1333(31)	0.0244(13)
		23.5	0.06852(47)	0.3145(26)	−0.1292(38)	0.0232(17)
		24.0	0.06599(24)	0.3102(13)	−0.1250(19)	0.02187(85)
	4	8.0	0.058(13)	0.771(41)	−0.290(28)	

Table 2: fit results with the improved action

		Wilson action		Improved action	
N_C	D	β	reduced χ^2	β	reduced χ^2
3	3	18.0	1.53	18.0	0.26
		18.5	2.25	18.5	1.04
		19.0	3.48	19.0	0.42
	4	5.9	0.53	4.5	0.49
		6.0	1.21		
4	3	32.0	15.91	23.0	0.91
		33.5	65.21	23.5	2.07
		34.0	86.83	24.0	0.79
		30.0	1.81		
	4	11.0	0.55	8.0	0.98

Table 3: The reduced χ^2 for each of the fits.

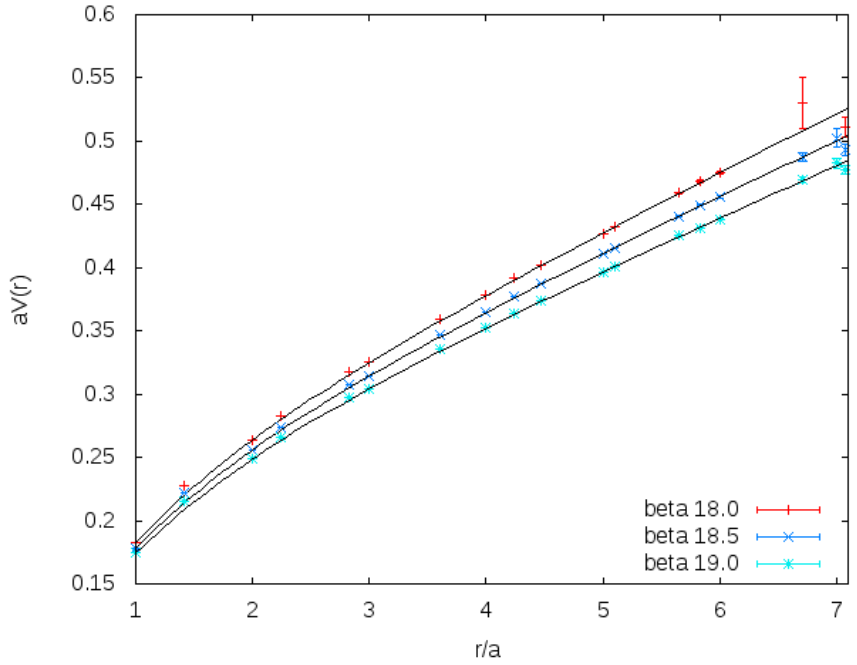

Figure 2: SU(3), in 3 dimensions, with the Wilson action. 4000 measurements, lattice size 48×24^2.

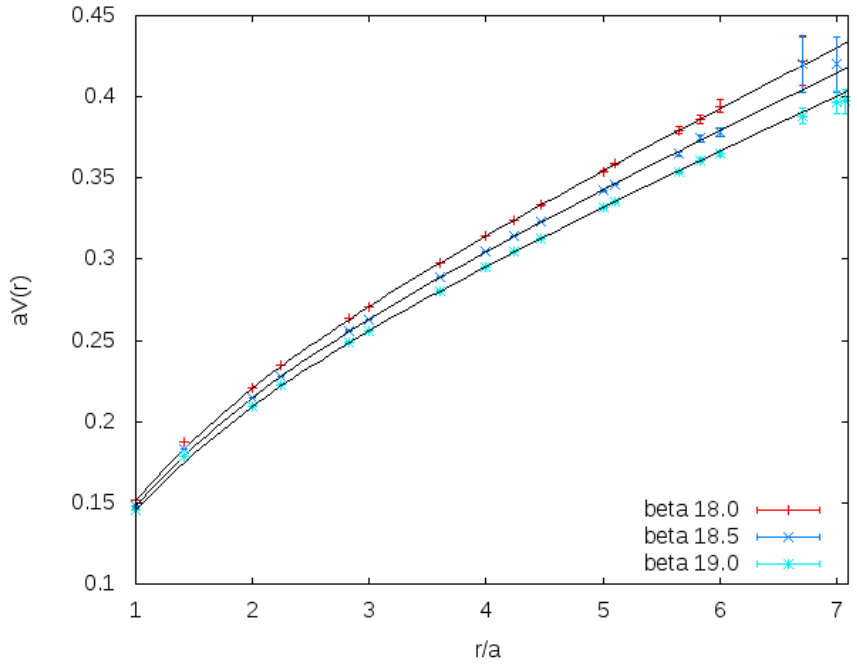

Figure 3: SU(3), in 3 dimensions, with the improved action. 4000 measurements, lattice size 48×24^2.

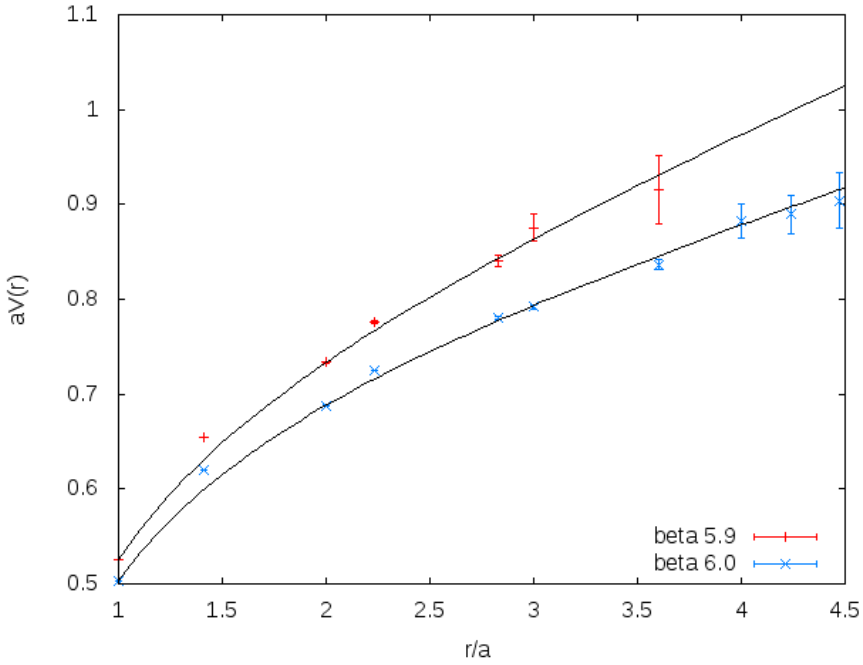

Figure 4: SU(3), in 4 dimensions, with the Wilson action. 4000 measurements, lattice size 24×16^3.

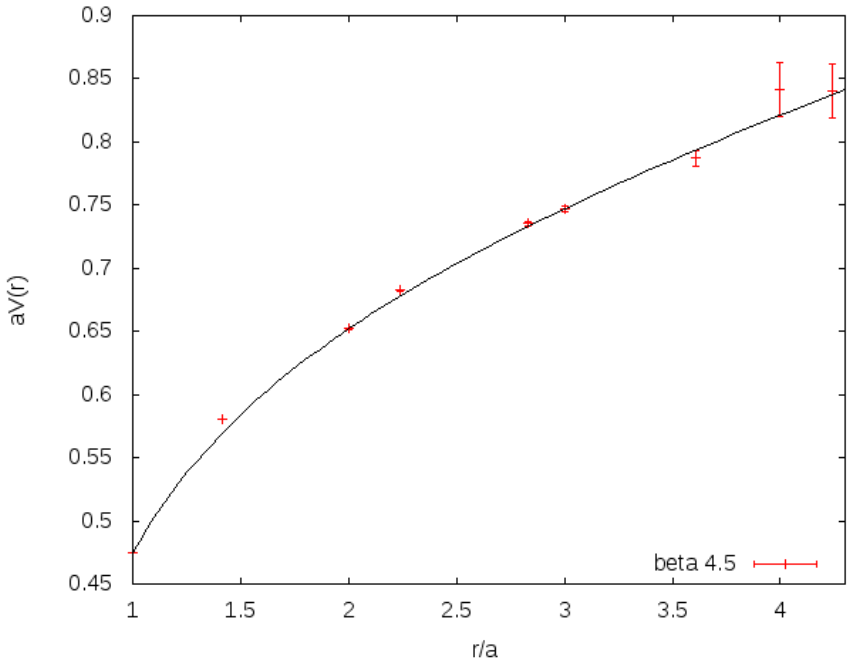

Figure 5: SU(3), in 4 dimensions, with the improved action. 3000 measurements, lattice size 24×16^3.

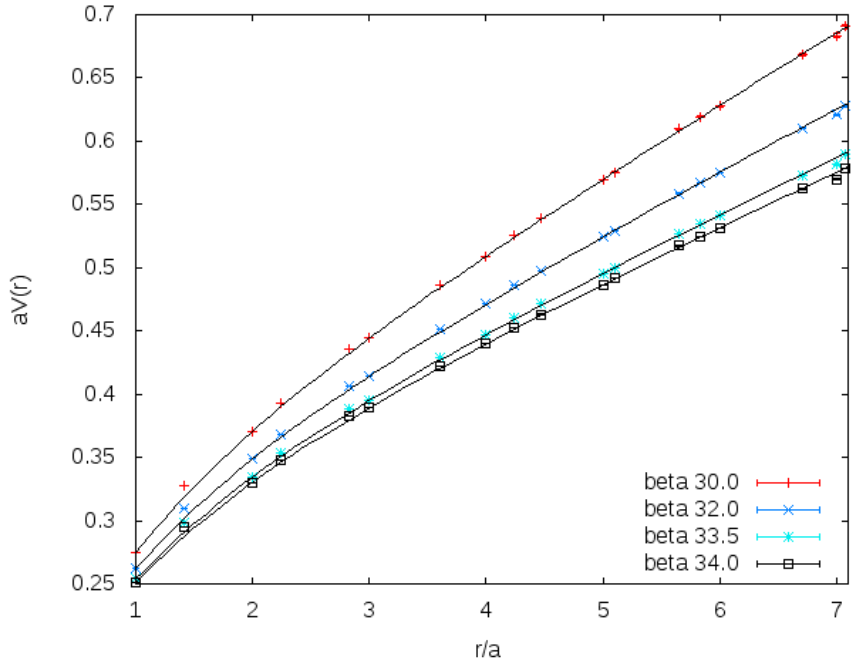

Figure 6: SU(4), in 3 dimensions, with the Wilson action. 5000 measurements, lattice size 24×16^2.

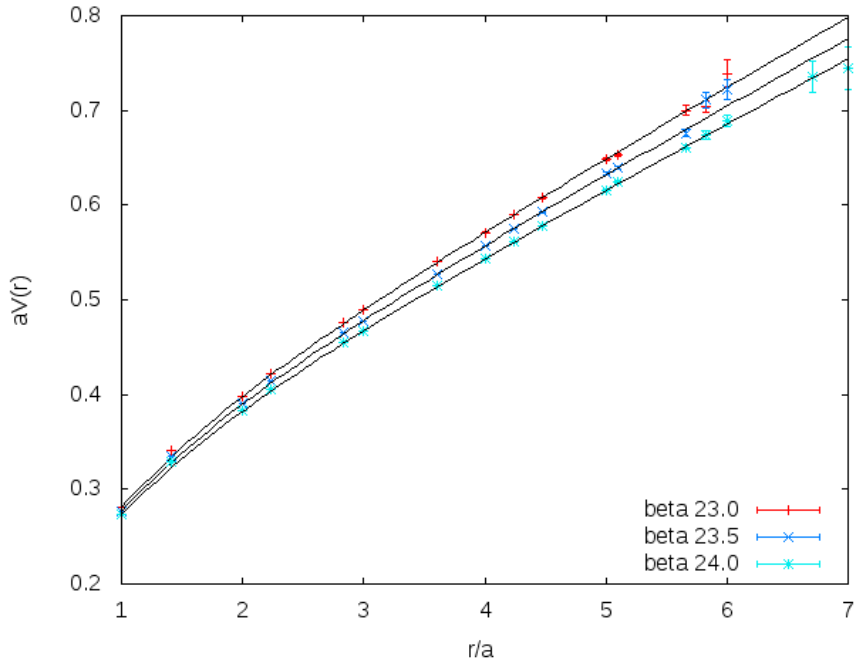

Figure 7: SU(4), in 3 dimensions, with the improved action. 5000 measurements, lattice size 24×16^2.

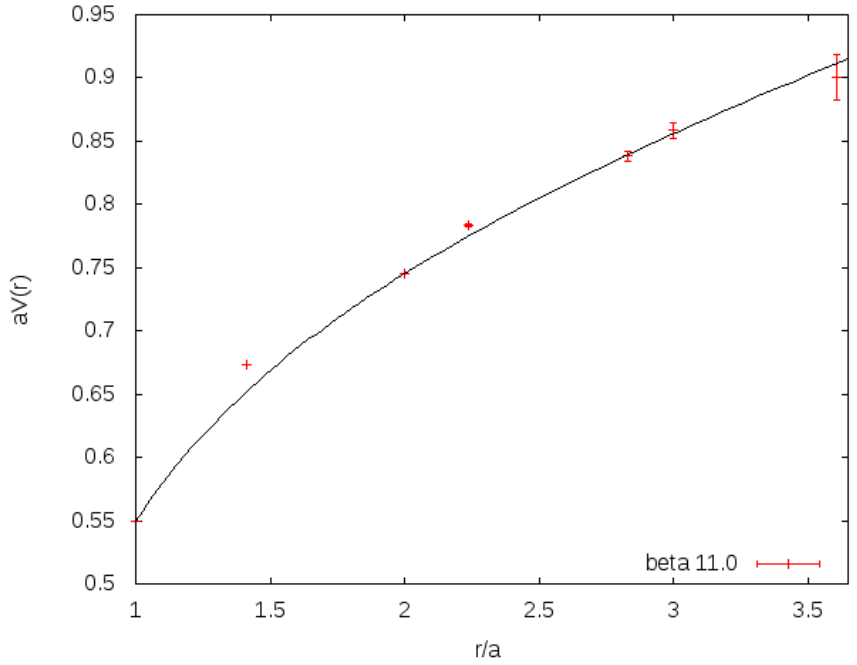

Figure 8: SU(4), in 4 dimensions, with the Wilson action. 3300 measurements, lattice size 24×16^3.

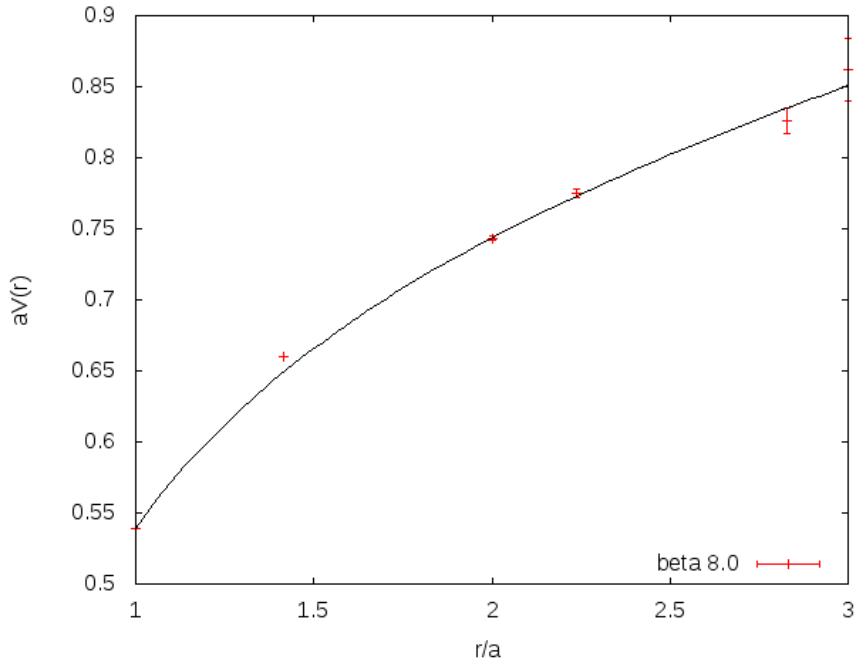

Figure 9: SU(4), in 4 dimensions, with the improved action. 1100 measurements, lattice size 24×16^3.

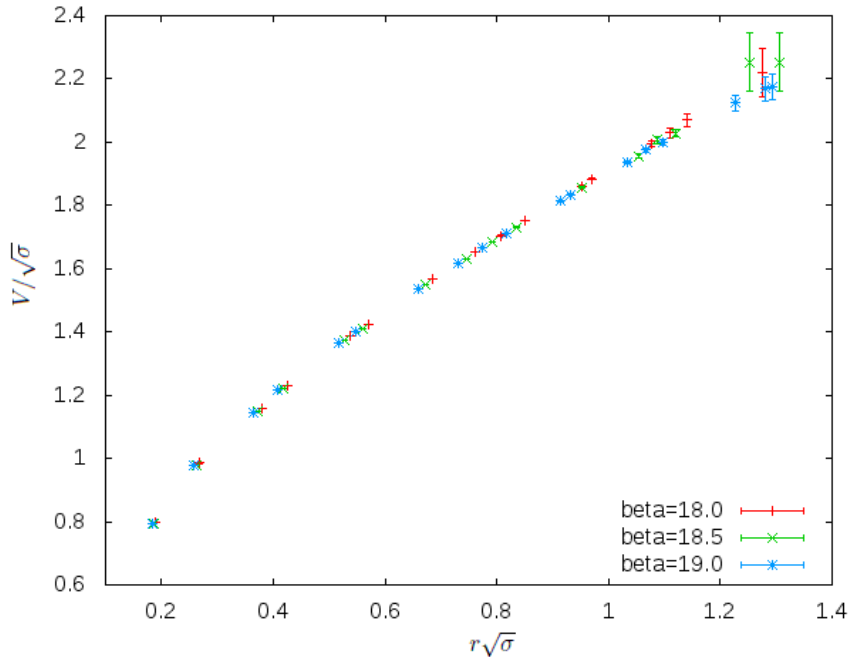

Figure 10: The physical values calculated from the results obtained with SU(3) in 3 dimensions, with the improved action

Wilson action as with the improved action. Also, we can see that the results obtained with SU(4) agree with the results of SU(3), and in fact, the bosonic string prediction for the Lüscher term is met more accurately with SU(4).

Besides the calculations of the static quark potential, multilevel algorithms can be used in many other contexts, such as in the computation of glueball masses and the correlation functions related to the transport coefficients of the quark-gluon plasma. For future endeavors, in principle the multilevel algorithm for the improved gauge action could also be used in graphics processing unit (GPU) implementations. As an example of this type of application, very recently this has been done for the compact U(1) lattice gauge theory with the standard Wilson action, in [77].

Another possible useful application for a high-precision multilevel algorithm with the improvement in $3D$ could be in the context of dimensionally-reduced effective theories for hot QCD, which, for example, very recently have been used to compute certain non-perturbative contributions to the jet-quenching parameter in [78, 79].

Acknowledgements

I would like to acknowledge support from the Academy of Finland grant 1134018 and the Magnus Ehrnrooth Foundation. I also thank K. Kajantie, M. Panero and K. Rummukainen for valuable comments and discussions. The simulations were carried out at the Finnish IT Center for Science (CSC).

References

[1] M. Lüscher and P. Weisz. Locality and exponential error reduction in numerical lattice gauge theory. *JHEP*, 09:010, 2001.

[2] H. B. Meyer. The Yang-Mills Spectrum from a Two-Level Algorithm. *JHEP*, 0401:030, Jan 2004. arXiv:hep-lat/0312034v2.

[3] H. B. Meyer. A calculation of the shear viscosity in SU(3) gluodynamics. *Phys.Rev.D*, 76:101701, 2007. arXiv:0704.1801v1 [hep-lat].

[4] H. B. Meyer. A calculation of the bulk viscosity in SU(3) gluodynamics. *Phys.Rev.Lett.*, 100:162001, 2008. arXiv:0710.3717v1 [hep-lat].

[5] M. Laine, H.B. Meyer, K. Rummukainen, and M. Shaposhnikov. Effective gauge theories on domain walls via bulk confinement? *JHEP*, 0404:027, 2004. arXiv:hep-ph/0404058v2.

[6] M. Lüscher and P. Weisz. Quark confinement and the bosonic string. *JHEP*, 0207:049, Jul 2002. arXiv:hep-lat/0207003v1.

[7] M. Lüscher, K. Symanzik, and P. Weisz. Anomalies of the free loop wave equation in the Wkb approximation. *Nucl. Phys. B*, 173:365, 1980.

[8] M. Lüscher. Symmetry breaking aspects of the roughening transition in gauge theories. *Nucl. Phys. B*, 180:317, 1981.

[9] Y. Nambu. QCD and the string model. *Phys. Lett. B*, 80:372, 1979.

[10] J. Ambjørn, P. Olesen, and C. Peterson. *Phys. Lett. B*, 142:410, 1984. Nucl. Phys. B244 (1984) 262.

[11] P. de Forcrand, G. Schierholz, H. Schneider, and M. Teper. *Phys. Lett. B*, 160:137, 1985.

[12] B. Lucini and M. Teper. *Phys. Rev. D*, 64:105019, 2001.

[13] S. Necco and R. Sommer. The $N_f = 0$ heavy quark potential from short to intermediate distances. *Nucl. Phys. B*, 622:328, 2002. arXiv:hep-lat/0108008v1.

[14] M. Caselle, R. Fiore, F. Gliozzi, M. Hasenbusch, and P. Provero. String Effects in the Wilson Loop: a high precision numerical test. *Nucl. Phys. B*, 486:245, 1997. arXiv:hep-lat/9609041v1.

[15] R. Lohmayer and H. Neuberger. Rectangular Wilson Loops at Large N, Jun 2012. arXiv:1206.4015v1.

[16] A. Athenodorou, B. Bringoltz, and M. Teper. Closed flux tubes and their string description in $D = 3 + 1$ SU(N) gauge theories. *JHEP*, 1102:030, 2011. arXiv:1007.4720v2 [hep-lat].

[17] A. Athenodorou, B. Bringoltz, and M. Teper. Closed flux tubes and their string description in $D = 2 + 1$ SU(N) gauge theories, Mar 2011. arXiv:1103.5854v1 [hep-lat].

[18] P. Weisz. *Nucl. Phys. B*, 212:1, 1983.

[19] G. Curci, P. Menotti, and G. Paffuti. Symanzik's improved Lagrangian for lattice gauge theory. *Phys.Lett. B*, 130:205, 1983.

[20] P. Weisz and R. Wohlert. *Nucl. Phys. B*, 236:397, 1984.

[21] M. Lüscher and P. Weisz. Computation of the Action for On-Shell Improved Lattice Gauge Theories at Weak Coupling. *Phys.Lett. B*, 158:250, 1985.

[22] B. Beinlich, F. Karsch, E. Laermann, and A. Peikert. *Eur. Phys. J.*, C6, 1999. arXiv:hep-lat/9707023.

[23] Sz. Borsányi, G. Endrődi, Z. Fodor, S. D. Katz, and K. K. Szabó. Precision SU(3) lattice thermodynamics for a large temperature range. Jul 2012. arXiv:1204.6184v2 [hep-lat].

[24] S. Gupta, K. Hübner, and O. Kaczmarek. Renormalized Polyakov loops in many representations. *Phys.Rev.D*, 77:034503, 2008.

[25] A. Mykkänen, M. Panero, and K. Rummukainen. Casimir scaling and renormalization of Polyakov loops in large-N gauge theories. *JHEP*, 1205:069, 2012. arXiv:1202.2762v2 [hep-lat].

[26] T. Karavirta, A. Mykkänen, J. Rantaharju, K. Rummukainen, and K. Tuominen. Nonperturbative improvement of SU(2) lattice gauge theory with adjoint or fundamental flavors. *JHEP*, 1106:061, 2011.

[27] M. Caselle, M. Hasenbusch, and M. Panero. String effects in the $3d$ gauge Ising model. *JHEP*, 0301:057, Jan 2003. arXiv:hep-lat/0211012.

[28] K. J. Juge, J. Kuti, and C. Morningstar. QCD String formation and the Casimir Energy, Jan 2004. arXiv:hep-lat/0401032.

[29] P. Giudice, F. Gliozzi, and S. Lottini. The conformal anomaly of k-strings. *JHEP*, 0705:010, 2007. arXiv:hep-th/0703153v1 16 Mar 2007.

[30] M. Panero. A numerical study of confinement in compact QED. *JHEP*, 0505:066, May 2005. arXiv:hep-lat/0503024v3.

[31] M. Panero. A numerical study of a confined $Q\bar{Q}$ system in compact U(1) lattice gauge theory in $4D$. *Nucl.Phys.Proc.Suppl.*, 140:665–667, 2005. arXiv:hep-lat/0408002v3.

[32] Y. Koma, M. Koma, and P. Majumdar. Static potential, force, and flux-tube profile in $4D$ compact U(1) lattice gauge theory with the multi-level algorithm. *Nucl. Phys. B*, 692:209–231, Jun 2004. arXiv:hep-lat/0311016v2.

[33] M. Caselle, M. Pepe, and A. Rago. Static quark potential and effective string corrections in the $(2+1)-d$ SU(2) Yang-Mills theory. *JHEP*, 10:005, Jun 2004. arXiv:hep-lat/0406008v1.

[34] M. Caselle, M. Pepe, and A. Rago. String effects in SU(2) lattice gauge theory. *Nucl. Phys. Proc. Suppl.*, 129:721, 2004. arXiv:hep-lat/0310005.

[35] C. Bonati. Finite temperature effective string corrections in $(3+1)D$ SU(2) lattice gauge theory, Aug 2011. arXiv:hep-lat/1106.5920v3.

[36] K. J. Juge, J. Kuti, and C. Morningstar. Fine Structure of the QCD String Spectrum. *Phys. Rev. Lett.*, 90:161601, 2003. arXiv:hep-lat/0207004.

[37] G. S. Bali. QCD forces and heavy quark bound states. *Phys. Rept.*, 343:1–136, May 2001. arXiv:hep-ph/0001312.

[38] A. Athenodorou, B. Bringoltz, and M. Teper. The closed string spectrum of SU(N) gauge theories in $2+1$ dimensions. *Phys. Lett. B*, 656:132, 2007. arXiv:hep-lat/0709.0693.

[39] B. Bringoltz and M. Teper. Strings in SU(N) gauge theories in $2+1$ dimensions: beyond the fundamental representation, 2007. arXiv:0708.3447 [hep-lat].

[40] F. Gliozzi, S. Lottini, M. Panero, and A. Rago. Random percolation as a gauge theory. *Nucl.Phys.*, B719:255–274, 2005.

[41] P. Giudice, F. Gliozzi, and S. Lottini. The confining string beyond the free-string approximation in the gauge dual of percolation, Jan 2009. arXiv:0901.0748 [hep-lat].

[42] Ofer Aharony, Steven S. Gubser, Juan Martin Maldacena, Hirosi Ooguri, and Yaron Oz. Large N field theories, string theory and gravity. *Phys.Rept.*, 323:183–386, 2000.

[43] D. Mateos. String Theory and Quantum Chromodynamics. *Class.Quant.Grav.*, 24:S713–S740, 2007. arXiv:0709.1523v1 [hep-th].

[44] Y. Nambu. Symmetries and Quark Models. ed. R. Chand, (Gordon and Breach, New York, 1970).

[45] T. Goto. *Prog. Theor. Phys*, 46:1560, 1971.

[46] Y. Nambu. *Phys. Rev. D*, 10:4262, 1974.

[47] J. F. Arvis. The exact $q\bar{q}$ potential in Nambu string theory. *Phys. Lett. B*, 127:106, 1983.

[48] O. Alvarez. Static potential in string models. *Phys. Rev. D*, 24:440, 1981.

[49] M. Caselle, A. Feo, M. Panero, and R. Pellegrini. Universal signatures of the effective string in finite temperature lattice gauge theories. *JHEP*, 1104:020, Apr 2011. arXiv:hep-lat/1102.0723.

[50] M. Lüscher, G. Münster, and P. Weisz. *Nucl. Phys. B*, 180:1, 1981.

[51] F. Gliozzi and M. Meineri. Lorentz completion of effective string (and p-brane) action. arXiv:1207.2912v1 [hep-th].

[52] H. B. Meyer. Poincaré invariance in effective string theories. *JHEP*, 05:066, 2006. arXiv:hep-th/0602281.

[53] O. Aharony and M. Field. On the effective theory of long open strings. *JHEP*, 1101:065, 2011. arXiv:1008.2636 [hep-th].

[54] O. Aharony and M. Dodelson. Effective String Theory and Nonlinear Lorentz Invariance. *JHEP*, 12:008, 2012. arXiv:1111.5758 [hep-th].

[55] O. Aharony, M. Field, and N. Klinghoffer. The effective string spectrum in the orthogonal gauge. *JHEP*, 04:048, 2012. arXiv:1111.5757 [hep-th].

[56] G. Bali and A.M. Green. Two Quark Potentials, Oct 2004. arXiv:nucl-th/0410080v2.

[57] J. Kuti. Lattice QCD and String Theory, 2006. PoS JHW2005, 009 (2006), arXiv:hep-lat/0511023.

[58] M. Caselle, M. Panero, and P. Provero. String effects in Polyakov loop correlators. *JHEP*, 0206:061, June 2002. arXiv:hep-lat/0205008.

[59] P. Majumdar. The string spectrum from large Wilson loops. *Nucl. Phys. B*, 664:213, 2003. arXiv:hep-lat/0211038v3.

[60] M. Caselle, M. Hasenbusch, and M. Panero. Short distance behaviour of the effective string. *JHEP*, 0405:032, May 2004. arXiv:hep-lat/0403004.

[61] P. Majumdar. Continuum limit of the spectrum of the hadronic string, Jun 2004. arXiv:hep-lat/0406037.

[62] M. Caselle, M. Hasenbusch, and M. Panero. Comparing the Nambu-Goto string with LGT results. *JHEP*, 0503:026, May 2005. arXiv:hep-lat/0501027.

[63] K. J. Juge, J. Kuti, and C. J. Morningstar. Quark Confinement and Surface Critical Phenomena. *Nucl. Phys. Proc. Suppl.*, 83:503, 2000. arXiv:hep-lat/9911007.

[64] K. J. Juge, J. Kuti, and C. Morningstar. The Casimir Energy Paradox of the QCD String. *Nucl. Phys. Proc. Suppl.*, 129:686, 2004. arXiv:hep-lat/0310039.

[65] B. B. Brandt. Probing boundary-corrections to Nambu-Goto open string energy levels in $3d$ SU(2) gauge theory. *JHEP :,*, 1102:040, 2011. arXiv:1010.3625v2 [hep-lat].

[66] J. Polchinski and A. Strominger. Effective string theory. *Phys. Rev. Lett.*, 67:1681, 1991.

[67] J. M. Drummond. Universal subleading spectrum of effective string theory. arXiv:hep-th/0411017; J. M. Drummond, Reply to hep-th/0606265, arXiv:hep-th/0608109.

[68] N. D. Hari Dass and P. Matlock. Universality of correction to Luescher term in Polchinski-Strominger effective string theories. arXiv:hep-th/0606265; N. D. H. Dass and P. Matlock, Our response to the response hep-th/0608109 by Drummond, arXiv:hep-th/0611215; N. D. Hari Dass and P. Matlock, Covariant Calculus for Effective String Theories, arXiv:0709.1765 [hep-th].

[69] M. Lüscher and P. Weisz. String excitation energies in SU(N) gauge theories beyond the free-string approximation. *JHEP*, 0407:014, Jul 2004. arXiv:hep-th/0406205.

[70] O. Aharony and E. Karzbrun. On the Effective Action of Confining Strings, Mar 2009. arXiv:hep-th/0903.1927v4.

[71] M. Caselle, M. Hasenbusch, and M. Panero. The interface free energy: Comparison of accurate Monte Carlo results for the $3D$ Ising model with effective interface models. *JHEP*, 0709:117, 2007. arXiv:0707.0055 [hep-lat].

[72] B. Bringoltz and M. Teper. Closed k-strings in SU(N) gauge theories: $2+1$ dimensions. *Phys. Lett. B*, 663:429, 2008. arXiv:0802.1490 [hep-lat].

[73] A. Athenodorou, B. Bringoltz, and M. Teper. On the spectrum of closed $k=2$ flux tubes in $D=2+1$ SU(N) gauge theories, Dec 2009. arXiv:0812.0334 [hep-lat].

[74] C. P. Korthals Altes and H. B. Meyer. Hot QCD, k-strings and the adjoint monopole gas model. arXiv:hep-ph/0509018.

[75] C. B. Lang and C. Rebbi. Potential And Restoration Of Rotational Symmetry In SU(2) Lattice Gauge Theory. *Phys.Lett. B*, 115:137, 1982.

[76] C. Legeland, B. Beinlich, M. Lütgemeier, A. Peikert, and T. Scheideler. The string tension in SU(N) gauge theory from a careful analysis of smearing parameters. *Nucl.Phys.Proc.Suppl.*, 63:260–262, 1998. arXiv:hep-lat/9709147v1.

[77] A. Amado, N. Cardoso, M. Cardoso, and P. Bicudo. Study of compact U(1) flux tubes in 3+1 dimensions in lattice gauge theory using GPU's, Aug 2012. arXiv:1208.0166v1 [hep-lat].

[78] M. Benzke, N. Brambilla, M. A. Escobedo, and A. Vairo. Gauge invariant definition of the jet quenching parameter, Aug 2012. arXiv:1208.4253 [hep-ph].

[79] M. Laine. A non-perturbative contribution to jet quenching, Aug 2012. arXiv:1208.5707 [hep-ph].